BONE TISSUE ENGINEERING UTILIZING ADULT STEM CELLS IN BIOLOGICALLY FUNCTIONALIZED HYDROGELS

A Dissertation
Presented to
The Academic Faculty

by

Christopher Ryan Dosier

In Partial Fulfillment of the Requirements for the Degree of
Doctor of Philosophy in Bioengineering

Georgia Institute of Technology
May 2013

BONE TISSUE ENGINEERING UTILIZING ADULT STEM CELLS IN BIOLOGICALLY FUNCTIONALIZED HYDROGELS

Approved by:

Dr. Robert E. Guldberg, Advisor
School of Mechanical Engineering
Georgia Institute of Technology

Dr. Barbara D. Boyan
Dean, School of Engineering
Virginia Commonwealth University

Dr. Andrés J. García
School of Mechanical Engineering
Georgia Institute of Technology

Dr. Alexandra Peister
Department of Biology
Morehouse College

Dr. Zvi Schwartz
Department of Biomedical Engineering
Georgia Institute of Technology

Date Approved: March 28, 2013

For September 13, 2007.

ACKNOWLEDGEMENTS

Professional golfer Greg Norman once said, “I owe a lot to my parents, especially my mother and father.” I too owe a lot to my parents, Margrit and Bob Dosier, along with my brothers Jamie and Matt, for their unending support throughout my educational endeavors. Whenever I doubted myself or the decisions I had made, you all were there to tell me to stay the course and everything would work out in the end. Unconditional love is the greatest and perhaps most underappreciated gift one can receive in this world, and I am truly grateful to have all of you as my family. I hope I have made you all as proud of me as I am of you. An equal appreciation goes to my extended family, most of which would ask me what I was doing down in Atlanta, to only admit they did not know what in the world I had just described to them. That’s OK though, because a lot of the times I didn’t really know either.

I next need to thank Bob Guldberg. To say that I knew what I was getting into when I came into the Bioengineering program in 2006 would be a lie. I think it is also safe to say that Bob did not know what he was getting into either when he asked me to join the lab. Countless jabs back and forth, a few instances of vomit, a new haircut (or lack thereof), and now a Ph.D. are just some of the indelible marks the lab has left on me. I know I have not been the easiest student you have ever had, but I like to think me being the way I am has at least made you a more effective advisor. So you’re welcome for that. But honestly, your advice during my thesis has been measured, insightful, and a blueprint for how to guide a student through their project and get the most out of them.

I next need to thank the members of my thesis committee. All of them have known me for quite some time, which makes me wonder why they agreed in the first place to serve on my committee. Gluttons for punishment I guess… or maybe payback? Whatever your motivations, I hope you know how truly grateful I am for all for the guidance you have given me over the course of my research.

Alex first met me when I joined the Guldberg lab and was given the unenviable task of training me cell culture techniques. I don't think Alex had high hopes for me at the time. It was a year or so later when I was helping with one of the day long Guldberg Lab surgeries and I was telling her a sob story about how I would be in the lab until 2 A.M. and then back in surgery the next day at 8 A.M. when she said, "Wow. You've actually become a grad student!" I knew then I was on the right track. From the early training that ended up becoming vital for completion of my project to your advice in guiding my final experiments, thank you for all you have done for me.

Dr. Boyan once informed me that she was also my advisor. This was her subtle way of telling me to get my rear end in gear after I had presented a rather shoddy project update. Along with your enforcer, Zvi, the Boyan lab has assisted me so much in my research that it would take too long here to list all of the contributions they have made to my work. I always look forward to the meetings with you and Zvi as it is almost like watching a live action version of 'The Honeymooners'. But it would be an injustice to not say that those meetings have been some of the most productive bits of time during my thesis. I would often come in with an overly complicated and elaborate experimental design trying to answer multiple questions at once, only to leave 30 minutes later with a

streamlined experiment that would answer my questions more concisely and with less work. To a graduate student, that is invaluable.

Last but not least I would like to thank the final member of my thesis committee, Andrés Garcia. Bill Cosby had a Russian science teacher in high school and stated, "That man traveled all the way from Russia, just to bother me." At first, I thought Andrés has traveled all the way from Puerto Rico, just to bother me. But in the end I would see that he had my interest in mind more than anything else. In essence, he was challenging me to justify my choices and to think harder about my data. This ultimately led to better experiments and better interpretations of my data. In return, I am glad that I was able to add a story about getting exotic drinks reimbursed into his rotation of tales of former graduate students.

Aside from my thesis committee members, I would be remiss to not thank past and present members of the Guldberg lab and members of the Lair of Inefficiency. There are way too many people to list here, but some deserve honorable mention. Angela Lin. My Dublin BFF. We showed Dublin how it's done. And we were good. To the members of the 'Cypress Core', a term I just coined: Ted Lee, Vince Fiore, Ashley Allen, Alison Douglas, Brent Uhrig, Devon Headen, and Nick Willet (when it is not yoga night), thanks for the beers, the wings, and the laughs. I also need to send a special shout out to Dave Dumbauld, perhaps the only man in the world who can quote 'Top Gun' more than I can. I don't know how many text messages have been sent with lines from that movie, but I am sure it would fill a cargo plane from Hong Kong. I would also like to thank Dave and many members of the Cypress Core for that heat stroke in Turner Field's

parking lot in the middle of July. That was awesome. It was also the only time it was acceptable to eat mac n' cheese out of a red Solo cup (in a public setting).

A big thank you goes to Hazel Stevens and Vivian Johnson. As loathe she may be to admit it, I actually think Hazel enjoyed having me in the lab. I guess now that I am wrapping up in the lab, she can stop looking at everyone's feet as the occurrence of 'Jesus creepers' in wing 2D will take an exponential dive. The poor woman probably has scoliosis from looking at my feet for 6 years. I'm sure I'll be back now and then sans lab coat, covered toe shoes, and eye protection just to keep Hazel on her game. I also want to thank Vivian for all her help over the years from scheduling meetings for me, ordering all the materials I needed for my experiments, handling travel reimbursements, but most of all just asking me how I am doing form time to time and actually listening.

And finally a thank you to my friends outside of work, who have provided many a night to escape the pressures of graduate school. Proper decorum prohibits my saying anything further, but I can say thanks for the memories, the concerts and festivals, and the things I never thought I'd see but can only be described as Atlanta nightlife.

And that's all I got to say, 'bout that.

TABLE OF CONTENTS

	Page
ACKNOWLEDGEMENTS	iv
LIST OF TABLES	xv
LIST OF FIGURES	xvi
LIST OF SYMBOLS AND ABBREVIATIONS	xviii
SUMMARY	xxi
CHAPTERS	
1 CHAPTER 1: SPECIFIC AIMS	1
Introduction	1
Specific Aim I	4
Specific Aim II	4
Specific Aim III	5
Significance	6
2 CHAPTER 2: LITERATURE REVIEW	7
Bone Structure and Function	7
Bone Function	7
Types of Bones	7
Cortical and Trabecular Bone	8
Bone Extracellular Matrix	9
Bone Cells and Bone Remodeling	10
Bone Development and Maturation	13
Bone Fracture and Non-healing Defects	14
Bone Fracture and Healing Response	14

Non-healing Bone Defects and Clinical Implications 15
Cell Based Tissue Engineering Strategies for Bone Regeneration 16
Premise of Tissue Engineering 16
Scaffolds and Biomaterials for Bone Tissue Engineering 17
Growth Factors for Bone Tissue Engineering 22
Stem Cell Sources for Bone Tissue Engineering 24
Bone Marrow Mesenchymal Stem Cells for Bone Tissue Engineering 26
Adipose Derived Stem Cells for Bone Tissue Engineering 27
Summary 30
3 CHAPTER 3: RESVERATROL AS A PHARMACOLOGICAL AGENT TO INCREASE THE OSTEOGENIC POTENTIAL OF ADIPOSE DERIVED STEM CELLS 31
Abstract 31
Introduction 32
Methods 35
Cell Isolation and Culture 35
Measurement of Osteogenic Differentiation Markers 36
PCL/Collagen 3-D Scaffold Preparation 37
Treatment Regimen Effect on rADSC and hADSC Osteogenic Differentiation 38
Cell Distribution and Seeding Efficiency in the 3-D Environment 38
Micro-CT Imaging 39
Dose Dependent Resveratrol Pre-treatment of rADSCs and hADSCs 39

Concurrent Resveratrol and BMP-2 Treatment of rADSCs 40
Fluorescent Imaging and Histological Evaluation 40
Surface Characterization and SEM Imaging 41
Statistical Analysis 41
Results 42
Resveratrol Treatment Effect on Osteogenic Markers for rADSCs in 2-D 42
Effect of Treatment Regimen on rADSC 3-D Mineralization 42
hADSC Cell Distribution and Seeding Efficiency on PCL/Collagen Scaffolds 45
Resveratrol Pre-treatment and Continuous Treatment on hADSC Mineralization 45
Dose Dependent Effect of Resveratrol on hADSC and rADSC Osteogenic Differentiation 49
hADSC and rADSC Mean Density of Mineralized Matrix 52
Histological Analysis of Mineralized Matrix of hADSC and rADSC Constructs 52
Surface Examination of hADSC and rADSC Constructs 55
SEM Imaging 55
TGA Analysis 55
XPS Analysis 57
Concurrent Resveratrol and BMP-2 Treatment of rADSCs 59
Discussion 63
Summary 66

4 CHAPTER 4: EVALUATION OF SYNTHETIC AND NATURALLY BASED HYDROGELS AS AN INJECTABLE CELL DELIVERY VEHICLE FOR BONE TISSUE ENGINEERING 67

Abstract 67

Introduction 68

Methods 71

Isolation of GFP ADSCs and BMMSCs 71

PEG Formulation and RGD Incorporation 72

PCL Nanofiber Mesh Tube Formation 72

Molded and Injected PEG Hydrogel Preparation 73

Alginate Hydrogel Preparation 74

Cell Viability and Histomorphometric Analysis 74

Alginate Digestion and DNA Quantification 75

Wet Weight Alginate Degradation Calculation 76

Subcutaneous Ectopic Mineralization Model 76

Micro-CT Imaging for Mineralized Tissue 76

Histological Analysis and GFP Immunohistochemistry 79

Statistical Analysis 79

Results 80

Cell Viability in Molded and Injected PEG Hydrogels 80

In vivo Ectopic Mineralization in PEG Hydrogels 82

Cell Viability in Alginate Hydrogels 83

Degradation Kinetics of Irradiated and Oxidized-Irradiated Alginate Hydrogels *In vitro* 89

Subcutaneous Ectopic Mineralization in Alginate Hydrogels 89

Histological Analysis of Harvested Alginate Hydrogels 91
Discussion 95
Summary 98
5 CHAPTER 5: EFFECT OF DELIVERY TIME ON THE REGENERATION OF BONE IN A NON-HELAING SEGMENTAL BONE DEFECT 99
Abstract 99
Introduction 100
Methods 103
GFP BMMSC Isolation 103
Alginate Hydrogel Formation 103
PCL Nanofiber Mesh Tube Formation 104
Surgical Procedures 105
Faxitron Radiograph Imaging 108
Micro-CT Imaging 108
Histological Analysis 108
Statistical Analysis 109
Results 109
Empty Defect Characterization 109
Percutaneous Delivery of Hydrogels to Segmental Bone Defect 115
Immediate versus Delayed Bone Formation with 2nd Procedure 119
Histological Analysis 126
Discussion 130
Summary 133

6 CHAPTER 6: SUMMARY AND IMPLICATIONS 134

Synopsis 134

Specific Aim I 135

Resveratrol Treatment of Rat ADSCs 135

Resveratrol Treatment of Human ADSCs 136

Comparison of rADSC and hADSC Mineralized Matrix 136

Concurrent Treatment of Resveratrol and BMP-2 137

Implications 137

Specific Aim II 138

In vitro Cell Viability in PEG Hydrogels 138

PEG Hydrogels as a Cell Delivery Vehicle for Bone Tissue Engineering 138

In vitro Cell Viability in Alginate Hydrogels 139

Degradation Kinetics of Irradiated and Oxidized-Irradiated Alginate Hydrogels 139

Alginate Hydrogels as a Cell Delivery Vehicle for Bone Tissue Engineering 140

Implications 140

Specific Aim III 141

Characterization of Empty Defects 141

Percutaneous Delivery of Injectable Alginate Hydrogels 142

Immediate versus Delayed Bone Formation with 2nd Procedure 143

Histological Analysis of Bone Formation and Implanted Cell Presence 144

Implications 145

Conclusions 146

7 CHAPTER 7: FUTURE DIRECTIONS 147

Role of Cells 147

Role of the Cell Carrier 148

Role of Timing of Delivery 150

Mimicking a Clinical Situation 151

APPENDIX A: Motivation for Adopting Hydrogels as a Cell Delivery Vehicle 152

APPENDIX B: Stability of GFP Signal in ADSCs and BMMSCs 154

APPENDIX C: Modified Fixation Plate Drawings to Allow Percutaneous Delivery of Hydrogels 155

REFERENCES 156

LIST OF TABLES

Page

Table 4.1: PEG Based Groups Tested for *In vivo* Ectopic Mineralization 77

Table 4.2: Alginate Based Groups Tested for *In vivo* Ectopic Mineralization 78

Table 5.1: Groups for Percutaneous Delivery of Hydrogel 106

Table 5.2: Groups for 2nd Procedure Delivery of Hydrogel 107

LIST OF FIGURES

	Page
Figure 2.1: Mechanical Properties of Common Bone Scaffolds	18
Figure 2.2: The Mesengenic Process	26
Figure 3.1: Resveratrol Effect on rADSC Osteogenic Markers in 2-D	43
Figure 3.2: Cell Distribution and Seeding Efficiency of rADSCs on PCL	44
Figure 3.3: Treatment Regimen of Resveratrol Treated rADSCs in 3-D	46
Figure 3.4: Cell Distribution and Seeding Efficiency of hADSCs on PCL	47
Figure 3.5: Treatment Regimen of Resveratrol Treated hADSCs in 3-D	48
Figure 3.6: Resveratrol hADSC Dose Dependency in 3-D	50
Figure 3.7: Resveratrol rADSC Dose Dependency in 3-D	51
Figure 3.8: Mean Density of rADSC and hADSC 3-D Mineralization	53
Figure 3.9: Histological Analysis of rADSC and hADSC 3-D Mineralization	54
Figure 3.10: SEM Analysis of rADSC and hADSC Mineralized Matrix	56
Figure 3.11: TGA and XPS Analysis of 3-D Mineralized Matrix	58
Figure 3.12: Concurrent Treatment of Resveratrol and BMP-2 2-D Results	60
Figure 3.13: Concurrent Treatment of Resveratrol and BMP-2 3-D Results	61
Figure 3.14: Histological Analysis of Concurrent Treatment in 3-D Culture	62
Figure 4.1: ADSC Viability in PEG Hydrogels *In vitro*	81
Figure 4.2: BMMSC Viability in PEG Hydrogels *In vitro*	82
Figure 4.3: *In vivo* Ectopic Mineralization in PEG Hydrogels	84
Figure 4.4: Histological Analysis of *In vivo* Bone Formation in PEG Hydrogels	85
Figure 4.5: *In vitro* Cell Viability in Alginate Hydrogels	86
Figure 4.6: Quantification of Live Cells *In vitro*	87

Figure 4.7: DNA Levels in Alginate Hydrogels *In vitro* 88

Figure 4.8: Degradation Kinetics of Alginate Hydrogels 90

Figure 4.9: ADSC *In vivo* Ectopic Mineralization in Alginate Hydrogels 92

Figure 4.10: BMMSC *In vivo* Ectopic Mineralization in Alginate Hydrogels 93

Figure 4.11: Histological Analysis of Explanted Alginate Hydrogels 94

Figure 5.1: Micro-CT Bone End Characterization 110

Figure 5.2: Day 3 Empty Defect Characterization 112

Figure 5.3: Day 7 Empty Defect Characterization 113

Figure 5.4: Day 14 Empty Defect Characterization 114

Figure 5.5: Cell Loaded Percutaneous Delivery Bone Formation 116

Figure 5.6: Cell Free Percutaneous Delivery Bone Formation 117

Figure 5.7: Carrier Free Percutaneous Delivery Bone Formation 118

Figure 5.8: Delayed Percutaneous Delivery Bone Formation 120

Figure 5.9: 2nd Procedure 4 week *In vivo* Bone Formation 122

Figure 5.10: 2nd Procedure 8 week *In vivo* Bone Formation 123

Figure 5.11: 2nd Procedure 12 week *In vivo* Bone Formation 124

Figure 5.12: Mean Density of Newly Formed Bone 125

Figure 5.13: H&E Staining of Newly Formed Bone 127

Figure 5.14: Safranin-O Staining of Newly Formed Bone 128

Figure 5.15: Immunohistochemistry for Implanted Cells 129

Figure A.1: Micro-CT Reconstruction of PCL/Collagen *In vivo* Bone Formation 152

Figure A.2: Presence of GFP Cells on Mesh in Segmental Defect 153

Figure B.1: Fluorescence of GFP ADSCs and BMMSCs Over Multiple Passages 154

Figure C.1: Drawings of Modified Internal Fixation Plate 155

LIST OF ABBREVIATIONS

ADSC	Adipose Derived Stem Cell
BMMSC	Bone Marrow Mesenchymal Stem Cell
MSC	Mesenchymal Stem Cell
Sirt1	Silent Mating Type Information Regulation 2 Homolog 1
PPAR-γ	Peroxisome Proliferator-Activated Receptor Gamma
Runx-2	Runt-related transcription factor-2 (also known as Cbfa-1)
ECM	Extra Cellular Matrix
2-D	Two Dimensional
3-D	Three Dimensional
PCL	Poly (ε – caprolactone)
BMP-2	Bone Morphogenetic Protein 2
Micro-CT	Micro Computed Tomography
PEG	Poly-ethylene Glycol
GFP	Green Fluorescent Protein
BMPs	Bone Morphogenetic Proteins
RANKL	Receptor Activator of Nuclear Factor Kappa-B Ligand
β-TCP	Beta-Tricalcium Phosphate
PGA	Poly-glycolic Acid
PLA	Poly-lactic Acid
TGF-β	Transforming Growth Factor-Beta
ESC	Embryonic Stem Cell
iPSCs	Induced Pluripotent Stem Cell
PLGA	Poly-(Lactic-co-Glycolic) Acid

CD(#)	Cluster of Differentiation (Number)
RGD	Arginine-Glycine-Aspartic Acid
rADSCs	Rat Adipose Derived Stem Cells
hADSCs	Human Adipose Derived Stem Cells
SEM	Scanning Electron Microscopy
XPS	X-ray Photoelectron Spectroscopy
TGA	Thermogravimetric Analysis
PBS	Phosphate Buffered Saline
ALP	Alkaline Phosphatase
OCN	Osteocalcin
GM	Growth Media
OM	Osteogenic Media
OPG	Osteoprotegerin
FBS	Fetal Bovine Serum
ANOVA	Analysis of Variance
resADSC	Resveratrol Treated Adipose Derived Stem Cells
w/v	Weight to Volume
HBSS	Hank's Balanced Salt Solution
PEGDA	Poly-ethylene Glycol Diacrylate
PEG-SVA	Poly-ethylene Glycol Succinimidyl Valerate
TEMED	Tetramethylethylenediamine
APS	Ammonium Peroxidisulfate
α-MEM	Minimum Essential Medium-Alpha
RSA	Rat Serum Albumin
RNU	Rowett Nude

iPEG	Injected Poly-ethylene Glycol
mPEG	Molded Poly-ethylene Glycol
Acell	Acellular
CF	Carrier Free
NBF	Neutral Buffered Formalin
DAPI	4',6-Diamidino-2-Phenylindole, Dihydrochloride
H&E	Hematoxylin and Eosin
PNCs	Polymorphonuclear Cells

SUMMARY

Repair of large bone defects remains a clinical challenge for orthopedic surgeons. Current treatment strategies such as autograft and allograft are limited by the amount of available tissue in the case of the former, and failure of revascularization effecting engraftment in the case of the latter. Tissue engineering offers an alternative approach to this challenging clinical problem. The general principle of tissue engineering for bone regeneration prescribes delivery of osteoinductive factors to induce an endogenous response within the host to repair a defect that will not normally heal. One such tissue engineering approach is cell based therapy, and this is attractive in the cases of patients with a lack of endogenous osteoprogenitors cells due to volumetric loss of tissue/ageing.

Stem cell therapy has emerged as a possible alternative to current treatment modalities, however many challenges to clinical translation remain. Central to these challenges for bone tissue engineering are lingering questions of which cells to use and how to effectively deliver those cells. The goal of this thesis was to elucidate more effective ways to enhance bone repair utilizing adult stem cells. First, we investigated adipose derived stem cells (ADSCs) as a viable cell source for bone tissue engineering. Upon isolation, adipose derived stem cells are a heterogeneous population of multipotent cells predisposed to adipogenic differentiation. We developed an enrichment protocol that demonstrated the osteogenic potential of ADSCs can be enhanced in a dose dependent manner with resveratrol, which had been demonstrated to up-regulate Runx-2 expression. This enrichment strategy produced an effective method to enhance the osteogenic potential of ADSCs while avoiding cell sorting and gene therapy techniques, thus bypassing the use of xenogenic factors to obtain an enriched source of

osteoprogenitor cells. This protocol was also used to investigate differences between human and rat ADSCs and demonstrated that rat ADSCs have a higher osteogenic potential than human ADSCs *in vitro*.

The second major thrust of this thesis was to develop an injectable hydrogel system to facilitate bone formation *in vivo*. Both a synthetic and a naturally based polymer system were investigated, the results of which demonstrated that the naturally based alginate hydrogel was a more effective vehicle for both cell viability *in vitro* and bone formation *in vivo*. Our results also demonstrated that despite the ability to increase the osteogenic potential of ADSCs *in vitro* with resveratrol treatment, this was insufficient to induce bone formation *in vivo*. However, the inclusion of bone marrow mesenchymal stem cells (BMMSCs) in BMP-2 functionalized alginate hydrogels resulted in significantly greater mineralization than acellular hydrogels. Finally, the effect of timing of delivery of therapeutics to a non-healing segmental bone defect in the femur was investigated. We hypothesized that delivery of biologics after the initial inflammation response caused by injury to the host tissue would result in greater regeneration of tissue in terms of newly formed bone. Contrary to our initial hypothesis, these experiments demonstrated that delayed implantation of therapeutics has a detrimental effect on the overall healing response. It was, however, demonstrated that the inclusion of BMMSCs results in greater bone volume regenerated in the defect site over acellular hydrogels.

In conclusion, this work has rigorously investigated the use of adipose derived stem cells for bone tissue engineering, and further produced an injectable hydrogel system for stem cell based bone tissue engineering. This work also demonstrated that the

inclusion of adult stem cells, specifically BMMSCs, can enhance the regeneration response in a non-healing bone defect model relative to acellular hydrogels.

CHAPTER 1: SPECIFIC AIMS

INTRODUCTION

Current treatment modalities for management of large bone defects are limited and often ineffective. Presently, the clinical gold standard for treatment of large segmental bone defects is autologous bone grafting. This procedure, however, is severely constrained by a limited supply of available graft material, insufficient structural properties, and significant donor site morbidity (Bauer and Muschler 2000, Nandi, Roy et al. 2010). An alternative treatment is processed bone allografts. Again, this treatment possesses significant limitations, including an unacceptably high rate of post-implantation failure, largely attributable to the inability of the graft tissue to fully revascularize and remodel (Wheeler and Enneking 2005, Nandi, Roy et al. 2010). Stem cell therapy has emerged as an attractive alternative to current treatment modalities. Bone marrow mesenchymal stem cells (BMMSCs) are often employed as the cell source for bone tissue engineering applications; however, adipose derived stem cells (ADSCs) have also been shown to be osteogenic and offer the advantage of greater abundance than bone marrow mesenchymal stem cells. The literature however suggests that the osteogenic potential of adipose derived stem cells may be inferior to bone marrow mesenchymal stem cells (Niemeyer, Fechner et al. 2010). Thus a method to increase the osteogenic differentiation potential of the cells from adipose tissue may translate into increased bone formation when applied to a bone defect.

Gene therapy via viral transfection is a widely studied technique for controlling cell behavior, but has several drawbacks in the terms of clinical translation (Li and Huang

2000). A pharmacological approach would provide a simpler method to promote differentiation along a given lineage. Reports have shown that resveratrol is able to modulate both osteogenesis and adipogenesis (Backesjo, Li et al. 2006, Costa, Rohden et al. 2011). The mechanism of action has been shown to be stimulation of the Sirt1 pathway, which simultaneously promotes osteogenic differentiation and inhibits adipogenic differentiation. Thus, adipogenesis is down-regulated in the presence of resveratrol by inhibition of peroxisome proliferator-activated receptor gamma (PPAR-γ), a key player in the control of adipocyte differentiation (Maroni, Brini et al. 2012). Furthermore, reports have shown that resveratrol treatment on mouse mesenchymal stem cells (MSCs) promoted osteogenic differentiation due to up-regulation of the Sirt1 pathway which ultimately leads to increased Runt-related transcription factor 2 (Runx-2) expression stimulating osteogenic differentiation (Backesjo, Li et al. 2006). These data demonstrate that resveratrol is a good candidate to promote osteogenic differentiation while simultaneously inhibiting adipogenesis in ADSCs, thereby increasing the utility of ADSCs for bone tissue engineering purposes.

Along with promotion of differentiation down a specific pathway, another criterion for cell based tissue engineering is a viable method of cell delivery. We have shown that a majority of the cells initially implanted into a defect site lacking vascularity die within the first 72 hours post implantation (Appendix A). As such, positive therapeutic outcomes for cell incorporation are difficult to obtain. Hydrogels offer a potential avenue to increase the effectiveness of cell delivery and have advantages in several key areas specific for cell based tissue engineering. First, hydrogels are able to facilitate cell adhesion via peptide incorporation. As stem cells are adherent cells,

mimicking of the natural extracellular matrix (ECM) is vital to proper function of cells. Lack of adhesive peptides can cause stem cells to undergo anoikis leading to cell apoptosis. Second, many groups have demonstrated that cell delivery also requires growth factor co-delivery to promote differentiation of the implanted cells (Awad, Quinn Wickham et al. 2004, Huang, Kaigler et al. 2004, Simmons, Alsberg et al. 2004). Encapsulation of growth factors into hydrogels has shown to be effective in inducing new tissue formation (Phelps, Landazuri et al. , Boerckel, Kolambkar et al. 2011, Kolambkar, Boerckel et al. 2011, Kolambkar, Dupont et al. 2011). Hydrogels are able to serve as a barrier to the initial host inflammatory response, but eventually permit host cell invasion and vascularization to regenerate a functional tissue. Finally, hydrogels may allow for the system to be injectable. An injectable system would allow for the generation of larger pores facilitating mass transport, which may in turn increase cell viability. Moreover, an injectable system would allow for delivery of stem cells at a delayed time point post injury creation. This would avoid implanting the therapeutic during the initial inflammatory response, which may lead to greater implanted cell viability and an increase in active growth factor presentation to endogenous progenitor cells.

The *overall objective* of this thesis was to evaluate the potential of adult stem cell sources to treat a critically sized non healing bone defect in the femur of the rat utilizing injectable, biologically functionalized hydrogels. The *central hypothesis* was that inclusion of adult stem cells would lead to a greater bone regeneration response than acellular counterparts. The objective of this thesis was evaluated via the following Specific Aims:

SPECIFIC AIM I

Evaluate pharmacological enrichment of rat and human adipose derived stem cells to promote osteogenic differentiation in vitro. The objective of this aim was to develop an enrichment protocol using resveratrol to increase the osteogenic differentiation of ADSCs *in vitro*. The *working hypothesis* was that pharmacological treatment of adipose derived stem cells with resveratrol would promote greater mineralized matrix production than that observed in untreated cells. This was tested both in two dimensions (2-D) standard culture on tissue culture plastic and a three dimensional (3-D) differentiation system using a polymer scaffold consisting of poly (ε – caprolactone) (PCL) and collagen type I. Rat and human ADSCs pretreated with varying concentrations of resveratrol in 3-D culture were assessed for mineralized tissue formation via micro computed tomography (micro-CT) imaging over a 12 week time course. Finally, we tested concurrent treatment of resveratrol and bone morphogenetic protein-2 (BMP-2) in both the 2-D and 3-D differentiation systems. The outcomes of this Specific Aim are discussed in Chapter 3.

SPECIFIC AIM II

Evaluate synthetic and naturally based hydrogels as an injectable cell delivery system in terms of cell viability and subcutaneous osteogenic differentiation. The objective of this aim was to evaluate the use of poly-ethylene glycol (PEG) and alginate hydrogels to serve as an injectable hydrogel for bone tissue engineering. The *working hypothesis* was that extrusion of the hydrogel via injection would facilitate greater cell viability *in vitro* than traditionally mold cast hydrogels, ultimately leading to greater

ectopic mineralization *in vivo* with the incorporation of BMP-2 when applied to a subcutaneous mineralization model. The hypothesis was first tested using PEG hydrogels and a histomorphometric analysis of green fluorescent protein (GFP) expressing ADSCs and BMMSCs *in vitro*. The amount of GFP expressing cells and the amount of dead cells was quantified after 14 days in culture. We next tested the PEG system for *in vivo* mineralization with adult stem cell and BMP-2 co-delivery and found limited mineralized tissue due to lack of resorption of the PEG hydrogel. Therefore irradiated and oxidized irradiated alginate hydrogels were then tested as cell delivery vehicles. Cell viability was assessed over a 14 day time course using a histomorphometric analysis and confirmed via DNA content. *In vivo* ectopic mineralization was then evaluated in a subcutaneous implant model, with the presence of implanted cells assessed after 8 weeks. The outcomes of this Specific Aim are discussed in Chapter 4.

SPECIFIC AIM III

Determine the effect of timing of therapeutic delivery on the bone regeneration process in a non-healing bone defect model. The objective of this aim was to determine whether delaying the time a therapeutic is delivered to a bone defect has an effect on the amount of tissue regenerated in a critically sized femoral defect. The *working hypothesis* was that delaying the implantation time from the creation of the defect would lead to greater mineralized tissue volume by avoiding the initial host inflammation response. To evaluate this hypothesis, we first evaluated the host tissue invasion into empty defects over a 14 day time course to assess the amount of tissue and types of cells present in the defect site. Next, we attempted to deliver both acellular and cell loaded BMP-2

functionalized alginate hydrogels percutaneously into the segmental defect both at the time of the creation of the defect and 14 days following the creation of the defect. Inaccurate delivery and lack of bone volume resulted in a follow up study where a second minor surgery was performed allowing the defect site to be visible to the surgeon. Constructs were implanted immediately and 7 days after the creation of the defect. The results of this Specific Aim are discussed in Chapter 5.

SIGNIFICANCE

This thesis presents a *significant* contribution to the field of bone tissue engineering utilizing adult stem cell based therapeutics. The effectiveness of adult stem cells from both adipose tissue and bone marrow were assessed in multiple types of hydrogels for bone tissue engineering, and further, the effect of timing of delivery of therapeutics was evaluated. This work produced the following outcomes: 1) Produced a pharmacological enrichment strategy to increase the *in vitro* differentiation potential of adipose derived stem cells from both human and rat donors, 2) Demonstrated differences in PEG and alginate based hydrogels in terms of maintaining cell viability *in vitro* and bone formation *in vivo*, 3) Demonstrated that delaying the delivery of therapeutics inhibits the amount of regenerated bone tissue in a non-healing bone model, 4) Demonstrated that inclusion of BMMSCs causes a significant increase in the amount of mineralized tissue over comparable acellular hydrogels.

CHAPTER 2: LITERATURE REVIEW

BONE STRUCTURE AND FUNCTION

Bone Function

Bone is one of the primary organs constituting the musculoskeletal system. It serves a variety of physiological functions in vertebrates including: ion homeostasis, particularly in the case of calcium which is important for cell function and signaling; production of hematopoietic precursors in the medullary cavities, giving rise to red and white blood cells; and the site of mesenchymal precursors, which mobilize and repair injured sites in the musculoskeletal system (Marks and Popoff 1988, Cohen 2006). In addition to its physiological functions, bone also serves as the major structural component of the musculoskeletal system. Bone serves as the protecting structure for the vital organs including the heart and lungs, as well as the central nervous system comprising the brain and spinal cord. Bone also is the anchoring point for muscles, tendons, and cartilage, giving rise to articulating joints providing movement (Baron 1993). Injury or loss of bone tissue inhibits the ability for joints to articulate properly, motivating the need for treatment options for bone repair.

Types of Bones

Bone has a hierarchal organization consisting of the whole bone level, the apparent bone level, and the ultrastructural level (Weiner 1998). On the whole bone level, there are five major categories of bones generally based on their shape or function and categorized as flat, short, long, irregular, and sesamoid bones (Buckwalter 1996). Flat bones reside primarily in the cranium, but are also found in the shoulder region and

pelvic region. These bones generally have the characteristic of a small thickness relative to their length and width. Short bones are characterized by having relatively the same dimensions in all directions, and are primarily found in the hands and feet. Irregular bones are normally categorized as such due their specialized geometry suited for their specific function. Examples of irregular bones are vertebrae, the mandible, and the sacrum in the pelvic region. Similarly, sesamoid bones are categorized as such due to their function. Sesamoid bones are embedded in tendon tissue and serve as structural component to maintain constant moments across joints. The typical example of a sesamoid bone is the patella in the knee. Finally, long bones are defined as bones with a length greater than their width. These are the primary bones comprising the limbs of most vertebrates. Long bones are defined by three regions: the diaphysis, metaphysis, and epiphysis, and are delineated relative to their position of the epiphyseal plate. The epiphyseal plate, or growth plate, is an area of cartilaginous tissue responsible for elongation of long bones during growth and development. The epiphyses are located on both ends of bone and are covered by cartilage to facilitate articulation of joints. The metaphysis is the area of bone between the epiphysis and diaphysis and the region that contains the epiphyseal plate. The diaphysis is the center of long bones and contains the medullary cavity which is the site of hematopoiesis and progenitor cells (Alberts 2002).

Cortical and Trabecular Bone

On the apparent bone level, the primary classifications of structures of bone are cortical bone and trabecular bone (Buckwalter 1996, Buckwalter 1996). Cortical bone is described as a highly compact tissue with limited porosity. Cortical bone is comprised of a series of neighboring osteons. Osteons in turn are comprised of lamellae with

interconnecting canaliculi. At the center of the osteon is a channel where osteocytes (described below) reside called lacunae. Lacunae form the Haversian system that allows signaling between osteons and ultimately allows bone to remodel to stimuli. These Haversian canals are generally oriented parallel to the diaphyseal surface (Alberts 2002). The highly compact nature of cortical bone gives rise to its primary function to bear mechanical loads. Conversely, trabecular bone, or cancellous bone, is often termed 'spongy' and is noted by its rod and plate structure, giving rise to large interconnected cavities. Trabecular bone is found in the ends of long bones and inside the medullary cavity of long bones. It is highly vascularized, and is characterized by its relative lack of density compared to cortical bone. The vascularity along with its high surface area due to its plate and rod structure results in trabecular bone being primarily responsible for metabolic and physiologic functions such as ion homeostasis (Marks and Popoff 1988).

Bone Extracellular Matrix

The ultra-structural level of bone consists of the bone extracellular matrix (ECM) and the cellular components of bone. The extracellular matrix of bone consists of two phases: an organic component containing connective proteins, proteoglycans, and growth factors; and an inorganic component comprised of mineral ions mainly in the form of hydroxyapatite. The primary component of the organic phase of bone is collagen I comprising 90% of the organic phase of bone ECM (Buckwalter 1996). Collagen I has a triple helical structure giving it high tensile strength (Patino, Neiders et al. 2002). The inorganic component consists predominately of hydroxyapatite and is noted by its high content of calcium and phosphate groups, which serve as reservoirs for ion homeostasis. The collagen network forms nucleation sites for mineral precipitation, giving rise to both

the tensile and compressive properties of bone tissue. The other components of the bone ECM include growth factors responsible for maintenance of bone structure. One of the most studied family of growth factors are the bone morphogenetic proteins (BMPs) described further below (Wozney 2002). This family of growth factors has been shown to be highly potent in their osteoinductivity and induce bone formation in both orthotopic and ectopic sites. As such, this family of growth factors has been shown to be effective in the generation of alternative strategies to regenerate bone (Luca, Rougemont et al. , Knippenberg, Helder et al. 2006, Usas, Ho et al. 2009).

Bone Cells and Bone Remodeling

Depositing and remodeling the bone extra cellular matrix are the cells residing in bone tissue. The main cell types in bone are osteoblasts, osteoclasts, and osteocytes (Marks and Popoff 1988). Osteoblasts are derived from osteoprogenitor cells located in the periosteum and the medullary cavity. These osteoprogenitor cells will begin to differentiate when presented with growth factors such as BMPs. As the osteoprogenitors mature into osteoblasts, they will begin to express and secrete proteins such as collagen type I, osteocalcin, and alkaline phosphatase. Once mature, osteoblasts are located on the surface of bone and when depositing new tissue, or osteoid, align themselves with other osteoblasts to generate a newly formed surface. Osteoid is an unmineralized matrix of organic components, mainly collagen type I, but also contains chondroitin sulfate and osteocalcin (Bono and Einhorn 2005). This large secretion of proteins is made possible by the osteoblasts having a large endoplasmic reticulum and Golgi apparatus, which are two of the primary organelles responsible for protein export out of the cell. As the

osteoid matures, it serves as the nucleation point of the inorganic mineral phase of bone matrix.

As osteoblasts deposit matrix, some become entrapped in the mineralized tissue. Once entrapped, these cells will slow down their metabolic function and reduce their protein machinery to become osteocytes. Osteocytes are located in the lacunae described previously at the apparent bone level. Osteocytes are responsible for the maintenance of the bone tissue and provide paracrine signaling to active osteoblasts, thus regulating bone formation. This is achieved through canaliculi which are cytoplasmic protrusions from the cell body that allow nutrient and waste transport via gap junctions (Marks and Popoff 1988). When an osteocyte undergoes apoptosis, it will release receptor activator of nuclear factor kappa-B ligand, or RANKL, which will recruit osteoclasts to the bone tissue around the osteocyte to promote bone resorption (Kurata, Heino et al. 2006). As a controller of osteoblast and osteoclast activity, the osteocyte is the critical cell in regulating bone turnover.

The final primary cell type found in bone is the osteoclast. As mentioned above, the osteoclast is responsible for resorption of bone. Osteoclasts are derived from monocytes and upon stimulation from RANKL will undergo fusion of precursor cells to form a multinucleated cell (Suda, Kobayashi et al. 2001). The mechanism of resorption is through proton pumps, which create an acidic environment on the bone surface to break down the organic phase of the bone matrix (Suda, Kobayashi et al. 2001). To increase the surface area of the resorption site, the osteocyte has a folded membrane on the bone surface to form the resorptive pit (Howships lacuna).

In adults, bone is remodeled and turned over at a rate of approximately 10% per year (Fernández-Tresguerres Hernández-Gil 2006). The signaling between osteoblasts, osteocytes, and osteoclasts is responsible for this bone turnover. Once osteocytes undergo apoptosis, they will activate osteoclast precursors to differentiate into mature osteoclasts and resorb the bone in the area. Once resorbed, osteoblasts will hone to the site and deposit new osteoid thus creating new bone tissue (Feng and McDonald 2011). This system of bone turnover is carefully balanced, and tipping of the scales to favor resorption or deposition results in poor quality bone with diminished mechanical properties. The two most prominent pathological conditions that arise from an imbalance in bone remodeling are osteoporosis, where resorption outpaces deposition, and osteopetrosis, where deposition outpaces resorption (Feng and McDonald 2011).

In addition to the primary cell types discussed previously, there are also populations of cells specific to certain areas of bone. As mentioned previously, the medullary cavity is the site of hematopoiesis and contains precursors for blood cells. In addition to hematopoietic precursors, the medullary cavity also contains mesenchymal stem cells which are osteoprogenitor cells that differentiate to become osteoblasts. Another site for osteoprogenitor cells is the periosteum (Kojimoto, Yasui et al. 1988, Iwasaki, Nakahara et al. 1995, Perka, Schultz et al. 2000). The periosteum is a membrane of connective tissue that covers the outside of cortical bone in long bones, and contains its own population of osteoprogenitor cells that have been shown to be important in fracture repair. Cells isolated from the periosteum have been incorporated into biomaterials to heal calvarial defects in rodents (Breitbart, Grande et al. 1998). A similar membrane is found coating the inside of the medullary cavity and is termed the

endosteum, however this is not normally used a as a source for progenitor cells given its location and difficulty in obtaining cells from that tissue.

BONE DEVELOPMENT AND MATURATION

There are two primary mechanisms for bone development: endochondral and intramembranous ossification (Ornitz and Marie 2002, Mackie, Ahmed et al. 2008). Endochondral ossification is denoted by the presence of a cartilaginous matrix prior to mineralization. This type of ossification occurs in long bones and short bones. In this method of development, progenitor cells condense and differentiate into chondrocytes, which then produce a cartilage template of the developing tissue. Mineralization and growth of the tissue occurs in the 'bone collar', which is a region rich in proliferating chondrocytes (Mackie, Ahmed et al. 2008). The proliferating chondrocytes continue to form new matrix, until cells begin to degrade the chondrogenic material. The cells will then undergo apoptosis, leaving a void where blood vessels will invade. Once vascularized, osteoprogenitors are recruited to the cartilaginous matrix and begin to differentiate into osteoblasts and mineralize the cartilaginous template. This process continues outwards from the bone collar thus elongating the developing tissue. Eventually two areas of growth develop that continue this process and become the epiphyseal plates as described previously. In the developing tissue the deposited osteoid is unorganized and is characterized as woven bone. Over time, the deposited osteoid tissue is continually remodeled into a compact structure and becomes lamellar bone.

Intramembranous ossification occurs without the development of a cartilaginous template. In this method of ossification, there are regions of dense progenitor cells that form multiple ossification centers. These ossification centers grow out radially via bone

spicules and fuse together to form a mature bone structure. The bone spicules follow areas that are vascularized, and osteoblasts are recruited via the vasculature and continue to deposit more osteoid. The most common bones that undergo intramembranous ossification are the flat bones in the cranium, the scapula in the shoulder, and the bones that form the pelvic region.

Despite the two mechanisms of bone development there are common traits between both types. First, both types rely on progenitor cells to differentiate into osteoblasts and deposit osteoid. Second, both tissues rely on vascular invasion to recruit osteoprogenitor cells to form bone matrix. In common fracture healing, it is an interplay of both methods that results in fully regenerated bone tissue (González, Cerrolaza et al. 2009).

BONE FRACTURE AND NON-HEALING DEFECTS

Bone Fracture and Healing Response

The cellular components of bone engender its ability to heal itself in cases of fracture. In the case of a simple fracture, there are three phases that typically occur in order to form a fully healed tissue. These phases are the reactive phase, the reparative phase, and the remodeling phase (Einhorn 1998). The reactive phase begins with bleeding occurring at the fracture site. The pooling of blood eventually forms a fibrin clot defined as a hematoma. The development of the hematoma is followed by cellular death and the formation of granular tissue. With the formation of the granular tissue, the reparative phase initiates. Cells from the neighboring periosteum begin to form a cartilaginous matrix on both ends of the fracture. Once these ends meet, a fracture callus

is formed. Recruitment of osteoprogenitor cells from the medullary cavity and the periosteum occurs, and the cells begin to undergo endochondral ossification forming a woven bone structure. During this stage of repair, much of the bone resembles trabecular bone in terms of mineral content and composition. The final phase of fracture healing is the remodeling phase. This phase is noted by osteoclast resorption of the newly formed trabecular bone, followed by the deposition of compact cortical bone by osteoblasts ultimately resulting in functionally regenerated tissue.

Non-healing Bone Defects and Clinical Implications

In severe cases of fracture the normal repair process is unable to restore function. This is also true in the case of volumetric bone loss, such as in the case of traumatic injury or in tumor resection. Loss of progenitor cells or damage to surrounding tissue can limit the endogenous healing capacity of the patient, resulting in nonunion of the defect (Bruder and Fox 1999). There is a large clinical for effective treatment strategies for such defects. According to the United States Bone and Joint Decade, musculoskeletal conditions are the most commonly reported health conditions in U.S. citizens, occurring in roughly 48% of the population. Beyond the associated physical afflictions is the enormous financial burden - $849 billion in 2004 alone (Decade 2009). In addition, these injuries are of specific concern to the United States Armed Forces as trauma to the extremities remains the most prevalent combat injury of troops admitted to the theater (Baer 2004). Bone grafting procedures have an annual occurrence greater than 500,000 resulting in a cost greater than $2.5 billion in the United States alone (Laurencin, Khan et al. 2006).

Current clinical treatment modalities for management of large bone defects are limited and often ineffective. The clinical gold standard for treatment of large segmental bone defects is autologous bone grafting. This procedure, however, is severely constrained by a limited supply of available graft material, insufficient structural properties, and significant donor site morbidity. Another often-employed treatment is allograft tissue obtained from cadavers. Again, this treatment possesses significant limitations, including an unacceptably high rate of post-implantation failure. This is largely attributable to an inability of the graft tissue to fully revascularize and remodel leading to decreased integration of the graft to the host tissue. There are also additional concerns with regard to disease transmission and immune rejection with allograft use (Nandi, Roy et al. 2010). The occurrence of refracture varies depending on the size of the graft, but has been reported to be as high as 25-35% (Sorger, Hornicek et al. 2001). As such, alternative treatment strategies are warranted to address the shortcomings of current treatment modalities.

CELL BASED TISSUE ENGINEERING STRATEGIES FOR BONE REGENERATION

Premise of Tissue Engineering

Tissue engineering offers an attractive alternative to current clinical treatment methods as stem cells, scaffolds, and growth factors can be delivered to augment the host response to heal critically sized defects. In particular, cell based therapies have the potential to alleviate the use of grafts from host tissue and allogeneic tissue sources (Bruder and Fox 1999, Kimelman, Pelled et al. 2007). Ideally, a cell-based tissue

engineering approach would incorporate the use of an autologous cell source and a biodegradable scaffold to allow for graft incorporation and eventual tissue remodeling *in vivo*. Autologous cell therapies eliminate the risk of graft rejection due to an immune response. However, a body of work suggests that stem cells from the mesenchymal lineages have immune privilege such that they could be transplanted allogeneically without rejection (Dominici, Le Blanc et al. 2006, Niemeyer, Kornacker et al. 2007). Incorporation of a resorbable scaffold would provide short-term retention of therapeutics while facilitating host tissue invasion in the long term. In addition, co-delivery with growth factors would promote recruitment of host cells to a defect site as well as promote the differentiation of implanted cells. These tools allow for a large assortment of potential strategies to address many developmental diseases and traumatic injuries.

Scaffolds and Biomaterials for Bone Tissue Engineering

Scaffolds for bone tissue engineering can be used for mechanical support, a delivery vehicle for biologics, a conduit for host tissue invasion and remodeling, or any combination thereof. As such scaffolds should be biocompatible and allow for cellular attachment and differentiation. In terms of mechanics, the scaffold can be tailored to its environment and this may dictate the choice of material used. When the goal is to have completely remodeled host tissue, the scaffold must be biodegradable to allow the host tissue to remodel and degrade the scaffold. This can be achieved by incorporating a protease sensitive component that will allow the material to be enzymatically degraded by cells in the defect. Conversely, the ultimate outcome of using a rigid scaffold may be to integrate with the surrounding tissue while allowing new tissue growth inside the scaffold. This is generally the approach when using ceramics as the scaffold. The

advantage of using rigid scaffolds like ceramic is that the material properties are similar to native cortical bone, thus allowing mechanics that will not stress shield the native tissue and cause further resorption (Byrne, Lacroix et al. 2007). Common material categories for bone tissue engineering and their relative properties to native bone tissue are displayed below (Amini, Laurencin et al. 2012).

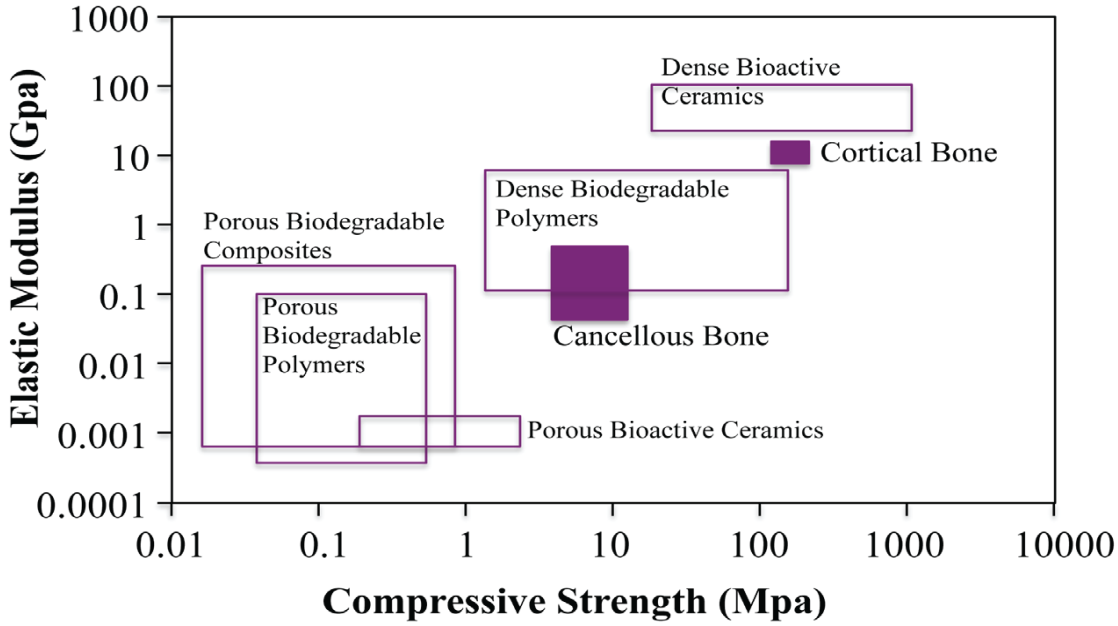

Figure 2.1 - Mechanical properties of common scaffold choices for bone tissue engineering relative to the mechanical properties of trabecular and cortical bone.

Ceramic materials for bone tissue engineering are generated by soaking a sponge with a high mineral content solution such as hydroxyapatite. The sponge is then sintered at an extremely high temperature to make a glass-like material (Teixeira, Fernandes et al. 2010). To increase cellular attachment, many ceramics will be coated with proteins such as collagen I or fibronectin. An alternative to a largely ceramic scaffold is the inclusion of ceramic particles into a polymer scaffold. Beta tri-calcium phosphate (β-TCP) particles can be used in conjunction with a polymer to create a composite material mimicking the organic and inorganic extracellular matrix of bone. Cao created a

composite material of poly-glycolic acid (PGA) and β-TCP particles and implanted them into a femoral defect. By varying the ratio of PGA to β-TCP the amount of bone formed in the defect was modulated and shown to obtain a mineral density comparable to native hydroxyapatite (Cao and Kuboyama 2010).

Polymer scaffolds for bone tissue engineering can be made of both natural and synthetic materials. The most commonly employed natural polymers employed are collagen, fibrin, alginate, and silk fibroin (Luca, Rougemont et al. , Karageorgiou, Meinel et al. 2004, Yang, Bhatnagar et al. 2004, Fini, Motta et al. 2005, Murphy, Haugh et al. 2010, Boerckel, Kolambkar et al. 2011, Kolambkar, Boerckel et al. 2011, Kolambkar, Dupont et al. 2011, Sheyn, Kallai et al. 2011). With the high collagen content found in bone, collagen is an ideal candidate for bone tissue engineering. However, natural polymers, including collagen scaffolds, have weak mechanical properties, and thus necessitate the use of fixation devices in the early healing process. Cross-linking can help increase the mechanical strength of the polymer, but still is not adequate to bear loads immediately. Collagen scaffolds are currently used clinically with BMP-2 for spinal fusion treatment. In this procedure, a collagen sponge is soaked in BMP and placed between vertebrae to fuse them together and recapitulate mechanical integrity. Fibrin is able to be cross-linked to form a gel that can then be injected into defect sites and has demonstrated promotion of bone formation. Fibrin has also been shown to be highly favorable for cell viability, and cell mobility and attachment can be controlled by varying the fibrin concentration (Hale, Goodrich et al. 2012). Sheyn showed that incorporation of genetically modified adult stem cells into a fibrin gel is able to double the amount of bone volume formed in a vertebral bone defect model (Sheyn, Kallai et al.

2011). Alginate has similarly been shown to be an effective natural polymer for bone tissue engineering, and is discussed in more detail below.

Synthetic materials offer high plasticity in formulation, ultimately allowing the material to be tailored to a specific application. Synthetic polymers can be functionalized by including cell adhesion peptides, growth factors, and protease sensitive motifs to facilitate enzymatic degradation. There are a wide range of synthetic polymers available for tissue engineering, including poly-lactic acid (PLA), PGA, poly-(ε -caprolactone) (PCL), and poly-ethylene glycol (PEG) (Majola, Vainionpää et al. 1991, Breitbart, Grande et al. 1999, Burdick 2002, Hu, Zhang et al. 2003, Richardson, Curran et al. 2006, Dupont, Sharma et al. 2010). A potential deficit of using synthetic polymers such as PLGA and PGA based materials is that when degraded the products formed can be acidic thereby inducing an inflammatory response or having a detrimental effect on the function of the cells surrounding the material.

An effective strategy for using both natural and synthetic polymers for cell-based therapies is to form a hydrogel. A hydrogel is characterized by its high water content with insoluble polymers that form a cross-linked network to retain a shape. The high water content gives the hydrogels mechanical properties similar to soft tissue and in itself is insufficient to maintain the mechanical loads in a segmental defect (Park 2011). As such, a fixation device needs to be employed in conjunction with the hydrogel for load bearing sites. Our lab uses a guided bone regeneration technique that utilizes an internal fixation plate, a membrane, and a hydrogel to treat femoral segmental defects. Guided bone regeneration is defined as the use of a membrane along the periosteal surface to control the area of bone formation (Kim, Jeong et al. 2005, Dahlin, Johansson et al.

2012). The membrane employed in our segmental defect model is a PCL nanofiber mesh tube and this is placed between the ends of the defect site. Once placed, a hydrogel with osteoinductive factors is injected filling the void. Two hydrogels that will be utilized in this thesis are both a synthetic PEG hydrogel and a naturally based alginate hydrogel using the guided bone regeneration technique.

While PEG has been used as a cell and drug delivery vehicle in various tissue engineering applications, its use in bone regeneration has been limited. PEG has no cell attachment domains, necessitating cell attachment motifs be tethered to the PEG backbone. A report has shown that functionalizing PEG with an RGD cell attachment peptide sequence, which mimics the cell adhesion site of fibronectin, leads to cell spreading in the hydrogel (Salinas and Anseth 2008). Comparison of soluble and tethered fibronectin sequences showed that tethering of a fibronectin sequence leads to greater cell spreading than soluble, as the cell is able to adhere to the PEG network versus a freely floating RGD sequence. Further, the amount of cell spreading was determined to be dose dependent as greater cellular area was observed with increased RGD concentration. Cellular attachment and spreading allows for cellular deposition of extra cellular matrix molecules, thus leading to the possibility of mineralized matrix within the hydrogel. This has been demonstrated by Burdick in which mineralized matrix was found on PEG hydrogels with tethered RGD (Burdick 2002). Betz demonstrated that modification of the PEG hydrogel to generate larger pore sizes resulted in increased osteoblastic gene activity and protein production by human mesenchymal stem cells (Betz, Yeatts et al. 2010). These studies demonstrate that PEG hydrogels are a viable osteoinductive delivery vehicle for bone tissue engineering applications.

Alginate has been shown to be an effective delivery vehicle for biologics for bone tissue engineering. Alginate is a polysaccharide derived from seaweed, and its properties can be manipulated by varying the concentration of its two primary components, mannuronic and guluronic acid. The backbone of alginate is highly negative which allows multiple chains to be cross-linked with a divalent cation such as calcium or magnesium. Further, the backbone chain of alginate can be manipulated with cell attachment motifs to facilitate cell adhesion and alter cell differentiation (Rowley and Mooney 2002, Comisar, Kazmers et al. 2007). Kolambkar demonstrated that when paired with BMP-2, alginate hydrogels are able to heal critically sized femoral segmental defects in rodents (Kolambkar, Boerckel et al. 2011, Kolambkar, Dupont et al. 2011). Mechanical testing showed that the regenerated bone tissue was not significantly different from intact bone, demonstrating successful functional repair of the defect. Boerckel followed this study with a dose dependency study demonstrating that the dose of BMP-2 affects the amount of regenerated tissue. Further, it was demonstrated in the rat that the alginate and BMP-2 system resulted in greater bone formation than the clinically used collagen sponge with an equal amount of BMP-2 (Boerckel, Kolambkar et al. 2011).

Growth Factors for Bone Tissue Engineering

As many of the previously highlighted studies show, growth factor delivery is a central tenant for bone tissue engineering. The most common growth factors employed for bone tissue engineering are bone morphogenetic proteins, or BMPs. BMPs were first discovered in 1965 when Marshall Urist implanted decellularized and decalcified allografts into intramuscular pockets and noted their osteoinductivity (Urist 1965). The

proteins responsible were later identified and termed bone morphogenetic proteins. Over 20 BMPs have been identified and have been shown to be instrumental in guiding tissue development throughout the body. The two most commonly used for bone tissue engineering are BMP-2 and BMP-7, belong to the transforming growth factor beta (TGF-β) superfamily (Wozney 2002). BMPs react with specific receptors on the cell surface initiating a signaling cascade. Dimerization of type I and type II TGF-β receptors activate the SMAD signaling cascade. SMADS are a family of intracellular proteins that specifically transduce extracellular signals from TGF-β to the nucleus initiating transcription of osteogenic genes. Runx-2 is one of these up-regulated genes, and is known as the master control switch for osteogenic differentiation. As such, this makes BMP delivery an effective tool for bone tissue engineering.

As mentioned previously, BMP-2 and BMP-7 have been widely studied as osteoinductive factors and are currently used clinically for spinal fusion. Both proteins have been approved by the FDA for use in grafting procedures. The use of BMPs has grown from .69% of all fusions in 2002 to 24.89% of all fusions in 2006 (Cahill, Chi et al. 2009). Medtronic developed its Infuse product which takes a bovine type I collagen sponge and soaks it in a high concentration of BMP-2 solution before being implanted. Stryker Biotech developed both a putty and an implant based on BMP-7 incorporation for lumbar spine fusion as well as nonunion of bone fractures. Despite their rising use in the clinic, reports have shown that supraphysiologic doses of BMP can result in poor bone quality (Razzouk and Sarkis 2011, Yu, Schindeler et al. 2012). The potency of BMPs results in large volumes of bone forming quickly and the tissue may not be able to be maintained long term. In addition, BMP use can cause adverse complications in wound

healing and have also been associated with a surge in costs of fusion procedures (Razzouk and Sarkis 2011). As such, reducing the amount of BMP needed for restoration of a defect may lead to better clinical outcomes. One such way to reduce BMP dosage is via stem cell co-delivery.

Stem Cell Sources for Bone Tissue Engineering

Stem cells are classified by their potency, or ability to differentiate into multiple tissues. The fertilized egg represents a totipotent cell and gives rise to all of the tissues found in an organism. Pluripotent cells have the capability of differentiation into any of the three germ layers: the endoderm which forms the inner linings of organs such as the lungs and gastrointestinal tract; the mesoderm which forms the muscle, bone, and blood cells; and the ectoderm which forms the nervous system and epidermal tissues such as skin. The most commonly referenced pluripotent cells are embryonic stem cells (ESCs) derived from the inner cell mass of a blastocyst. The harvesting of the inner cell mass results in the destruction of the embryo, giving rise to ethical concerns about their use for tissue engineering (de Wert and Mummery 2003). Moreover, the generation of osteogenic cells from ESCs is difficult as the ESC population is often heterogeneous and possibly tumorogenic (Arnhold, Klein et al. 2004, Amini, Laurencin et al. 2012). A recent report, however, did suggest that BMP-2 laden scaffolds seeded with ESCs are capable of forming mineralized tissue *in vivo* (Levi, Hyun et al. 2012). That study further demonstrated that fibroblasts genetically modified to a pluripotent state are also able to form bone *in vivo* under the direction of BMP-2. These cells are termed induced pluripotent stem cells (iPS cells). A report also suggests that a cocktail of proteins may also be able to induce the pluripotent state, thereby alleviating the need for viral vectors

(Zhang, Li et al. 2012). Both these techniques are in their nascent stage and their evaluation for *in vivo* bone regeneration is limited. Fetal stem cells have also been investigated as a potential cell source for bone tissue engineering. Stem cells from amniotic fluid have been demonstrated to be osteogenic both *in vitro* and *in vivo* (Peister, Porter et al. 2008, Peister, Deutsch et al. 2009, Dupont, Sharma et al. 2010, Peister, Woodruff et al. 2011). Reports suggest these cells retain much of the potency of embryonic stem cells, in that they are able to undergo differentiation into the three germ layers (De Coppi, Callegari et al. 2007, Tsai, Hwang et al. 2007, Hauser, De Fazio et al. 2010, Antonucci, Stuppia et al. 2011, Park, Shim et al. 2011).

The next level in terms of potency is multipotent cells. These cells are more generally referred to as adult stem cells as these progenitor cells can be isolated from fully developed adult tissue. For bone tissue engineering, the most common adult stem cells used are mesenchymal stem cells. These cells are found in multiple tissues including bone marrow, adipose tissue, and muscle tissue. The cells from all three sources exhibit similar cell surface marker profiles despite their origin from different tissues, and are capable of differentiating down the mesodermal lineages of bone, muscle, cartilage, and fat (Deasy, Jankowski et al. 2001, Kern, Eichler et al. 2006). A similar source of mesenchymal stem cells is umbilical cord blood (Erices, Conget et al. 2000, Xu, Meng et al. 2010). Mekala was able to demonstrate that cells derived from umbilical cord are able to undergo osteogenic differentiation on PLGA scaffolds, implicating the possibility of their use for bone tissue engineering (Mekala, Baadhe et al. 2013). The two cell types studied in this thesis are bone marrow mesenchymal stem cells and adipose derived mesenchymal stem cells.

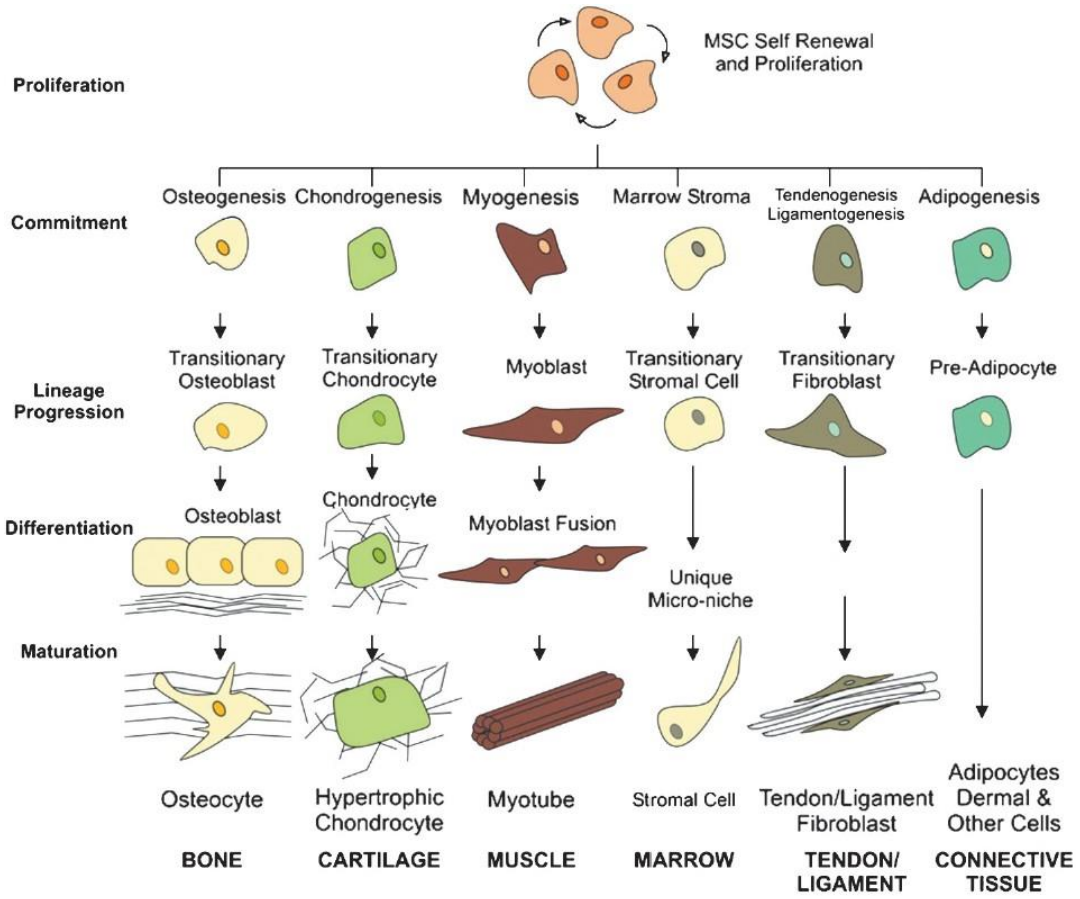

Figure 2.2 – Mesenchymal stem cells and differentiation pathways for multiple adult tissues of the mesoderm (Firth and Yuan 2012).

Bone Marrow Mesenchymal Stem Cells for Bone Tissue Engineering

Cells from bone marrow were first shown to be multipotent in 1924 when Alexander Maximow developed his theory that all blood cells come from one precursor hematopoietic cell (Maximow 1924). Similarly, another population of cells found in the bone marrow was shown to be multipotent. Bone marrow mesenchymal stem cells were first identified by Friedenstein and Owen (Friedenstein, Piatetzky et al. 1966, Owen 1988). Arnold Caplan developed a method to isolate and expand BMMSCs while maintaining their potency (Caplan 1991). It was later demonstrated that MSCs from bone marrow were capable of differentiating into multiple phenotypes including bone,

cartilage, muscle, adipose, and connective tissues if given certain cocktails of cytokines to induce their commitment to a lineage (Pittenger, Mackay et al. 1999). It has also been shown that differentiation of BMMSCs can be controlled by the stiffness of the substrate they are cultured on, demonstrating a mechanical component to the differentiation pathway (Pek, Wan et al. 2010). Given their location in the bone marrow, BMMSCs seem an intuitive choice for a cellular component in a tissue engineering approach to bone regeneration. When incorporated into biomaterials, it has been shown that inclusion of BMMSCs can increase the rate and overall volume of bone tissue formed (Amini, Laurencin et al. 2012). BMMSCs have been utilized in a variety of bone defect models including segmental defects, calvarial defects, and fusion of spinal vertebrae (Kadiyala, Jaiswal et al. 1997, Shang, Wang et al. 2001, Blum, Barry et al. 2003, Hasharoni, Zilberman et al. 2005, Gan, Dai et al. 2008, Dupont, Sharma et al. 2010).

Adipose Derived Mesenchymal Stem Cells for Bone Tissue Engineering

Adipose derived mesenchymal stem cells were first identified in 2001 as a potential cell source for tissue engineering applications. Zuk, et al. first characterized the cells and noted that the cells were able to undergo differentiation down the mesodermal lineages including the adipogenic, osteogenic, myogenic, and chondrogenic lineages. Compared to the more widely studied mesenchymal stem cells from bone marrow, adipose derived stem cells showed a similar cell marker expression profile staining positive for the cell markers CD29, CD44, CD71, CD90, CD105; while negative for endothelial cell markers CD34 and CD45 (Zuk, Zhu et al. 2002). When cultured in osteogenic media, ADSCs showed up-regulation of the osteogenic genes Runx-2, osteocalcin, and had increased alkaline phosphatase activity compared to cells in control

media in standard 2-D culture. Knippenberg later showed that ADSCs cultured in the presence of BMP- 2 and BMP- 7 showed greater osteogenic differentiation in terms of alkaline phosphatase activity compared to controls in standard 2-D culture (Knippenberg, Helder et al. 2006). Moreover, a major advantage of ADSCs is their relative abundance as well as their faster proliferation rate compared to bone marrow MSCs. This allows for more rapid expansion to obtain clinically relevant cell numbers (Cowan, Shi et al. 2004, Nakagami, Morishita et al. 2006). These reports demonstrate that ADSCs have similar osteogenic potential to MSCs with the added advantage of being highly abundant, compared to other cell sources for bone tissue engineering applications.

Bone tissue engineering research utilizing adipose derived stem cells has been limited with mixed outcomes and mainly focused on non-challenging orthopedic defects in animal models e.g. calvarial defects as well as defects in the radius and tibia (Rhee, Ji et al. , Cowan, Shi et al. 2004, Niemeyer, Fechner et al. 2010). Cowan showed that juvenile and adult ADSCs harvested from rats led to greater bone formation in a critically sized calvarial defect compared to untreated controls. Further, the deposited tissue had a greater radiopacity than uninjured bone suggesting robust mineralization. Niemeyer investigated the use of ADSCs in a tibial bone defect model. When undifferentiated ADSCs were implanted, little bone was formed and the ADSCs differentiated down the adipogenic lineage as evidenced histologically with the presence of lipid filled vacuoles in the defect site (Niemeyer, Fechner et al. 2010). However, a report in which adipose derived stem cells were infected with BMP-2 adenovirus showed complete healing of a radial defect in rabbits 12 weeks post-implantation (Wei Hao 2009). Hicok demonstrated human adipose derived stem cells produce osteoid *in vivo* when seeded onto a

hydroxyapatite tri-calcium phosphate scaffold and implanted subcutaneously into immune deficient mice (Hicok, Du Laney et al. 2004). Similarly, Park seeded ADSCs onto a poly(lactic)-glycolic acid (PLGA) scaffold and analyzed the regeneration in a tibia defect model. In order to achieve mineralization, the cells had to be cultured on the scaffold and differentiated prior to implantation (Park, Zhou et al. 2012). However pre-differentiation of ADSCs on the scaffold limits their proliferative capacity, and further obfuscates the role the cells play in the regeneration process as it is difficult to assess newly formed tissue post implantation. These reports demonstrate a critical criterion for the implantation of adipose derive stem cells for bone tissue engineering in that ADSCs require a degree of cell differentiation to control the behavior of the cells *in vivo*.

While pre-differentiation and gene therapy via viral transfection are widely studied techniques for controlling cell behavior, this has several drawbacks in the terms of clinical translation. A pharmacological approach would provide a simpler method to promote differentiation along a given lineage. Reports have shown that resveratrol is able to modulate both osteogenesis and adipogenesis. This appears to be caused by stimulating the Sirt1 pathway, which simultaneously promotes osteogenic differentiation and inhibits adipogenic differentiation (Backesjo, Li et al. 2006, Costa, Rohden et al. 2011, Tseng, Hou et al. 2011). Thus, adipogenesis is down-regulated in the presence of resveratrol by inhibition of PPAR-γ, a key player in the control of adipocyte differentiation. Further, Backesjo showed that resveratrol treatment on mouse MSCs promoted osteogenic differentiation due to up-regulation of the Sirt1 pathway (Backesjo, Li et al. 2006). The Sirt1 pathway ultimately leads to up-regulation of Runx-2 leading to osteogenic differentiation.

SUMMARY

Bone is a highly complex organ responsible for multiple physiologic functions. The cellular components of bone give it the ability to regenerate itself in the case of fracture. However, in catastrophic injuries or volumetric tissue loss, the regenerative capacity of bone may be insufficient for functional repair. Current grafting techniques such as autograft and allograft have their limitations and challenges. As such, tissue engineering has risen as a possible alternative for the treatment of these defects. By utilizing a scaffold or carrier along with growth factors and/or stem cells, new treatment strategies can be developed. In this thesis, we investigated a cell based tissue engineering approach by utilizing adult stem cells, specifically ADSCs and BMMSCs, to generate bone tissue in biologically active hydrogels.

CHAPTER 3: RESVERATROL AS A PHARMACOLOGICAL AGENT TO INCREASE THE OSTEOGNEIC DIFFERENTIATION OF ADIPOSE DERIVED STEM CELLS*

ABSTRACT

The goal of these studies was to investigate the effect of resveratrol treatment on the osteogenic potential of human and rat adipose derived stem cells both in a 2-D and 3-D culture environment. Adipose derived stem cells (ADSCs) have shown promise as a potential source of osteogenic progenitor cells. Resveratrol has been shown to inhibit adipogenic differentiation while simultaneously activating osteogenic differentiation. 2-D experiments with rat ADSCs identified 25 μM of resveratrol as an effective dose to increase the production of osteogenic genes. The effect of 25 μM resveratrol treatment was investigated in a pre-treatment and continuous treatment regimen in 3-D culture and demonstrated that pre-treatment was sufficient to increase the mineralized matrix production of rat ADSCs. We next sought to investigate whether this result was also observable with human ADSCs and found that the human cells did not respond to 25 μM

This chapter is adapted from the following publications:

Erdman, Christopher P. and Dosier, C. R., et al. "Effects of resveratrol on enrichment of adipose-derived stem cells and their differentiation to osteoblasts in two-and three-dimensional cultures." *Journal of Tissue Engineering and Regenerative Medicine* (2011).

Dosier, Christopher R., et al. "Resveratrol effect on osteogenic differentiation of rat and human adipose derived stem cells in a 3-D culture environment." *Journal of the Mechanical Behavior of Biomedical Materials* 11 (2012): 112-122.

resveratrol in a positive manner suggesting a species specific difference in resveratrol dosage. Therefore we next investigated multiple doses at or below 25 μM resveratrol for both rat and human ADSCs. We found that doses below 25 μM caused significantly more mineralization than 0 (untreated) and 25 μM treated cells in a 3-D culture environment. Furthermore, we observed species differences in the total amount of mineralized matrix, as well as the mean mineral density suggesting that the nature of mineralization of the extracellular matrix was different between species. Histological examination of the scaffolds showed that the human cell constructs remain highly cellular in nature with small pockets of mineralization; while rat cell constructs showed much larger and more mature mineralized nodules. Finally, we investigated concurrent treatment of resveratrol and BMP-2 in 2-D and 3-D. It was demonstrated that short-term exposure of BMP-2 had no added benefit in terms of mineralization. Taken together we demonstrate dose dependent differences in the mineralization response of human and rat ADSCs to resveratrol treatment, suggesting that *in vitro* pre-conditioning of 3D adipose-derived stem cell constructs may be an effective strategy to promote osteogenic differentiation prior to implantation.

INTRODUCTION

Adipose derived stem cells (ADSCs) were first identified in 2001 as a potential cell source for tissue engineering applications. Zuk, et al. first characterized the cells and noted that the cells were able to undergo differentiation down the mesodermal lineages including the adipogenic, osteogenic, myogenic, and chondrogenic lineages (Zuk, Zhu et al. 2001, Zuk, Zhu et al. 2002). Compared to the more widely studied mesenchymal stem

cells (MSCs) from bone marrow, adipose derived stem cells showed a similar cell marker expression profile, staining positive for the cell markers CD29, CD44, CD73, CD90, CD105; while negative for endothelial cell markers CD34 and CD45 (Gimble and Guilak 2003). When cultured in osteogenic media, ADSCs showed up-regulation of the osteogenic genes Cbfα-1 (Runx2), osteocalcin, and had increased alkaline phosphatase activity compared to cells in control media in standard 2-D culture (Hattori, Sato et al. 2004, Schaffler and Buchler 2007). Knippenberg later showed that ADSCs cultured in the presence of bone morphogenetic protein 2 and bone morphogenetic protein 7 showed greater osteogenic differentiation in terms of alkaline phosphatase activity compared to controls in standard 2-D culture (Knippenberg, Helder et al. 2006). Moreover, a major advantage of ADSCs is their relative abundance as well as their faster proliferation rate compared to bone marrow MSCs and this allows for more rapid expansion to obtain clinically relevant cell numbers compared to MSCs (Cowan, Shi et al. 2004, Fraser, Wulur et al. 2006, Nakagami, Morishita et al. 2006).

Bone tissue engineering research utilizing adipose derived stem cells has been limited with mixed outcomes and mainly focused on orthopedic defects in animal models, e.g. calvarial defects as well as defects in the radius and tibia (Niemeyer, Fechner et al. 2010, Rhee, Ji et al. 2010). Cowan showed that implantation of juvenile and adult ADSCs harvested from rats led to greater bone formation in a critically sized calvarial defect compared to untreated controls (Cowan, Shi et al. 2004). Niemeyer investigated the use of ADSCs in a tibial bone defect model. When undifferentiated ADSCs were implanted, little bone was formed and the ADSCs differentiated along the adipogenic lineage as evidenced histologically by the presence of lipid filled vacuoles in the defect

site (Niemeyer, Fechner et al. 2010). However, a recent report in which adipose derived stem cells were transduced with a BMP-2 plasmid-containing adenovirus showed complete healing of a radial defect in rabbits 12 weeks post-implantation (Wei Hao 2009). These conflicting reports nevertheless demonstrate a critical criterion for the implantation of adipose derive stem cells for bone tissue engineering in that they appear to require a degree of cell differentiation to direct the behavior of the cells *in vivo*.

While gene therapy via viral transduction is a widely studied technique for controlling cell behavior, this has several drawbacks in the terms of clinical translation. A pharmacological approach would provide a simpler method to promote differentiation along a given lineage. Reports have shown that resveratrol is able to modulate both osteogenesis and adipogenesis (Rayalam, Della-Fera et al. 2011). This appears to be caused by stimulating the Sirt1 pathway, which simultaneously promotes osteogenic differentiation and inhibits adipogenic differentiation. Thus, adipogenesis is down regulated in the presence of resveratrol by inhibition of PPAR-γ, a key player in the control of both osteogenic and adipogenic differentiation (Shockley, Lazarenko et al. 2009). Further, studies have shown that resveratrol treatment of mouse MSCs promoted osteogenic differentiation due to up-regulation of the Sirt1 pathway (Boissy, Andersen et al. 2005, Backesjo, Li et al. 2006, Costa, Rohden et al. 2011). These data demonstrate that resveratrol is a good candidate to promote osteogenic differentiation while simultaneously inhibiting adipogenesis in ADSCs and may therefore promote mineralization of ADSCs for bone tissue engineering purposes.

The goal of these studies was to investigate the effect of resveratrol treatment on the osteogenic potential of human and rat adipose derived stem cells both in a 2-D and 3-

D culture environment. Dose dependency experiments were performed with rat ADSCs to identify therapeutic doses of resveratrol. We next investigated treatment regimens in 3-D to determine the length of time need to induce a beneficial effect on osteogenic differentiation. We next sought to investigate whether this result was also observable with human ADSCs and found species differences in 3-D mineralization. Therefore we next investigated multiple doses at or below 25 μM resveratrol for both rat and human ADSCs in the 3-D culture environment. A histological evaluation of the scaffolds after mineralization was performed to investigate differences in the nature of mineral deposition in the extra cellular matrix. We analyzed the surface and chemical makeup of mineralized constructs using scanning electron microscopy (SEM), x-ray photoelectron spectroscopy (XPS), and thermogravimetric (TGA) analyses. Finally, we investigated concurrent treatment of resveratrol and BMP-2 in 2-D and 3-D for rat ADSCs.

METHODS

Cell Isolation and Culture

Rat ADSCs were isolated from inguinal fat pads, which are subcutaneous fat depots surrounding the thigh, were harvested from multiple 100-125g male Sprague-Dawley rats (Harlan, Indianapolis, IN) bilaterally according to a protocol approved by the Institutional Animal Care and Use Committee at Georgia Institute of Technology and the US Army Medical Research and Materiel Command Animal Care and Use Review Office. Briefly, the tissue was pooled and washed three times in Hank's balanced saline solution (HBSS), and digested in 0.25% trypsin for 30 minutes at 37˚C. The tissue was then cut into smaller pieces and digested in 9125 units of collagenase IA (Sigma, St.

Louis, MO) and 75 units of dispase (Gibco, Invitrogen, Carlsbad, CA) for three hours. The upper layer of adipocytes was removed, and the cell suspension was filtered through a 40µm cell strainer. The digestion was stopped with MSC growth media (GM) (Lonza, Basel, Switzerland), which contains fetal bovine serum, and the cells were collected by centrifugation. The cells were plated at 5,000 cells/cm^2 in T-75 flasks. Cultures were washed twice with phosphate buffered saline (PBS) and fed with GM at 24 and 48 hours after plating. Cell expansion was performed in which cells were grown to sub-confluence and then trypsinized and reseeded for 2 passages prior to being cryo-preserved.

Human ADSCs were isolated from adipose tissue obtained from an adolescent donor at the Children's Healthcare of Atlanta and cells were isolated and cultured as described above. The procuring and processing of the tissue was performed according to Georgia Institute of Technology Institute Review Board protocol H08244.

Passage 2 rADSCs and hADSCs were thawed and cultured in T75 flasks in GM (Lonza). At 80% confluence the cells were passaged and plated at 5000 cells/cm^2 in GM. Starting the following day, the ADSCs were then treated for 7 days with 0, 6.25, 12.5, and 25 µM resveratrol in GM. Media were changed every 48 hours.

Measurement of Osteogenic Differentiation Markers

Twenty-four hours prior to harvest, the media were replaced with fresh medium with and without resveratrol. At harvest the conditioned media were collected, and the cells were lysed with 0.05% Triton-X 100, 10 seconds of sonication, and one freeze-thaw cycle. Alkaline phosphatase (ALP) specific activity was measured in cell lysates as the release of p-nitrophenol from p-nitrophenylphosphate at pH 10.25. Protein levels were measured with a BCA protein assay kit (Pierce, Rockford, IL). Osteocalcin (OCN) levels

in the conditioned media were measured via the Human Osteocalcin Radioimmunoassay kit (Biomedical Technologies, Stoughton, MA). Osteoprotegerin (OPG) levels in the conditioned media were measured via the Osteoprotegerin ELISA (R&D Systems, Minneapolis, MN). Osteocalcin and osteoprotegerin assays were each run according to manufacturer's instructions and levels were normalized to DNA levels, quantified by fluorescent Picogreen labeling of double stranded DNA in the cell lysate (Invitrogen).

PCL/Collagen 3-D Scaffold Preparation

PCL scaffolds were prepared as described previously (Peister, Deutsch et al. 2009). Briefly, 100x100x9 mm sheets of medical grade poly ε-caprolactone (PCL, Osteopore International, Singapore) with 85% porosity were cut with a 5 mm diameter biopsy punch to yield a cylindrical scaffold. The scaffolds were then briefly treated with 5M sodium hydroxide to roughen the surface and facilitate cell attachment. Scaffolds were then washed three times with sterile water and sterilized overnight via 70% ethanol evaporation. Sterile PCL scaffolds were washed with excess sterile water three times and placed into a custom mold. Rat tail collagen type I (Trevigen, Gaithersburg, MD) was diluted with 0.05% acetic acid to 1.5 mg/mL, neutralized with 1M sodium bicarbonate, and aseptically pipetted into the mold to occlude the pores of the scaffold. The scaffold/collagen gel constructs were then placed in a -80°C freezer for 1 hour prior to being lyophilized overnight. Lyophilized scaffolds were placed in a sterile scaffold holder and into 24-well low-attachment cell culture plates (Corning, Lowell, MA) and stored until cell seeding.

Treatment Regimen Effect on rADSC and hADSC Osteogenic Differentiation

Cryo-preserved cells were thawed and plated for 24 hours. Cells were then trypsinized and plated at a density of 250 cells/cm^2 and cultured for one week in GM. One half of the cultures were treated with 25 µM resveratrol every two days. Cells were harvested, counted, and reconstituted at a density of 3 x 10^4 cells/µL. 100µL (3 x 10^6) of cells were then carefully pipetted onto the tops of the scaffold/collagen constructs and allowed to attach to the surface. After a 1-hour incubation, GM was added to the culture wells so that the cell-scaffold constructs were completely submerged in media. After 48 hours media were changed to osteogenic differentiation media consisting of α-MEM (Invitrogen) supplemented with 16% FBS (Atlanta Biologics, Lawrenceville, GA), 1% penicillin-streptomycin (Invitrogen), 50 µg/mL ascorbic acid 2-phosphate (Sigma), 50 ng/mL thyroxine (Sigma), 6 mM beta-glycerophosphate (Sigma), and 1 nM dexamethasone (Sigma). Cell/scaffold constructs on the continuous resveratrol treatment regimen were given osteogenic differentiation medium supplemented with 25µM resveratrol. Media were changed twice weekly during culture on the 3D scaffolds. Scaffolds were placed in a custom holder consisting of a plastic disk with four stainless steel pins, and cultured in a 24-well low-attachment cell culture plate. Cells were cultured dynamically on an orbital shaker (Stovall Life Scientific, Greensboro, NC) at a rate of 6.5 RPM in a 5 % CO_2 incubator.

Cell Distribution and Seeding Efficiency in 3D Environment

Cell/scaffold constructs were harvested 24 hours after seeding. Scaffolds were bisected. A live/dead assay was performed on one half with the LIVE-DEAD Viability/Cytotoxicity kit (Invitrogen). Qualitative distribution of the cells throughout

the scaffold was observed via fluorescent microscopy using a Zeiss Axio Observer (Göttingen, Germany) microscope at 4x magnification. Non-attached cells were collected from the media samples 24 hours after seeding and DNA quantified. The number of cells on the scaffold was determined using the Pico Green DNA assay (Invitrogen) together with a standard curve. Cell numbers were then normalized to the number of cells delivered.

Micro-CT Imaging

At 4, 8, and 12 weeks, cell scaffold constructs were aseptically removed from culture and placed in custom tubes for micro-CT scanning. Mineralized matrix in the cell/scaffold constructs was determined by using a VivaCT scanner (Scanco Medical, Brüttisellen, Switzerland) at 55 kVp, 109 mA, 1024 mu scaling, and a 200 ms integration time. The constructs were evaluated with a lower threshold of 80 with a filter width of 1.2 and a filter support of 1.0. The total volume of the mineralized matrix as well as the mean mineral density of the mineralized nodules was determined.

Dose Dependent Resveratrol Pre-treatment of rADSCs and hADSCs

Cryo-preserved cells were thawed and plated for 24 hours. Cells were then trypsinized and plated at a density of 250 cells/cm^2 and cultured for one week in GM, GM supplemented with 6.25 μM resveratrol, 12.5 μM resveratrol, or 25 μM resveratrol. Cells were grown for one passage and trypsinized at sub-confluence. Cells were then harvested and seeded onto PCL/collagen scaffolds as described in 2.3 and placed in osteogenic media after 48 hours and cultured on an orbital shaker. Micro-CT imaging was performed at 4, 8 and 12 weeks as described previously. At the end of 12 weeks, 3

scaffolds of each group were fixed in 10% neutral buffered formalin for 48 hours and then evaluated histologically. The remaining samples were used for fluorescent imaging.

Concurrent Resveratrol and BMP-2 Treatment of rADSCs

Cryo-preserved cells were thawed and plated for 24 hours. Cells were then trypsinized and plated at a density of 250 cells/cm^2 and cultured for one week in G or GM supplemented 12.5 μM resveratrol. Cells were grown for one passage and trypsinized at sub-confluence. Cells were then harvested and seeded either at 5000 cells/ cm^2 into tissue culture plastic for 2-D culture or onto PCL/collagen scaffolds for 3-D culture as described in 2.3 and placed in growth media supplemented with 500 ng of BMP-2 for 48 hours. Media was changed to osteogenic media and continuously cultured on an orbital shaker. 2-D samples were analyzed via von Kossa staining, DNA content, total calcium content and alkaline phosphatase activity after 14 days. Micro-CT analysis was performed at 4 and 8 weeks as described previously for the 3-D samples, and then processed for fluorescent histology as described previously.

Fluorescent Imaging and Histological Evaluation

Fluorescent imaging was performed on scaffolds following 24 hours of culture. Scaffolds were washed with PBS thrice and then sectioned longitudinally and stained with calcein and ethidium and imaged using a Zeiss Axio Observer (Göttingen, Germany) microscope at 4x magnification. Fixed samples were sectioned longitudinally and von Kossa staining for mineralized matrix was performed. Gross images of the cell/scaffold constructs were then taken using a digital camera.

Surface Characterization and SEM Imaging

The surface morphology of PCL, PCL/Col, PCL/Col-hADSCs, and PCL/Col-rADSCs was obtained by using a Hitachi S-3700 VP-scanning electron microscope (Hitachi high technologies America, Inc., USA) with an accelerating voltage of 15 kV. Elemental distribution of the substrates used in this study was analyzed by using the energy-dispersive x-ray spectroscopy (EDX) detector attached to the Hitachi S-3700N VP-SEM. In order to determine organic and inorganic contents of PCL, PCL/Col, PCL/Col-hADSCs, and PCL/Col-rADSCs, thermogravimetric analyses (TGA) were performed under nitrogen using a TA Instruments Q50 Thermogravimetric Analyzer (Delaware, USA). Substrates weighing approximately 10 – 30 mg were heated from 25 °C to 800 °C at a rate of 10 °C/minute and the weight loss percentage of each substrate is reported. The surface chemical composition and chemical mapping were carried out by using x-ray photoelectron spectroscopy (XPS; Thermo K-Alpha, Thermo Fisher Scientific Inc., MA, USA). The XPS analysis was performed under ultra-high vacuum (less than 10-9 Torr) with a monochromatic Al Kα X-ray source (hv = 1486.6 eV, 90° take-off angle). Thermo Advantage 4.43 software package (Thermo Fisher Scientific, Inc.) was used to evaluate the XPS spectra.

Statistical Analysis

Data were analyzed with a one-way ANOVA followed by a Tukey's post hoc analysis with a significance level of $p<0.05$. All groups had 6 independent samples per experiment unless otherwise noted.

RESULTS

Resveratrol Treatment Effect on Osteogenic Markers for rADSCs in 2-D

Resveratrol treatment for 7 days had no significant effect on DNA levels (Figure 3.1A). Alkaline phosphatase specific activity was increased in cells grown in osteogenic media (OM) compared to cells cultured in growth media (GM) (Figure 3.1B). Treatment with 25 µM resveratrol increased alkaline phosphatase-specific activity in both media. Similarly, OCN levels were higher in OM than in GM (Figure 4B). Osteocalcin levels were increased by resveratrol in both media, but at the lower concentration of 12.5 µM and with no further increase at the higher dose (Figure 3.1C). Osteoprotegerin (OPG) levels were reduced in cultures grown in OM compared to GM and resveratrol had no effect on this marker (Figure 3.1D).

Effect of Treatment Regimen on rADSC 3-D Mineralization

Both resveratrol treated and untreated cells readily attached to the PCL–collagen constructs by 24 hours, as seen on the live/dead images (Figure 3.2A). DNA quantification showed that resveratrol treatment had no significant effect on the seeding efficiency onto the PCL scaffolds (Figure 3.2B). After 4 weeks of dynamic cell culture in osteogenic medium, micro-CT imaging showed that resveratrol treated and untreated cells both produced mineralized matrix throughout the entirety of the scaffold (Figure 3.3A). Resveratrol-pretreated cells produced significantly higher mineralized matrix with an average 33% more mineralized matrix than untreated cells at 4 weeks. In addition, continuous treatment with resveratrol did not produce a more robust effect on mineralization (Figure 3.3B). The pre-treated group showed levels of mineralization

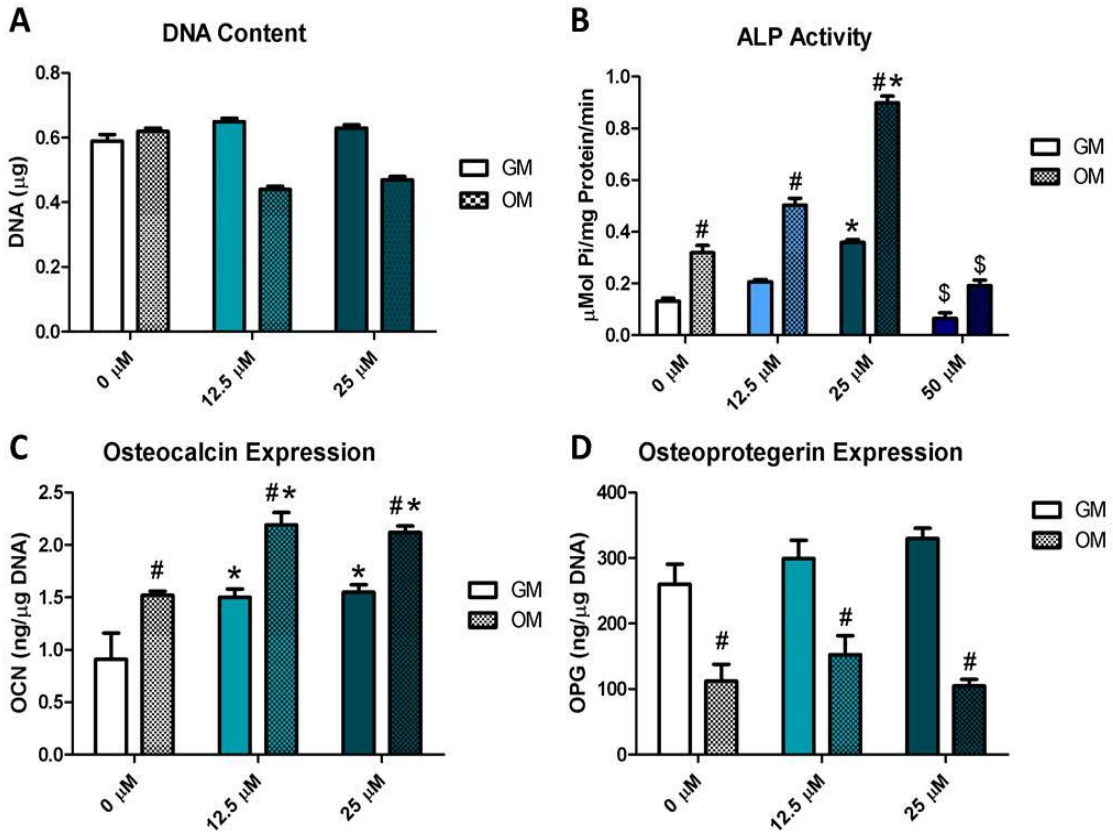

Figure 3.1. Effect of resveratrol on osteogenic biochemical markers. ADSCs were plated in 24-well plates and treated with 0, 12.5 and 25 µM resveratrol in GM and OM. After 7 days of treatment, DNA (A), alkaline phosphatase-specific activity (B), OCN levels (C), and OPG levels (D) were measured. Data represented are mean ± SEM of six independent samples; *$p<0.05$, Res vs 0mM; #$p<0.05$, OM vs GM.

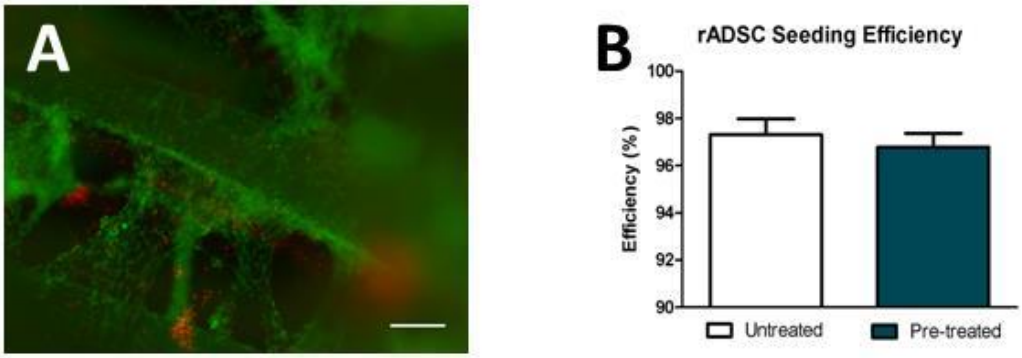

Figure 3.2. Live/Dead imaging demonstrating rADSC attachment to the scaffold as well as a cellular and collage network spanning the struts of the scaffold (A). Similar levels of seeding efficiency were seen in untreated and resveratrol treated ADSCs (B). Scale bar = 300 µm.

similar to that of the continuously treated group, suggesting that a 7 day pre-culture was sufficient to obtain the desired effect of early mineralization. After 8 weeks of culture, no significant differences in the treatment modalities were observed, although all groups continued to mineralize over time. This is most likely due to the amount of osteoprogenitors in the untreated cell group having sufficient time to catch up with the resveratrol-treated groups, resulting in equal amounts of mineralization. Results at week 12 were similar to those at week 8, albeit with increased mineralization in all groups from week 8 to week 12.

hADSC Cell Distribution and Seeding Efficiency on PCL/Collagen Scaffolds

Live/Dead imaging showed high cell attachment and viability for both groups. Cells were readily observable attached to the struts of the scaffold as well as forming cell/collagen networks that span in between the struts of the scaffold (Figure 3.4). This was confirmed by measuring the seeding efficiency via pico Green DNA assay. Cells that were pre-treated with 25 μM resveratrol had a seeding efficiency of 97.6±.4% while untreated cells had a 97.5±.9% of cells seeded.

Resveratrol Pre-treatment and Continuous Treatment on hADSC Mineralization

Human ADSCs readily produce mineral on the PCL/collagen scaffolds in the presence of osteogenic media as shown in Figure 3.5. At all time points, resveratrol pre-treatment (25 μM) resulted in significantly less mineralization than untreated cells. Continuous resveratrol treatment (osteogenic media + 25 μM resveratrol) further reduced mineralized matrix at all time points. It should be noted that at each successive time point there was a significant increase in mineralized matrix compared to the previous time point for each group respectively.

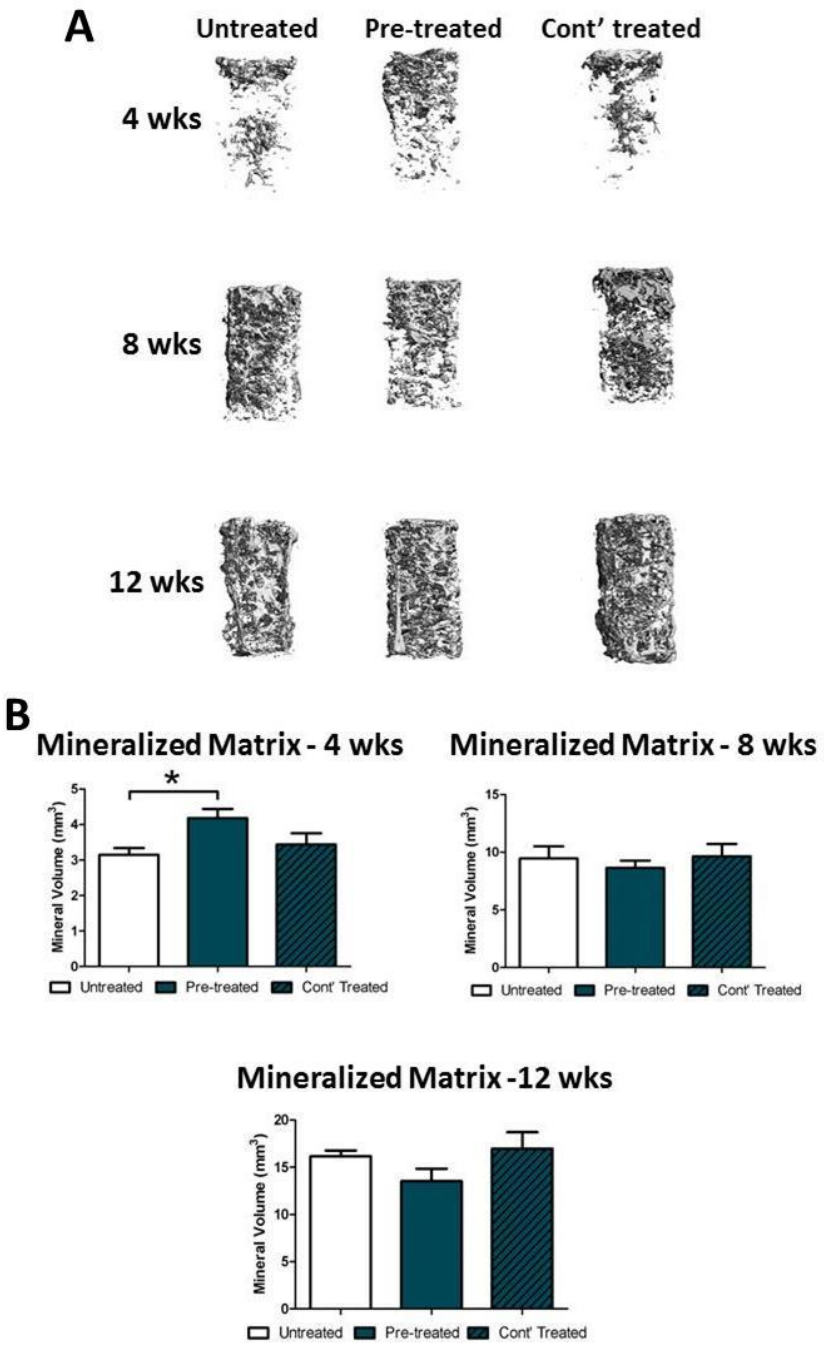

Figure 3.3. Micro-CT reconstructions of rADSC untreated, resveratrol pre-treated, and continuously resveratrol treated constructs over time (A). Quantification of mineralized matrix over time (B). *$p<0.05$ from untreated group.

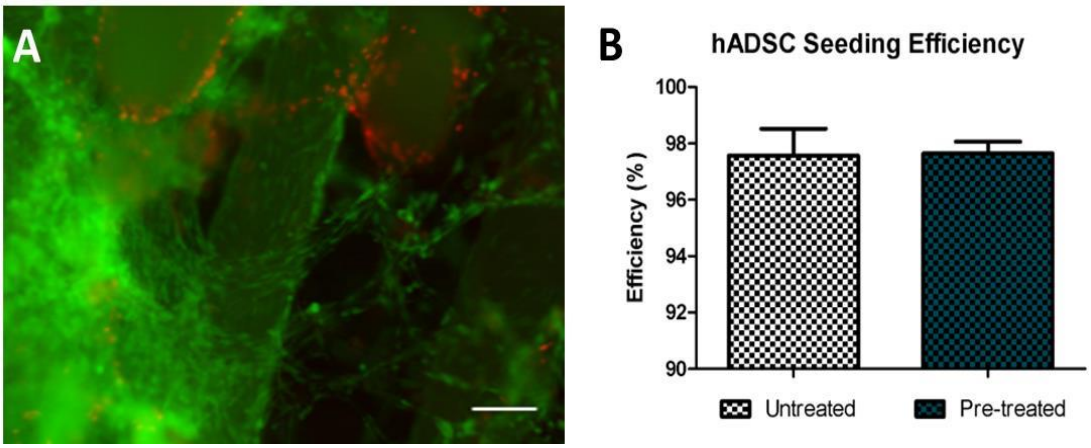

Figure 3.4. Live/Dead imaging demonstrating hADSC attachment to the scaffold as well as a cellular and collage network spanning the struts of the scaffold (A). Similar levels of seeding efficiency were seen in untreated and resveratrol treated ADSCs (B). Scale bar = 300 µm.

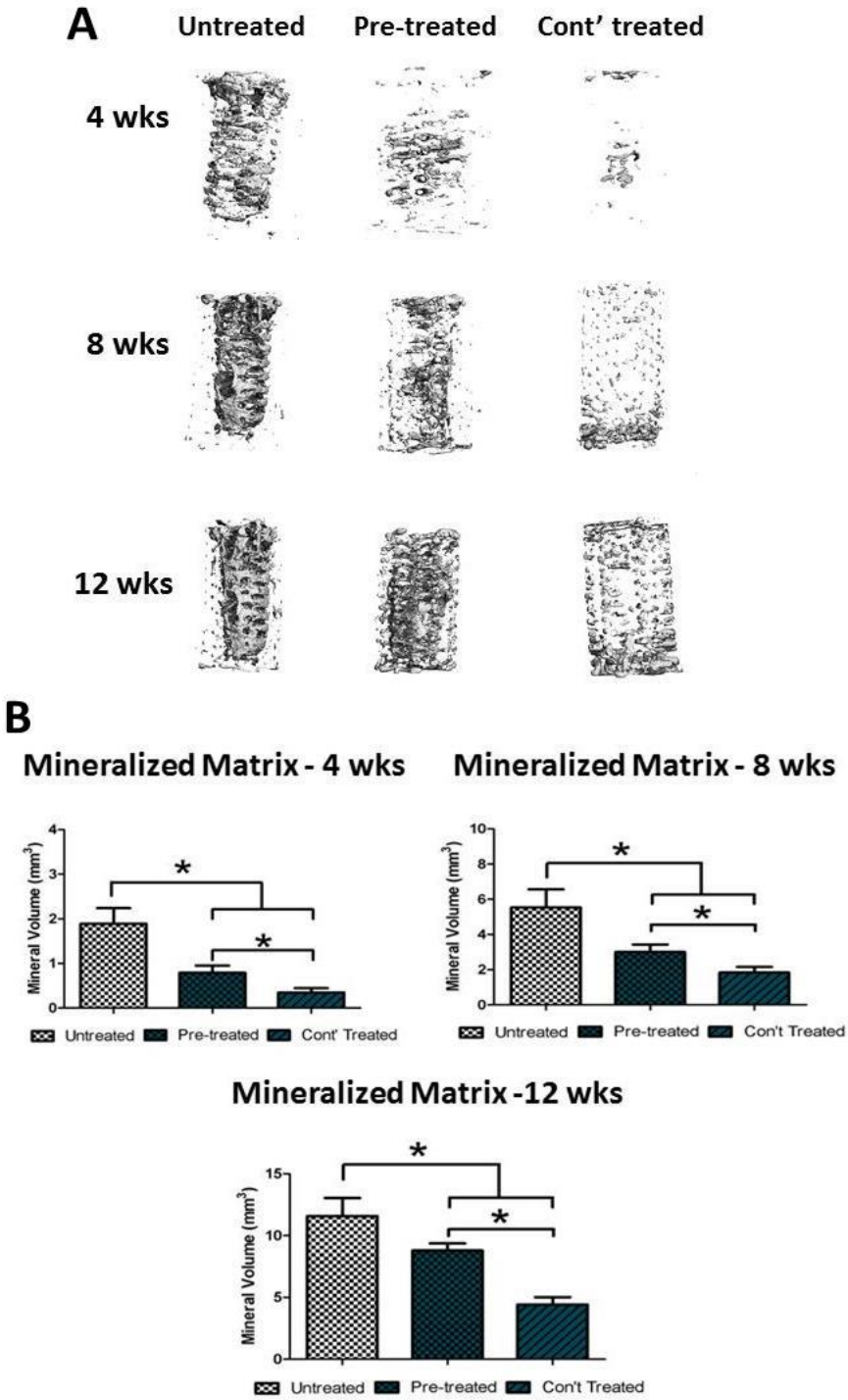

Figure 3.5. Micro-CT reconstructions of hADSC untreated, resveratrol pre-treated, and continuously resveratrol treated constructs over time (A). Quantification of mineralized matrix over time (B). *$p<0.05$ from untreated group.

Dose Dependent Effect of Resveratrol on hADSC and rADSC Osteogenic Differentiation

Micro-CT imaging demonstrated that at 4 weeks all groups of hADSCs were mineralizing throughout the entirety of the scaffold (Figure 3.6). At 4 weeks, the 12.5 μM group had significantly greater mineral volume than the 25 μM group, indicating that a high dose of resveratrol reverses its promotion of mineralization seen in lower dose groups (Figure 3.6B). The 12.5 μM group also approached significance compared to the 0 μM (untreated) group although it was not statistically significant. By 8 weeks, all groups continued to mineralize with their matrix volume being significantly higher than the 4 week time point. Interestingly, by 8 weeks the 6.25 μM group displayed the greatest amount of mineralized matrix and was significantly higher than the 25 μM group. Similar results were observed at 12 weeks, with a significant increase in mineralization of all groups compared to the 8 week time point. These data demonstrate that for resveratrol doses lower than 25 μM, pre-treatment of resveratrol is sufficient to increase mineralization of human ADSCs with higher doses promoting greater mineralization at early time points, and lower doses promoting greater mineralization at later time points.

Mineralization of rat ADSCs was robust in all treatment groups as seen on the representative micro-CT images (Figure 3.7). Quantification of the mineralized matrix showed that at 4 weeks the 12.5 μM group significantly increased the mineral volume

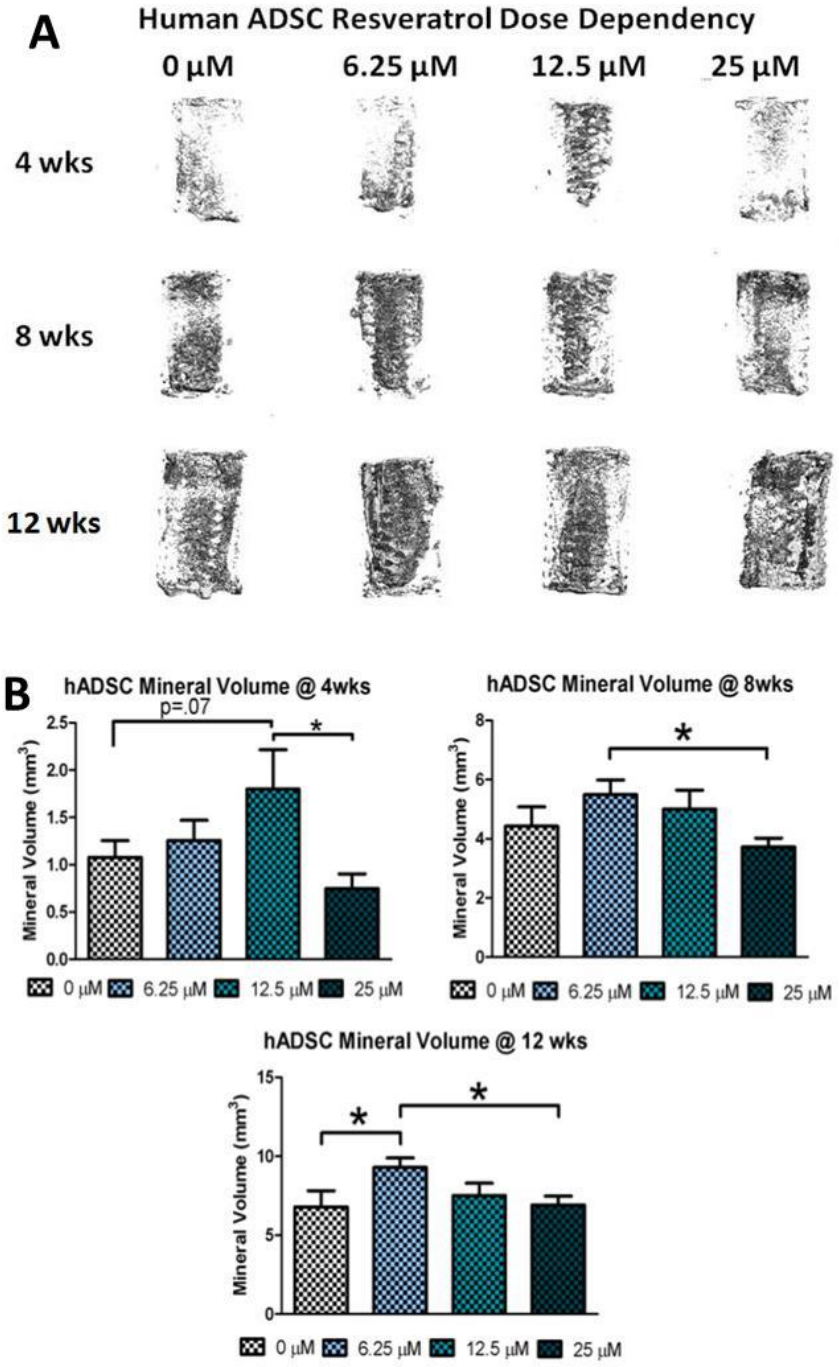

Figure 3.6. Micro-CT reconstructions of pre-treated hADSCs at multiple dosages of resveratrol (A). Quantification of mineralized matrix over time (B). *$p<0.05$ from untreated group except where otherwise noted.

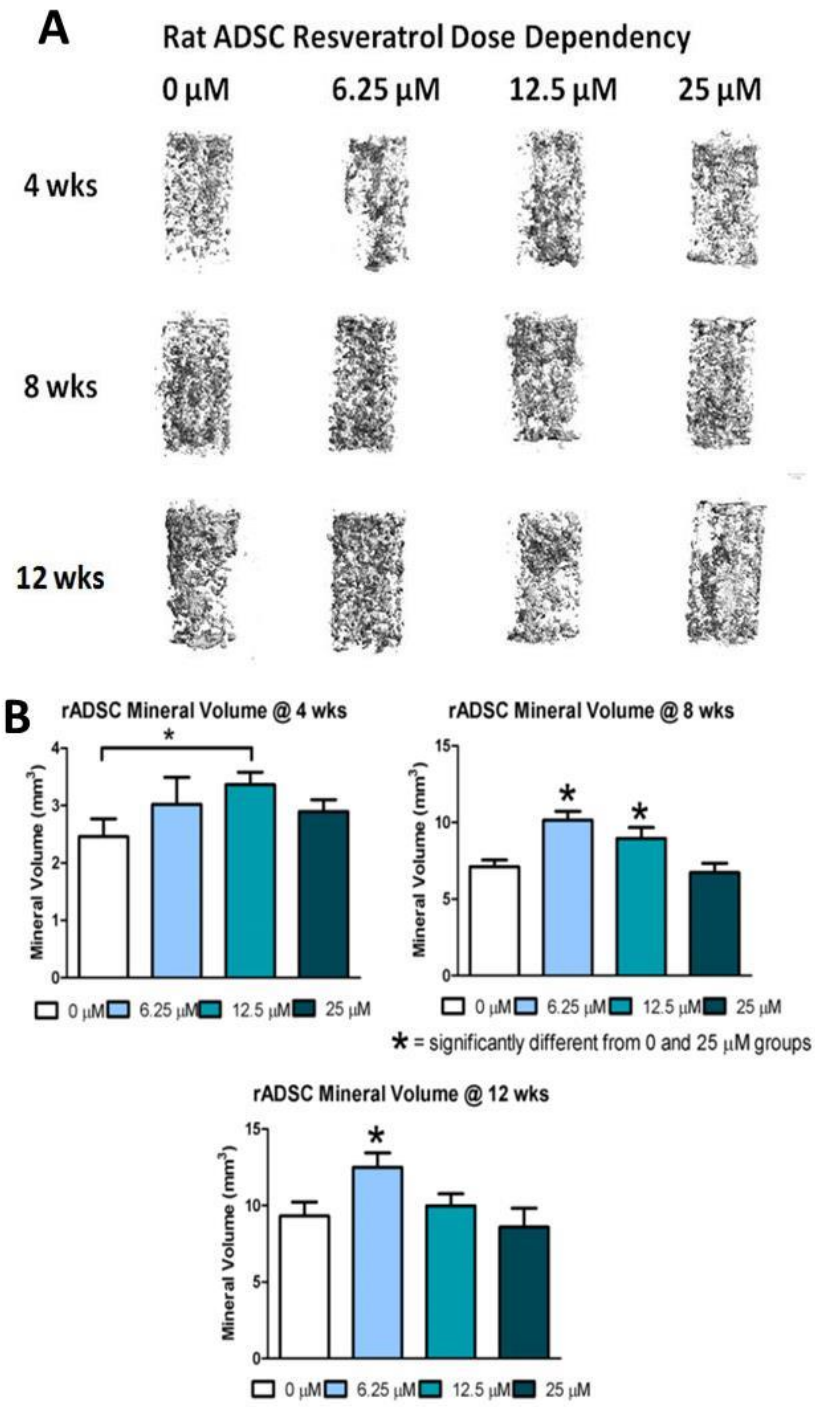

Figure 3.7. Micro-CT reconstructions of pre-treated rADSCs at multiple dosages of resveratrol (A). Quantification of mineralized matrix over time (B). *$p<0.05$ from untreated group except where otherwise noted.

compared to the 0 μM group. Similar results were observed at 8 weeks with both the 6.25 μM and 12.5 μM groups having more mineralized matrix than the 0 and 25 μM groups. By 12 weeks the 6.25 μM group was significantly higher than all other dosage groups. At all time points the mineralization increased compared to the previous time point for all resveratrol dosages. It should also be noted that the rat ADSC groups all produced more mineralized matrix than the corresponding human ADSC groups at all time points.

hADSC and rADSC Mean Density of Mineralized Matrix

Quantification of the mean density of the mineralized nodules showed that at 4 weeks rat and human ADSC constructs showed similar mineral density with only the 25 μM groups being significantly different (Figure 3.8A). However at 8 and 12 weeks there were significant differences in the mean density with rat cells showing higher mean density compared to human cells at all doses (Figure 3.8B and 3.8C). Interestingly, rat ADSC constructs increased in mean density significantly over time for all groups from 4 to 8 weeks. From 8 to 12 weeks the middle two doses were significantly different from the previous time point although all groups increased in mean density. At all time points human cells had a relatively consistent mean density regardless of resveratrol dose. Some groups did significantly increase over time, but the increases were lower than observed for the rADSCs.

Histological Analysis of Mineralized Matrix of hADSC and rADSC Constructs

Cell scaffold constructs from both species were sectioned longitudinally through the middle of the construct and calcein and ethidium imaging of the mineralized matrix was performed. Rat ADSC groups displayed large nodules of mineral with live cells

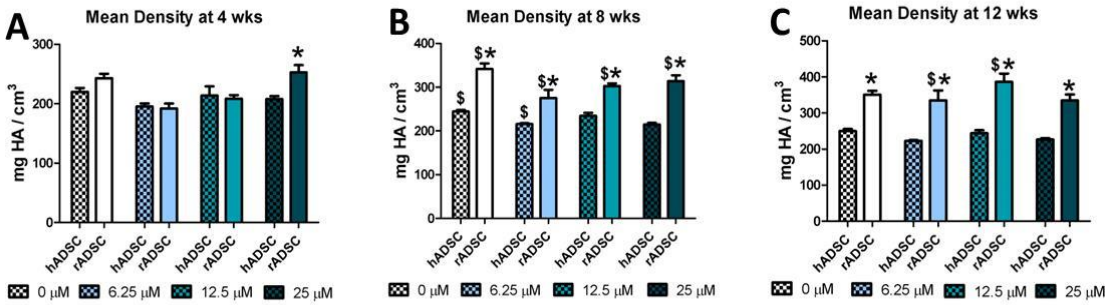

Figure 3.8. Mean mineral density from micro-CT reconstructions of pre-treated rADSC and hADSC constructs at multiple dosages of resveratrol at 4 weeks (A), 8 weeks (B), and 12 weeks (C). *$p<0.05$ species difference at that dose, \$ $p<0.05$ from previous time point for that group.

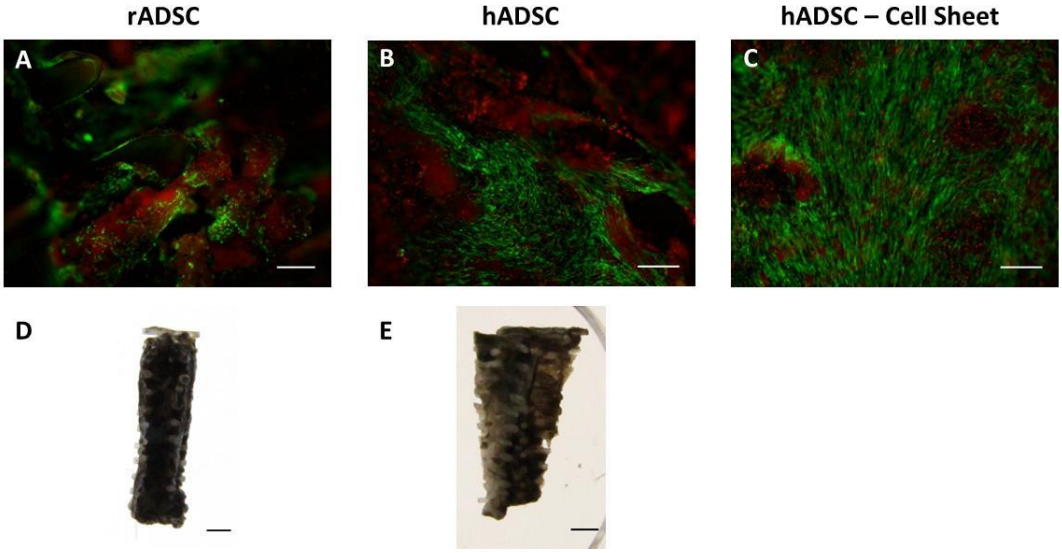

Figure 3.9. Fluorescence imaging of rADSC (A) and hADSCs (B & C) after12 weeks of culture in osteogenic media (scale bar = .5 mm; green = cells, red = mineral). Von Kossa staining of rADSC (D) and hADSC (E) cell seeded constructs after 12 weeks of culture in osteogenic media (scale bar = 1 mm).

being found on top of the mineralized nodules as well as on the struts of the scaffold (Figure 3.9A). Human ADSC constructs showed similar results with similar mineralized nodules (Figure 3.9B); however there were also large areas of confluent cells that were not observed in the rat ADSC constructs (Figure 3.9C). Von Kossa staining showed that both human and rat cell constructs had large deposits of mineral (Figure 3.9D and 3.9E). It should be noted that the rat cell groups stained darker and blacker than the human cell groups which had a more brownish color, confirming micro-CT results in which the rat cell groups had denser mineral nodules than human cell groups.

Surface Examination of hADSC and rADSC Constructs

SEM Imaging

SEM images of the scaffold with and without mineralized cells showed distinguishing features. Similar to the fluorescent imaging results, SEM images showed that human cell constructs had much more ECM compared to rat cells, however the rat cell constructs had much larger nodules compared to the human cells (Figure 3.10C, D, G, & H).

TGA Analysis

The weight percentage of organic and inorganic contents of substrates used in this study was determined by thermogravimetric analysis (TGA). The weight loss profile and percentage as a function of increasing temperature from 25 °C to 800 °C is shown in Figure 8A. PCL had 99.3% weight loss at 800 °C while PCL with lyophilized collagen had 98.8% weight loss. Human and rat cell mineralized constructs had 47%, and 68% weight loss, respectively. The weight loss of human bone and rat bone corresponded to

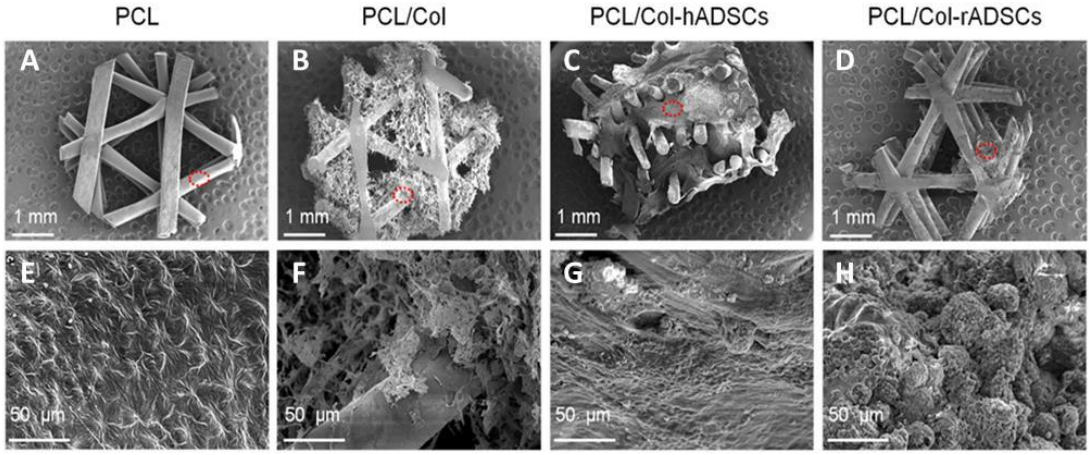

Figure 3.10. Scanning electron microscope images of PCL (A&E), PCL/Col (B&F), PCL/Col-hADSCs (C&G), and PCL/Col-rADSCs (D&H). The red dot circle indicates the area of higher magnification, shown in the second row of this figure.

34% and 33%, respectively. PCL and PCL/Col consist of organic components while PCL/Col-hADSCs (mineralized human constructs) and PCL/Col-rADSCs (mineralized rat constructs) consisted of both organic and inorganic materials like human and rat bones.

XPS Analysis

The inorganic contents of PCL/Col-hADSCs and PCL/Col-rADSCs were measured by X-ray photoelectron spectroscopy (XPS). Calcium (Ca2p, 347 eV) and phosphorous (P2p, 133 eV) peaks were detected in human bone, PCL/Col-hADSCs, rat bone, and PCL/Col-rADSCs, however these two peaks were not observed on PCL and PCL/Col surfaces (Figure 3.11B) demonstrating that inorganic mineral deposition by human and rat cells occurred in the tissue engineered constructs.

The distribution of Ca and P on human bone, PCL/Col-hADSCs, rat bone, and PCL/Col-rADSCs surfaces was obtained by XPS chemical mapping (Figure 3.11C). In human bone samples, Ca and P demonstrated stronger and more widespread intensity compared to rat bones. PCL/Col-hADSCs distinctly showed that Ca and P were locally concentrated rather than evenly spread. On PCL/Col-rADSCs constructs, Ca and P were present with strong intensity and relatively well spread. The XPS mapping showed higher intensity suggesting a denser mineralized matrix for the rat cell constructs compared to the human cell constructs, confirming the mean mineral density differences we obtained from micro-CT.

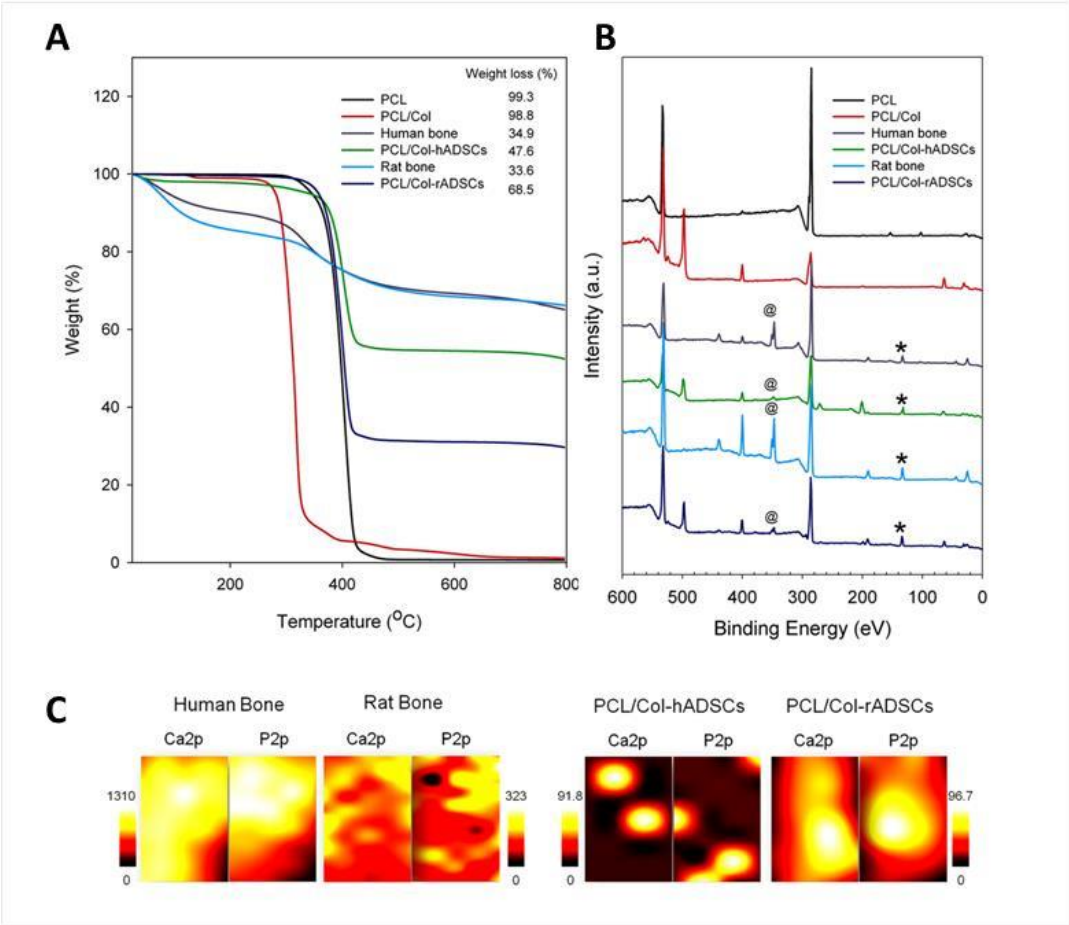

Figure 3.11. A) TGA decomposition profiles of PCL, PCL/Col, human bone, PCL/Col-hADSCs, rat bone, and PCL/Col-rADSCs under N_2 atmosphere; B) x-ray photoelectron spectroscopy (XPS) general survey spectra for PCL, PCL/Col, human bone, PCL/Col-hADSCs, rat bone, and PCL/Col-rADSCs (@ = Ca2p peak, * = P2p peak); C)XPS chemical mapping of Ca2p and P2p on human and rat bone (B) and PCL/Col-hADSCs and PCL/Col-rADSCs (Mapping area = 0.44 mm^2).

Concurrent Resveratrol and BMP-2 treatment of rADSCs

Von Kossa staining of 2-D cultures was similar among all groups, demonstrating that all groups did exhibit some mineralization of their extra cellular matrix as shown in Figure 3.12. Quantitative assays were also performed to further examine differences in the culture conditions. BMP-2 significantly reduces the DNA content of the cell cultures after 2 weeks in osteogenic media in non-resveratrol treated cells. There was a significant reduction in resveratrol treated cells in terms of DNA content compared to non-treated cells Figure 3.12B). Total calcium content showed a significant increase in resveratrol treatment (Figure 3.12C). Alkaline phosphatase activity indicated that the resveratrol and BMP-2 supplemented cultures exhibited significantly higher activity than the other groups (Figure 3.12D).

Our 3-D results indicated a significant increase in mineral volume in resveratrol treated ADSCs, consistent with our previous dose dependency and treatment regimen studies. Further, we did not see a significant increase in BMP-2 supplemented cultures in either resveratrol treated or non-treated cells, although the means were slightly higher in each treatment group respectively. Qualitatively, we observe that there is mineral throughout the entirety of the scaffold. Continuing the culture through 8 weeks we observed very similar results, although there were significantly higher levels of mineralization for all groups compared to the 4 week time point. Representative images and mineral volumes quantified via micro-CT reconstruction are shown in Figure 3.13. Resveratrol had a significant effect on the mineralization of the scaffolds, with no effect of BMP-2 being observed in both treated and non-treated cell groups. Fluorescent imaging showed that at the end of culture, there were still live cells present on the

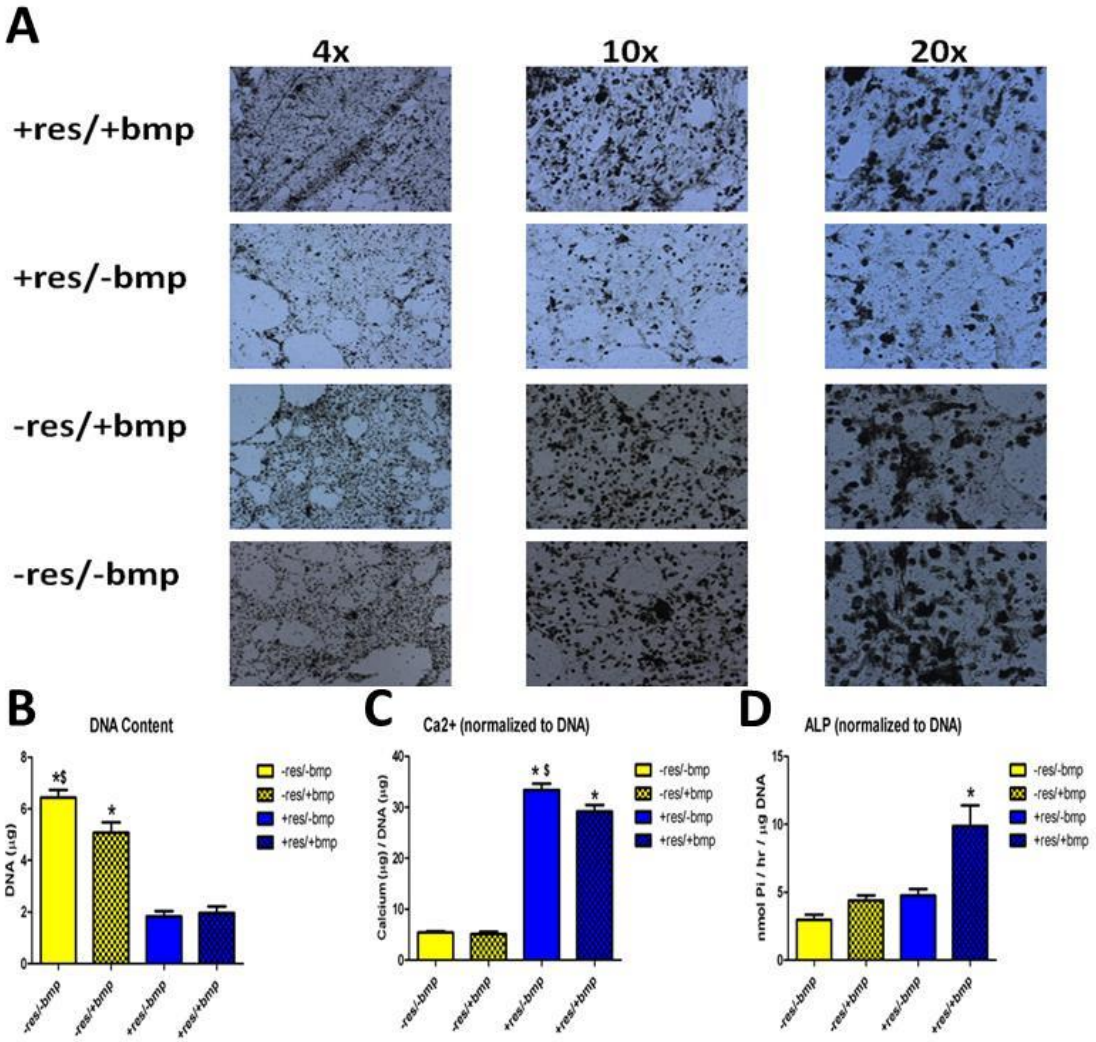

Figure 3.12. Von Kossa staining of concurrent resveratrol and BMP-2 treated samples in 2-D cultures (A). DNA (B), total cellular calcium content (C), and alkaline phosphatase activity (D) of 2-D samples after 14 days. * $p<0.05$ effect of resveratrol treatment, $ $p<0.05$ effect of BMP-2 treatment.

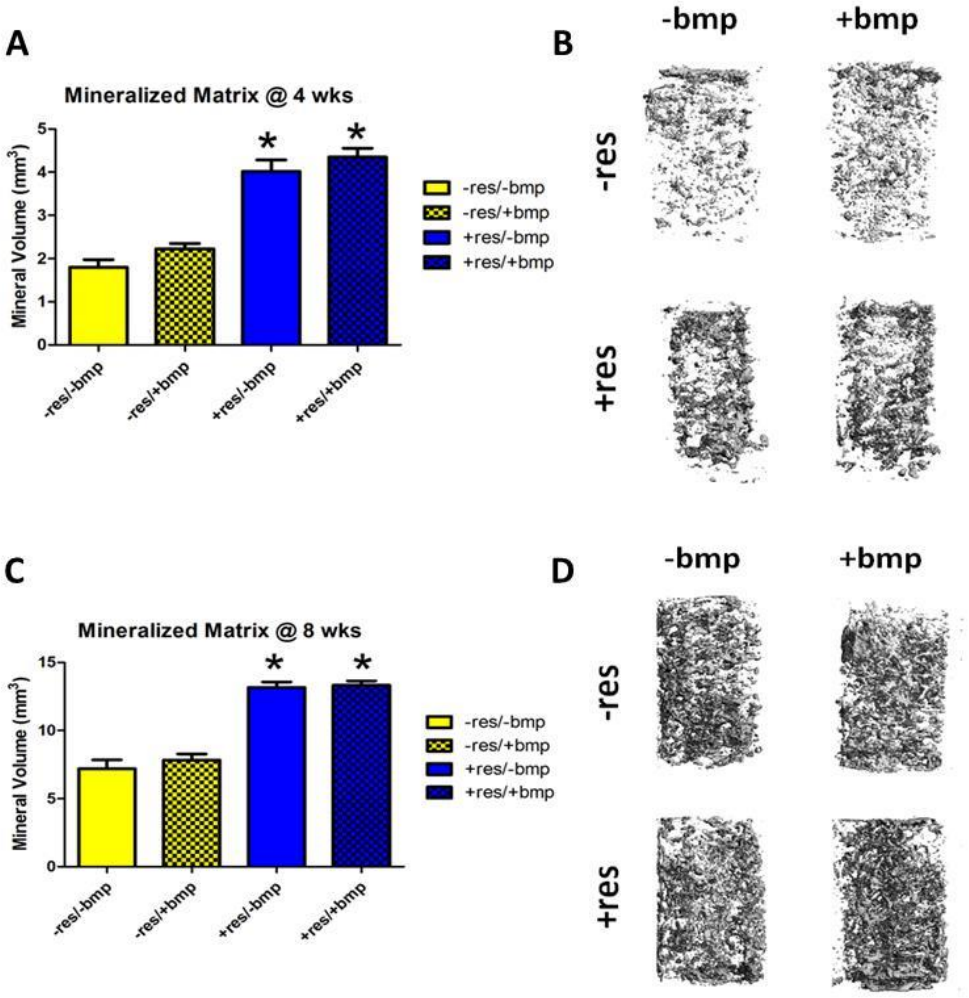

Figure 3.13. Micro-CT analysis of mineralized matrix at 4 and 8 weeks of rADSCs concurrently treated with resveratrol and BMP-2. Quantification of mineralized matrix at 4 weeks (A) and 8 weeks (C), and representative reconstructions at 4 weeks (B) and 8 weeks (D). *$p<0.05$ effect of resveratrol treatment.

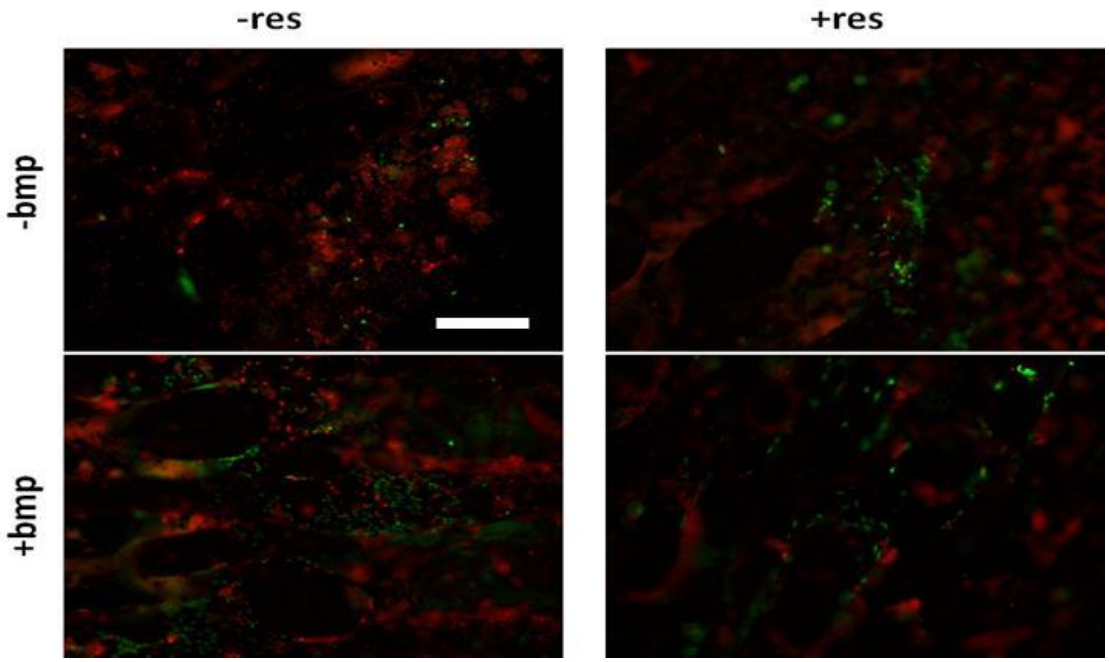

Figure 3.14. Fluorescent images of concurrent rADSC treated 3-D constructs after 8 weeks of culture. Scale Bar = 300 µm.

scaffold, suggesting that the mineralization is cell mediated and not caused by precipitation from the media (Figure 3.14).

DISCUSSION

This work examines the osteogenic potential of both rat and human adipose derived stem cells in a 3-D environment as well as the impact of pharmaceutical treatment to improve the osteogenic potential of the cell source. Most studies comparing cell sources from different species have focused on mesenchymal stem cells from bone marrow aspirates (Woodbury, Schwarz et al. 2000, Javazon, Colter et al. 2001, Ikeuchi, Ito et al. 2003, Osyczka, Diefenderfer et al. 2004, Zavan, Giorgi et al. 2007). Further, many studies focus on age related differences by comparing adult cells to fetal cells (De Coppi, Callegari et al. 2007, Guldberg, Oest et al. 2007, Peister, Woodruff et al. 2011). While age is an important consideration, the species from which the cell source is tested in tissue engineering models should also be considered in selecting a cell source. Such studies have been limited to examining different strains of mice (Peister, Mellad et al. 2004), and to our knowledge only one study has looked at the difference in osteogenic potential of adipose derived stem cells from different species (Ni, Zhou et al. 2009).

We show that there are differences in the osteogenic potential of the cell sources as well as dosage effects of resveratrol to improve osteogenic differentiation. Adipose derived stem cells obtained from rats showed greater mineralization at all time points compared to human cells. Further, the mean density of the nodules in rat cell constructs was higher than human at later time points suggesting a more mature mineralization in the rat cell constructs. A possible explanation for this is the use of lyophilized rat tail

collagen I in our PCL scaffold system. Rat cells may be able to assimilate the collagen I and remodel and mineralize it more efficiently than the human cells. This is supported by the differences seen at the early time point of four weeks as well as the larger mineral nodules observed in the rat cell constructs. Human cell mineralization may be altered in the presence of human collagen I and should be tested in the future. Another possible explanation for the observed differences in mineralization may be related to variations in resveratrol metabolism. Human cells and rat cells have been shown to metabolize resveratrol differently and this may influence the osteogenic differentiation of the cells (Yu, Shin et al. 2002).

Resveratrol has been shown to induce osteogenesis in preference to adipogenesis in mesenchymal and adipose derived stem cells (Backesjo, Li et al. 2006, Erdman, Dosier et al. 2011). Previous work in our lab demonstrated that rat adipose derived stem cells pre-treated with resveratrol produce more mineralized matrix than untreated and continuously treated cells (Erdman, Dosier et al. 2011). We extended this work to analyze human adipose derived stem cells. We observed that the human cells did not respond well to the 25 μM resveratrol dose regardless of treatment regimen. We therefore performed a dose dependency study evaluating pre-treatment with resveratrol for both human and rat adipose derived stem cells. We observed dosage differences in both rat and human cell constructs. For both rat and human cell constructs, 12.5 μM resveratrol pre-treatment resulted in greater mineralized matrix at 4 weeks. Doses higher than 12.5 μM led to decreased mineralized matrix suggesting a potentially cytotoxic effect. At later time points, a lower dose of 6.25 μM resveratrol had the greatest mineralized matrix. Taken together, this suggests that higher doses lead to more rapid

differentiation and thus higher mineralized matrix initially, while lower doses promote differentiation while retaining better cell viability, resulting in greater mineralized matrix at later time points. These results suggest that the resveratrol dosage should be taken into consideration and tailored for the bone tissue engineering application. For short time course studies, a higher dose may produce the best results in terms of mineral production, and contrarily for long time course studies a lower dose may be the most beneficial.

Concurrent treatment of resveratrol and BMP-2 did not result in any added benefit in terms of mineralization *in vitro*. Others have shown that short exposure times to BMP-2 are capable of inducing differentiation of ADSCs *in vitro* (Overman, Farre-Guasch et al. 2013). Our result is most likely due to the relatively short exposure time of BMP-2 relative to the long-term culture in osteogenic media. As such, any up-regulation of genes by BMP-2 is ameliorated by the 4 week time point. This agrees with our alkaline phosphatase data that demonstrated at 14 days there was an effect of BMP-2 in 2D culture.

The PCL/collagen system used in this study provides a consistent and reproducible method to evaluate the osteogenic potential of cells from a variety of sources. Our lab and others have used this to test cells from human bone marrow aspirates, amniotic fluid stem cells, mouse cells, and now adipose derived stem cells (Guldberg, Oest et al. 2007, Peister, Deutsch et al. 2009, Rai, Lin et al. 2010, Erdman, Dosier et al. 2011). An advantage of this system is the consistent porosity as each scaffold is punched from a uniform sheet of material. This eliminates the variable of poor mass transport due to varying porosity in the scaffold affecting the results. As such, any differences observed should be solely attributable to the osteogenic potential of the

cell source. When we mapped the mineral distribution of the mineralized matrix using XPS, we observed that the rat cells had higher mineral content compared to human constructs. As expected, when compared to native bone from both rats and humans however, the mineral content within the 3-D constructs was markedly lower, indicating a still immature mineralized extracellular matrix relative to bone tissue.

SUMMARY

In this study we evaluated the osteogenic potential of human and rat adipose derived stem cells subjected to pre-treatment with resveratrol prior to seeding within 3-D tissue-engineered constructs. We found that the dose of resveratrol has a significant effect on the mineralized matrix production of both cell sources. We further found that rat adipose derived stem cells produce a larger quantity and more mature mineralized matrix compared to the human cell constructs. Taken together we demonstrate that the species as well as resveratrol dose can have a significant effect on the mineralized matrix production of adipose derived stem cells.

CHAPTER 4: EVALUATION OF SYNTHETIC AND NATURALLY BASED HYDROGELS AS AN INJECTABLE CELL DELIVERY VEHICLE FOR BONE TISSUE ENGINEERING

ABSTRACT

The goal of these experiments was to evaluate synthetic and naturally based hydrogels as a cell delivery vehicle for bone tissue engineering. Poly-ethylene glycol (PEG) and alginate based hydrogels were studied for both *in vitro* cell viability and *in vivo* ectopic mineralization in a subcutaneous implant model. We first compared traditionally molded 10% w/v PEG hydrogels and injectable PEG hydrogels, as well as the incorporation of cell adhesive peptide RGD, for *in vitro* cell viability at 14 days. We found that the injectable hydrogels with a RGD sequence tethered to the backbone resulted in the greatest amount of cell viability. Therefore, we tested these hydrogels for *in vivo* ectopic mineralization by incorporating 1 million green fluorescent protein expressing adipose derived and bone marrow derived mesenchymal stem cells (ADSCs and BMMSCs respectively) co-delivered with 2 µg of BMP-2. Very little ectopic mineralization was observed in any of the groups, and the hydrogel remained largely intact most likely due to its high weight to volume percentage. We therefore tested a lower weight percentage hydrogel in alginate-based hydrogels. 2% w/v alginate hydrogels demonstrated high cell viability over a 14 day time course, and an increase in cell number was observed via DNA analysis. Further, alginate hydrogels were shown to be an effective delivery method for *in vivo* ectopic mineralization, with BMMSC loaded hydrogels resulting in greater mineralization than acellular hydrogels. We therefore

conclude that an injectable alginate hydrogel system may be an attractive option as a cell delivery vehicle for bone tissue engineering.

INTRODUCTION

In the case of volumetric bone loss, such as traumatic injury or in tumor resection, the loss of progenitor cells or damage to surrounding tissue can limit the endogenous healing capacity of the patient, resulting in nonunion of the defect (Bruder and Fox 1999). Presently, the clinical gold standard for treatment of large segmental bone defects is autologous bone grafting. This procedure, however, is severely constrained by a limited supply of available graft material, insufficient structural properties and significant donor site morbidity (Bauer and Muschler 2000, Nandi, Roy et al. 2010). An alternative treatment is processed bone allografts. Again, this treatment possesses significant limitations, including an unacceptably high rate of post-implantation failure, largely attributable to the inability of the graft tissue to fully revascularize and remodel (Wheeler and Enneking 2005, Nandi, Roy et al. 2010). Cell based tissue engineering strategies utilizing stem cells have the potential to augment the endogenous healing response resulting in restoration of tissue and function. However, questions remain in effective delivery strategies of stem cells to facilitate cell viability and differentiation *in vivo*.

Hydrogels have been studied as cell delivery vehicles for bone tissue engineering. A hydrogel is characterized by its high water content contained with insoluble polymers that form a cross-linked network to retain a shape. Hydrogels have many characteristics advantageous for cell viability. First, hydrogels are able to facilitate cell adhesion via peptide incorporation. As stem cells are adherent cells, mimicking of the natural ECM is

vital to allow proper functioning of cells. Lack of adhesive peptides can cause stem cells to undergo anoikis leading to cell apoptosis. Second, many have demonstrated that cell delivery also requires growth factor co-delivery to promote differentiation of the implanted cells. Encapsulation of growth factors into hydrogels has shown to be effective in inducing new tissue formation (Phelps, Landazuri et al. , Boerckel, Kolambkar et al. 2011, Kolambkar, Boerckel et al. 2011, Kolambkar, Dupont et al. 2011). In addition, hydrogels are able to serve as a barrier to the initial host inflammatory response, yet will permit host cell invasion and vascularization to regenerate a functional tissue. Finally, hydrogels allow for the system to be injectable. Extrusion of the hydrogel immediately after cross-linking will lead to generation of larger pores other than those inherent to the polymer chain length. This may ultimately lead to greater cell viability by possibly increasing the mass transport within the hydrogel.

Poly-ethylene glycol (PEG) based hydrogels are an attractive option for bone tissue engineering due to their ability to be manipulated to facilitate cellular attachment and differentiation. Cellular attachment and spreading allows for cellular deposition of extra cellular matrix molecules, thus leading to the possibility of mineralized matrix within the hydrogel. This has been demonstrated by Burdick in which mineralized matrix was found on PEG hydrogels with tethered RGD (Burdick 2002). Betz demonstrated that modification of the PEG hydrogel to generate larger pore sizes resulted in increased osteoblastic gene activity and protein production by human mesenchymal stem cells (Betz, Yeatts et al. 2010). These studies suggest that PEG hydrogels may be a viable platform as an injectable cell delivery vehicle for bone tissue engineering applications.

Alginate has been shown to be an effective delivery vehicle for biologics for bone tissue engineering. Kolambkar demonstrated that when paired with BMP-2, alginate hydrogels are able to heal critically sized femoral segmental defects in rodents (Kolambkar, Boerckel et al. 2011, Kolambkar, Dupont et al. 2011). Mechanical testing showed that the regenerated bone tissue was not significantly different from intact bone demonstrating successful functional repair of the defect. Boerckel followed this study with a dose dependency study demonstrating that the dose of BMP-2 affects the amount of regenerated tissue in a critically sized segmental bone defect. Further, it was demonstrated that the alginate and BMP-2 system resulted in greater bone formation than the clinically used collagen sponge with an equal amount of BMP-2 (Boerckel, Kolambkar et al. 2011). The backbone chain of alginate can be manipulated with cell attachment motifs to facilitate cell adhesion and cell differentiation (Rowley and Mooney 2002, Comisar, Kazmers et al. 2007). Alsberg demonstrated that RGD functionalized alginate hydrogels are able to support in vivo bone formation (Alsberg, Anderson et al. 2001). As such, alginate is an attractive platform to test as a potential injectable cell based bone tissue engineering delivery vehicle.

The aim of this study was to evaluate PEG and alginate based hydrogels as cell delivery vehicles for bone tissue engineering. Our hypothesis was that the generation of macropores via injection would facilitate greater cell viability *in vitro* than traditional mold cast hydrogels, ultimately leading to greater bone volume *in vivo* with the incorporation of bone morphogenetic protein 2 (BMP-2). The hypothesis was first tested using PEG hydrogels and a histomorphometric analysis of green fluorescent protein (GFP) expressing ADSCs and BMMSCs *in vitro*, quantifying the amount of GFP

expressing cells and the amount of dead cells over a 14 day time course. We next tested the PEG system for *in vivo* mineralization with adult stem cells and BMP-2 co-delivery and found limited mineralized tissue due to lack of resorption of the PEG hydrogel. Therefore low weight percentage irradiated and oxidized irradiated alginate hydrogels were then tested as cell delivery vehicles. Cell viability was assessed over a 14 day time course using a histomorphometric analysis and confirmed via DNA content. *In vivo* ectopic mineralization was then evaluated with a subcutaneous implant model, with the presence of implanted cells assessed after 8 weeks.

METHODS

Isolation of GFP ADSCs and BMMSCs

Genetically modified Sprague Dawley rats that express GFP ubiquitously (SD-Tg(GFP)2BalRrrc) were obtained from the Rat Resource and Research Center (RRRC, Columbia, MO). 3 males weighing 120-150 grams were euthanized and their adipose tissue and bone marrow harvested as described previously. Briefly, adipose tissue was pooled and washed three times in Hank's balanced saline solution (HBSS), and digested in 0.25% trypsin for 30 minutes at 37˚C. The tissue was then cut into smaller pieces and digested in 9125 units of collagenase IA (Sigma, St. Louis, MO) and 75 units of dispase (Gibco, Invitrogen, Carlsbad, CA) for three hours. The upper layer of adipocytes was removed, and the cell suspension was filtered through a 40µm cell strainer. The digestion was stopped with MSC growth media (GM) (Lonza, Basel, Switzerland), which contains fetal bovine serum, and the cells were collected by centrifugation. The cells were plated at 5,000 cells/cm^2 in T-75 flasks. Cultures were washed twice with

phosphate buffered saline (PBS) and fed with GM at 24 and 48 hours after plating and allowed to grow to 90% confluence. The cells were cryopreserved following expansion.

For bone marrow mesenchymal stem cells, femurs and tibias were harvested aseptically. Both epiphyseal ends were cut and the marrow flushed out in α-MEM into tissue culture plates (Gibco, Grand Island, NY). After 1 hour, the media was collected and then re-plated onto new tissue culture plates. 48 hours later the media was aspirated off and the adherent cells grown to 90% confluence, with media changes occurring every 48 hours. The cells were cryopreserved following expansion.

PEG Formulation and RGD Incorporation

A 3400 molecular weight PEG diacrylate (PEGDA) was the PEG system utilized in these studies (Laysan Bio, Arab, AL). The cell adhesive peptide sequence GGGRGDSP, containing the fibronectin cell attachment domain, was tethered to the PEG chain (Peptides International, Louisville KY). Briefly, a 3400 molecular weight PEG chain with a succinimydyl valerate reactive group on one end was reacted at 1:1 molar ratios with the peptide on a stir plate for 4 hours. Reacted products were purified by dialysis using a 3500 MW dialysis cassette for 24 hours (Thermo Scientific, Waltham, MA). After purification, the solutions were lyophilized for 48 hours to obtain a powder and then stored at minus 20°C until needed.

PCL Nanofiber Mesh Tube Formation

PCL nanofiber mesh tubes were produced as described previously (Kolambkar, Boerckel et al. 2011). Poly (ε-caprolactone) (PCL) pellets (Sigma-Aldrich, St. Louis, MO) were dissolved in a 90:10 volume ratio of hexafluoro-2-propanol (HFP):dimethylformamide (DMF) (Sigma-Aldrich) to obtain a 12% (w/v) polymer

solution. The solution was stirred overnight and until the solution was homogenous. The polymer solution was loaded in a 5 mL syringe (Becton-Dickinson, Franklin Lakes, NJ), and a 22 gauge blunt stainless steel needle (Jensen Global Inc., Santa Barbara, CA) was attached to the syringe end. The syringe was mounted on a syringe pump (Harvard Apparatus, Holliston, MA) set at a rate of 0.75 mL/hr. Electrospun fibers were collected on foil covering a copper plate (McMaster-Carr, Atlanta, GA) which was placed at a distance of 20-23 centimeters from the needle end. Fibers were electrospun for 5 hours at a voltage of 15-20 kV, supplied by a high voltage power supply (Gamma High Voltage Research, Ormond Beach, FL). The residual solvent from the meshes was allowed to evaporate by placing them in a dessicator until use. Sheets of electrospun nanofibers were cut via laser cutter (Universal Laser Systems, Scottsdale, AZ) into 12mm x 18 mm squares, with 1 mm holes perforating the middle of the mesh to allow nutrient transport. Meshes were removed from the foil by submerging them in 70% ethanol (VWR, West Chester, PA). The rectangular mesh samples were then wrapped around a stainless steel mandrel (McMaster-Carr, Atlanta, GA) to form a tube approximately 5 mm in diameter and 12 mm length. The overlapping edges of the mesh were secured via UV glue (DYMAX Corporation, Torrington, CT), which was cured with a LED spot curing lamp (DYMAX Corporation). Tubes were then placed in ethanol for overnight evaporation. Prior to use, tubes were washed thrice with PBS (Mediatech Inc., Manassas, VA.)

Molded and Injected PEG Hydrogel Preparation

PEGDA and RGD tethered PEG powders were mixed in a 3:1 mass ratio and re-suspended in PBS. Re-suspended polymers were mixed in multiple 1 mL syringes with 1 million cells and/or 2 μg of BMP-2 (R&D Systems, Minneapolis, MN) and a 10%

cross-linker consisting of tetramethylethylenediamine (TEMED) and ammonium peroxydisulfate (APS). For molded hydrogels, 150 µL of solution was injected into PCL nanofiber tubes placed in custom molds and the hydrogel cross-linked in the mold. After cross-linking, the PCL mesh tubes containing the hydrogel were placed into custom holders in a 24-well plate (Corning, Lowell, MA). Injected hydrogels were allowed to cross-link in the syringes and then injected into PCL nanofiber tubes placed in sterile custom holders in a 24 well plate. Samples were cultured for 14 days in α-MEM supplemented with 16% fetal bovine serum, and 1% pen-streptomycin L-glutamine with media exchanges occurring every 48 hours.

Alginate Hydrogel Preparation

Alginate hydrogels were prepared as described previously (Boerckel, Kolambkar et al. 2011). Sterile irradiated RGD functionalized alginate was obtained from FMC Biopolymer (FMC Biopolymer, Philadelphia, PA). Oxidized-irradiated alginate was kindly provided by Ovijit Chaudhuri of Harvard University. Alginate hydrogels were prepared by dissolving the lyophilized polymer in α-MEM to a 3% w/v solution. The 3% w/v solution was then diluted to a 2% solution with either α-MEM or α-MEM containing 1 million cells. For BMP-2 containing gels, rat serum albumin (RSA, Sigma Aldrich, St. Louis, MO) was dissolved in 4 mM hydrochloric acid to obtain a .1% solution and mixed with the lyophilized BMP-2 protein at a 10 µg / 100 µL concentration. The BMP-2 solution was added to a syringe at a concentration of 2 µg/150 µL of hydrogel. Non-BMP-2 containing hydrogels just received the RSA carrier solution. Alginate hydrogels were then cross-linked with a .21 g/mL calcium sulfate solution and then injected into PCL nanofiber mesh tubes placed in a custom holder in a 24 well plate.

Cell Viability and Histomorphometric Analysis

At times of harvest, hydrogels were taken out of culture and stained for dead cells using the ethidium-2-homodimer. A 1:1000 dilution of the ethidium-2-homodimer was prepared in PBS as per manufacturer instructions (Invitrogen, Eugene, Oregon) and the hydrogels were placed in 2 mL of solution and agitated gently on a rocker plate for 1 hour (Stovall Life Scientific, Greensboro, NC). Hydrogels were then pushed out of the PCL nanofiber mesh and placed on a circular cover slip then squeezed with another cover slip in a confocal imaging chamber. For each hydrogel, 3 regions were randomly selected and imaged at either 10X or 20 X magnifications on a Zeiss Axio Observer (Zeiss, Göttingen, Germany) and imaged for GFP positive cells and dead cells. Cell viability was expressed as the percentage of GFP positive cells normalized to the total cellular count.

Alginate Digestion and DNA Quantification

Alginate hydrogels in their PCL nanofiber mesh tubes were placed in a 1.5 mL Eppendorf tube (Eppendorf, Hamburg, Germany) and immersed in a sodium citrate digestion solution. The tubes were placed in a water bath at 37 degrees Celsius for 5 minutes. The PCL mesh tube was then removed, and samples were spun at 15,000 R.P.M. for 10 minutes. The digestion solution was then aspirated off leaving a cell pellet, and the cells were lysed with 0.05% Triton-X 100, a 10 second sonication, and one freeze-thaw cycle. DNA was measured per manufacturer instruction using the Picogreen DNA quantification assay (Invitrogen). Data was presented as a percentage of the DNA levels immediately following hydrogel formation (Day 0 levels).

Wet Weight Alginate Degradation Calculation

To assess the degradation of irradiated and oxidized-irradiated alginate hydrogels, the wet weight of the hydrogel construct was measured at multiple time points. First, the PCL nanofiber mesh and holder were immersed in PBS for 10 minutes and the weight of the mesh and holder was determined. 150 µL of alginate hydrogel was then injected into the tube and weighed again, giving the day 0 weight and allowing the weight of the gel to be determined. At each take down point, the hydrogel weight was determined and the amount of hydrogel lost presented as a percentage of the day 0 weight.

Subcutaneous Ectopic Mineralization Model

Female RNU Nude rats approximately 14 weeks of age underwent a subcutaneous implant procedure (Harlan, Tampa, FL). Aseptic procedures were followed. Two 2 cm incisions were made on the dorsal side of the rat. Two pockets were made lateral to the incision sites by debridement. Using a stainless steel tube and pole, the hydrogels were placed into individual pockets. Incisions were then closed with a subcutaneous suture and wound clips. All procedures were approved by the Georgia Tech Institute Animal Care and Use Committee according to protocol #A10021. The groups tested for *in vivo* mineralization are listed below. Carrier free was cells in media without hydrogel.

Micro-CT Imaging for Mineralized Tissue

Mineralized tissue of the constructs was determined by using a VivaCT scanner (Scanco Medical, Brüttisellen, Switzerland) at 55 kVp, 109 mA, 1024 mu scaling, and a

Table 4.1 PEG Based Groups Tested for *In vivo* Ectopic Mineralization

Group	Cell Type	Resveratrol Pre-treatment	2 µg BMP-2
iPEG-RGD	None	No	No
iPEG-RGD + BMP-2	None	No	Yes
iPEG-RGD w/ BMMSC	BMMSC	No	No
iPEG-RGD w/ BMMSC + BMP-2	BMMSC	No	Yes
iPEG-RGD w/ ADSC	ADSC	No	No
iPEG-RGD w/ ADSC + BMP-2	ADSC	No	Yes
iPEG-RGD w/ resADSC	ADSC	12.5 µM	No
iPEG-RGD w/ resADSC + BMP-2	ADSC	12.5 µM	Yes

Table 4.2 Alginate Based Groups Tested for *In vivo* Ectopic Mineralization

Group	Alginate Hydrogel	Cell Type	Resveratrol Pre-treatment	2 µg BMP-2
Acell	Yes	None	No	Yes
ADSC	Yes	ADSC	No	Yes
resADSC	Yes	ADSC	12.5 µM	Yes
Carrier Free (CF)-resADSC	No	ADSC	12.5 µM	Yes
BMMSC	Yes	BMMSC	No	Yes
BMMSC w/o BMP-2	Yes	BMMSC	No	No
Carrier Free (CF)-BMMSC	No	BMMSC	No	Yes

200 ms integration time. The constructs were evaluated with a lower threshold of 80 with a filter width of 1.2 and a filter support of 1.0. The total volume of the mineralized matrix was determined for each sample.

Histological Analysis and GFP Cell Immunohistochemistry

For PEG hydrogels, frozen sections were obtained and stained for mineral via von Kossa staining. Some samples were fixed and saved for GFP immunohistochemistry. Histological analysis of alginate hydrogels was performed using paraffin embedding. Samples were fixed in 10% neutral buffered formalin (NBF) for 48 hours and then decalcified over 2 weeks under mild agitation on a rocker plate. Following paraffin processing, 5 μm-thick sections were cut and stained with Haematoxylin and Eosin (H&E) and Safranin-O/Fast-green.

Depariffinized sections were stained for the presence of GFP using a primary GFP antibody according to manufacturer instructions (Abcam, Cambridge MA). Briefly, a 1:100 solution of primary GFP antibody to PBS was placed on sectioned tissue and incubated overnight at 4ºC. A secondary fluorescently tagged Texas-Red antibody was incubated for 1 hour. Samples were then cover slipped and imaged at 10X magnification using the Zeiss Axio Observer. Sections were also stained for all nuclei using DAPI (Invitrogen) to compare to GFP immunostaining to discern between host cells and implanted cells.

Statistical Analysis

Data are presented as the mean and standard error. Data was analyzed via ANOVA with a Tukey's post hoc test for significance. Significance was determined with an alpha level of .05.

RESULTS

Cell Viability in Molded and Injected PEG Hydrogels *In vitro*

Cell viability in injected and molded PEG based hydrogels was determined via histomorphometry. Results for the adipose derived stem cells (ADSCs) showed that the PEG-RGD containing hydrogel that was injected after cross-linking had the highest cell viability and was significantly higher than PEG injectable and the molded PEG (Figure 4.1). The injected PEG-RGD has a higher mean than the PEG-RGD mold, though it was not significantly different and this was most likely attributable to the limited sample size (n=3). It should also be noted that cell viability in the injected PEG hydrogel was significantly higher than the molded PEG hydrogel suggesting that injecting the gel after cross-linking provides a greater porosity and increases cell viability. Further, the data also demonstrate that for both injectable and molded gels, the incorporation of RGD has a positive effect on cell viability. This is expected at the 2 week time point as adipose derived stem cells are adherent cells and cells undergo anoikis and die without the presence of cell attachment peptides. As the images and quantification of GFP positive cells show, similar results were observed for both the ADSCs and BMMSCs (Figure 4.2). While the trends were near identical compared to the adipose derived stem cells, some differences did not reach significance. Of the differences that were significant however, we observed that for molded gels RGD tethering significantly increased cell viability.

In vivo Ectopic Mineralization in PEG Hydrogels

Analysis of mineralized matrix was performed using micro-CT imaging. Micro-CT showed small nodules of mineral interspersed throughout the hydrogel volume. Quantification of the mineralized matrix showed that BMMSC and ADSC cell seeded

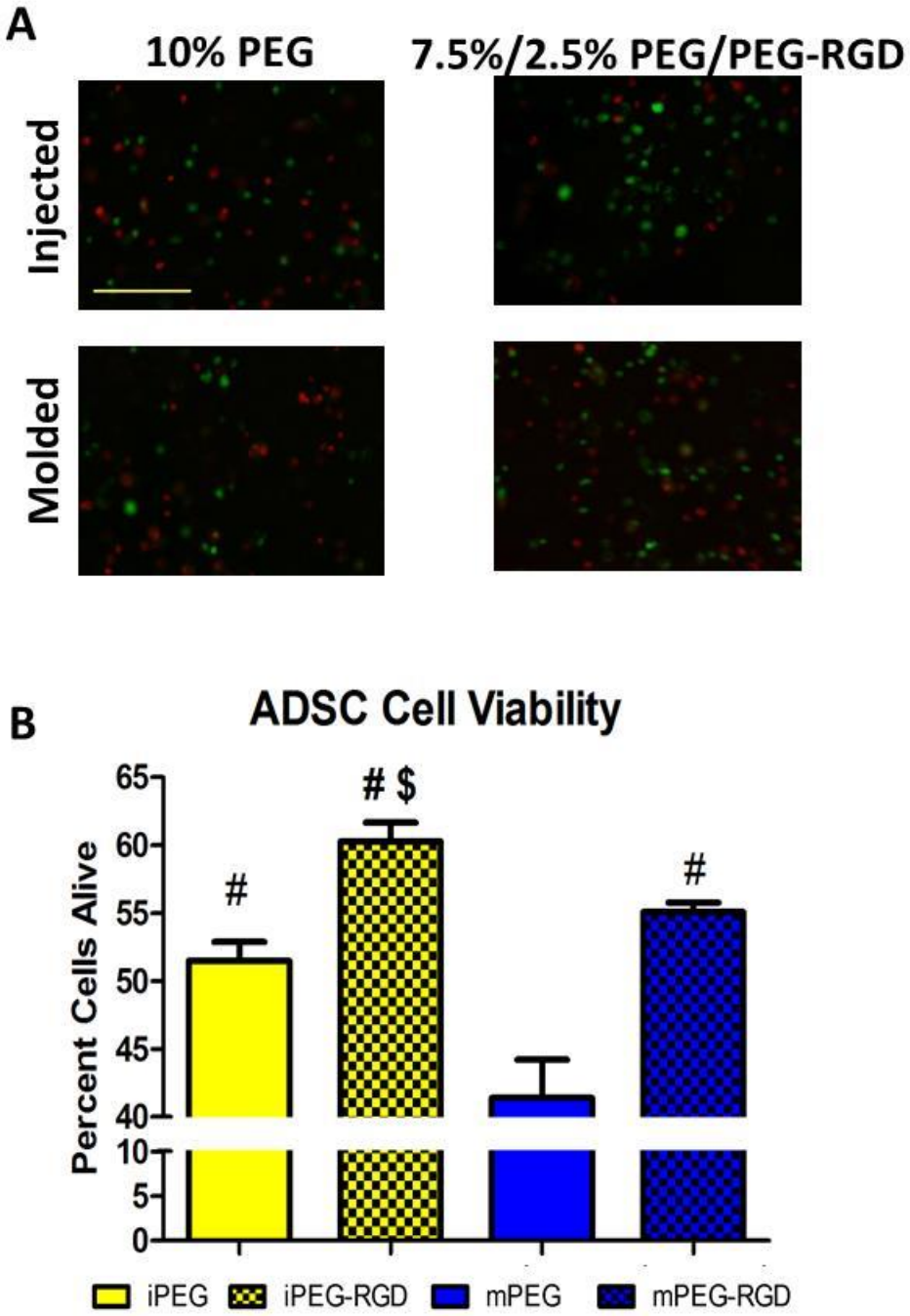

Figure 4.1 Representative images of GFP ADSC cell viability after 14 days in different PEG hydrogel conditions (A). Quantification of GFP positive cells normalized to total cell count (B). # $p<0.05$ from mPEG, $ $p<0.05$ from iPEG. Scale bar = 200 µm.

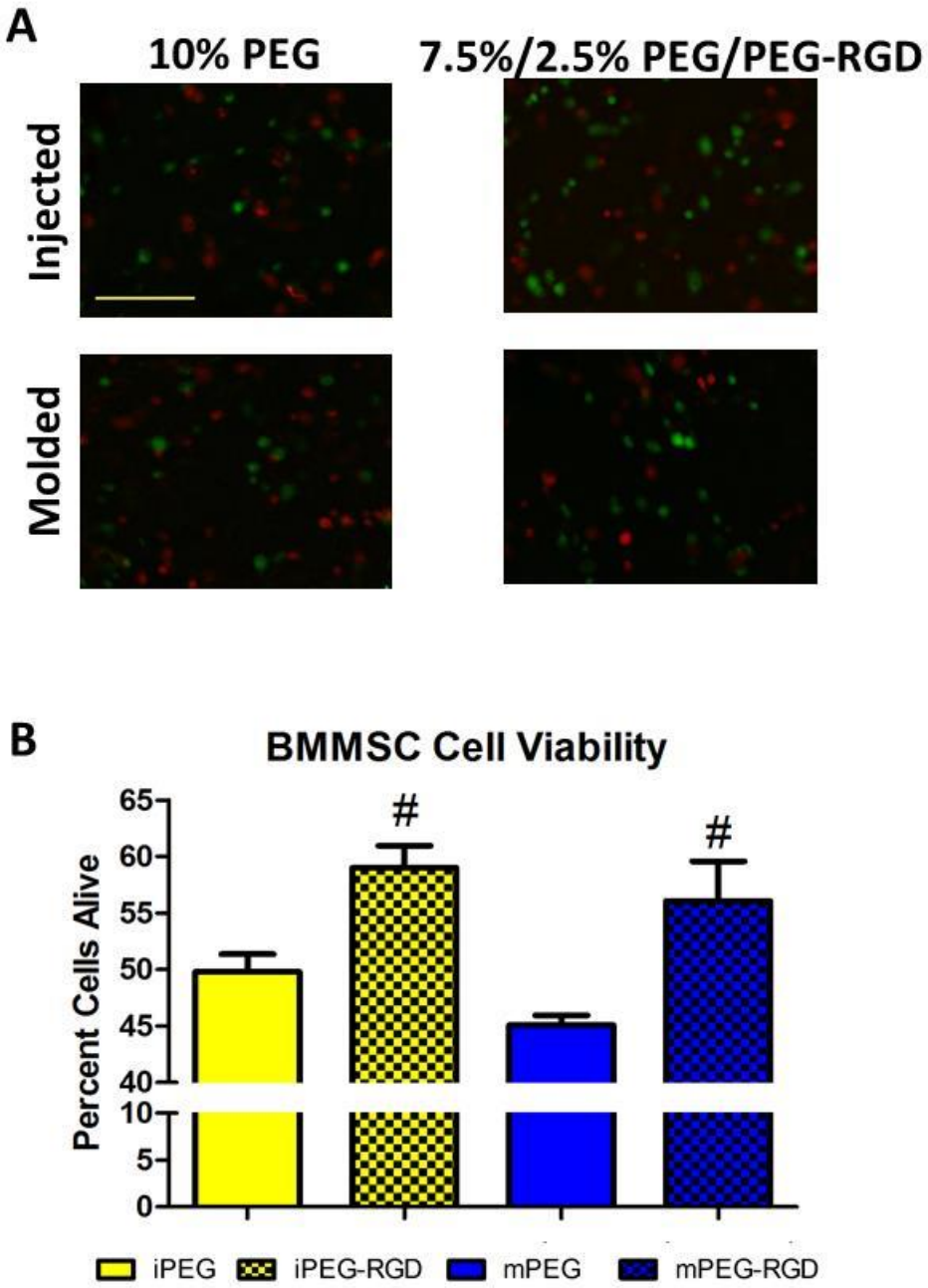

Figure 4.2 Representative images of GFP BMMSC cell viability after 14 days in different PEG hydrogel conditions (A). Quantification of GFP positive cells normalized to total cell count (B). # $p<0.05$ from mPEG. Scale bar = 200 µm.

groups had a greater mean than acellular hydrogels, although the results did not reach significance (Figure 4.3). There was no effect of pre-treating the cells with resveratrol on the mineralized matrix production of ADSCs. In addition, the incorporation of BMP-2 did not result in an increase in mineral production. The constructs on the whole largely did not mineralize. We next performed von Kossa staining on frozen sections to confirm the presence of mineral. Positive staining was found primarily where cells were present (Figure 4.4). This demonstrates that the mineralized matrix observed in the micro-CT imaging is cell-mediated. Further, we found cells in the acellular groups, demonstrating that there was some host cell invasion into the hydrogel constructs. We performed fluorescent staining with a GFP antibody to determine if the cells observed in the hydrogel are implanted cells or the host cells. While some positive GFP cells were present, the majority of the cells in the constructs were negative for GFP suggesting that most of the mineralized tissue is from the host cells, as shown in the images below.

Cell Viability in Alginate Hydrogels

Cell viability was also assessed in irradiated and oxidized-irradiated alginate hydrogels. We observed that a majority of the cells survive the mixing and injecting process of generating the hydrogel (Figure 4.5). Furthermore, the cell viability percentage was in the 80-90% range throughout the 14 day time period for all cell types and gel types, demonstrating a much higher percentage of live cells compared to the PEG hydrogel system described previously (Figure 4.6). We also observed that the cells appear much smaller at the later time points, hypothesized to be due to proliferation of the cells in the hydrogel causing crowding and a smaller phenotype. This was confirmed

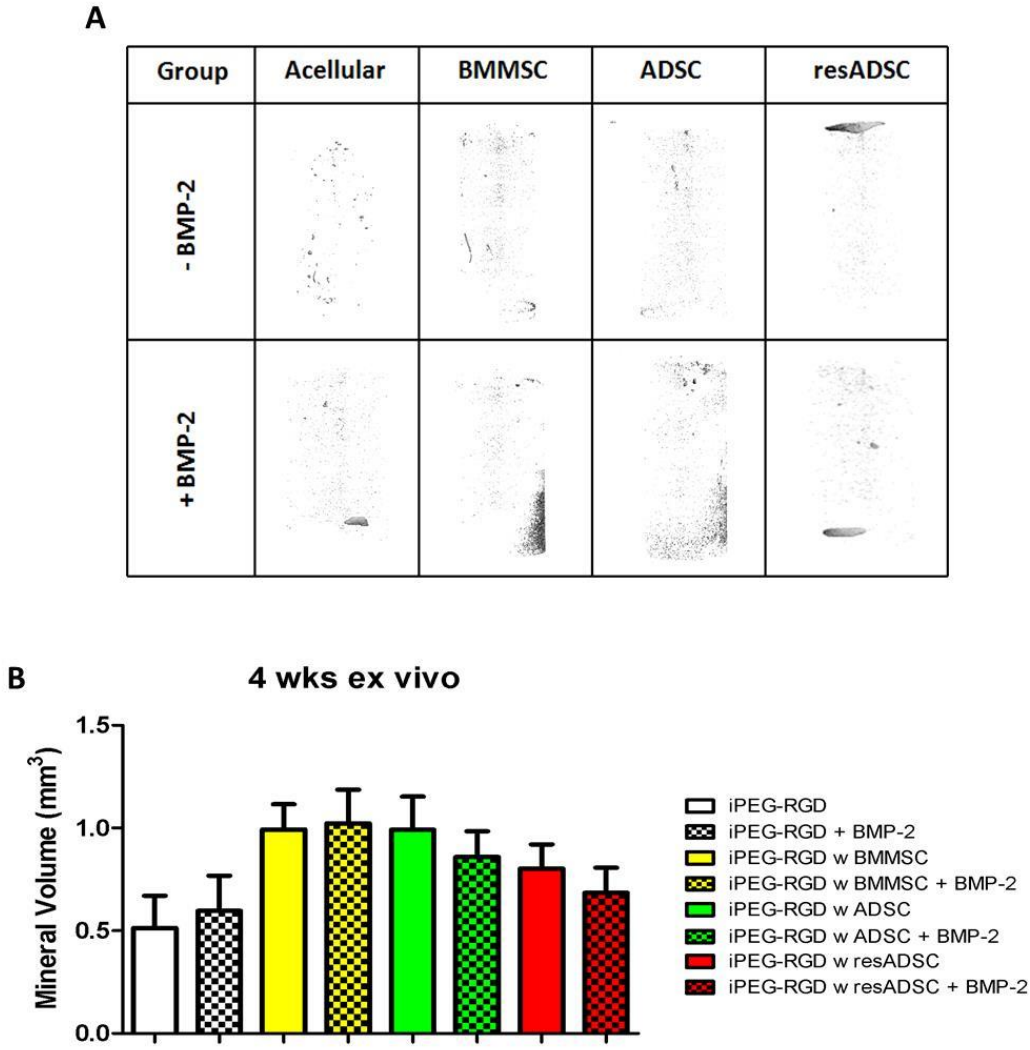

Figure 4.3 Representative micro-CT reconstructions of PEG hydrogels (A). Quantification of ectopic mineralized matrix (B).

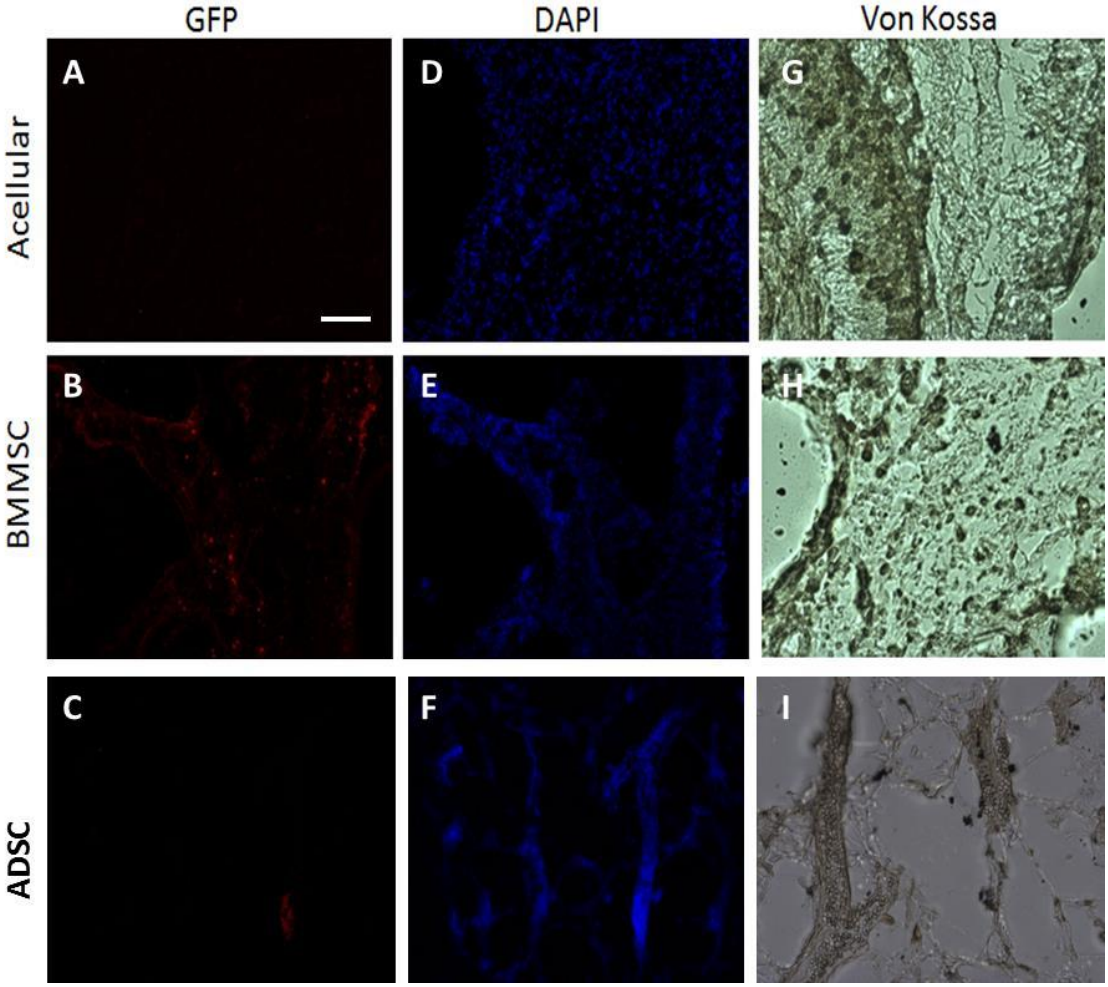

Figure 4.4 Representative images of acellular, GFP BMMSC, and GFP ADSC in PEG hydrogel following explanation. Staining for GFP (A-C), DAPI (D-F), and von Kossa staining for mineral (G-I). Scale Bar = 100 µm.

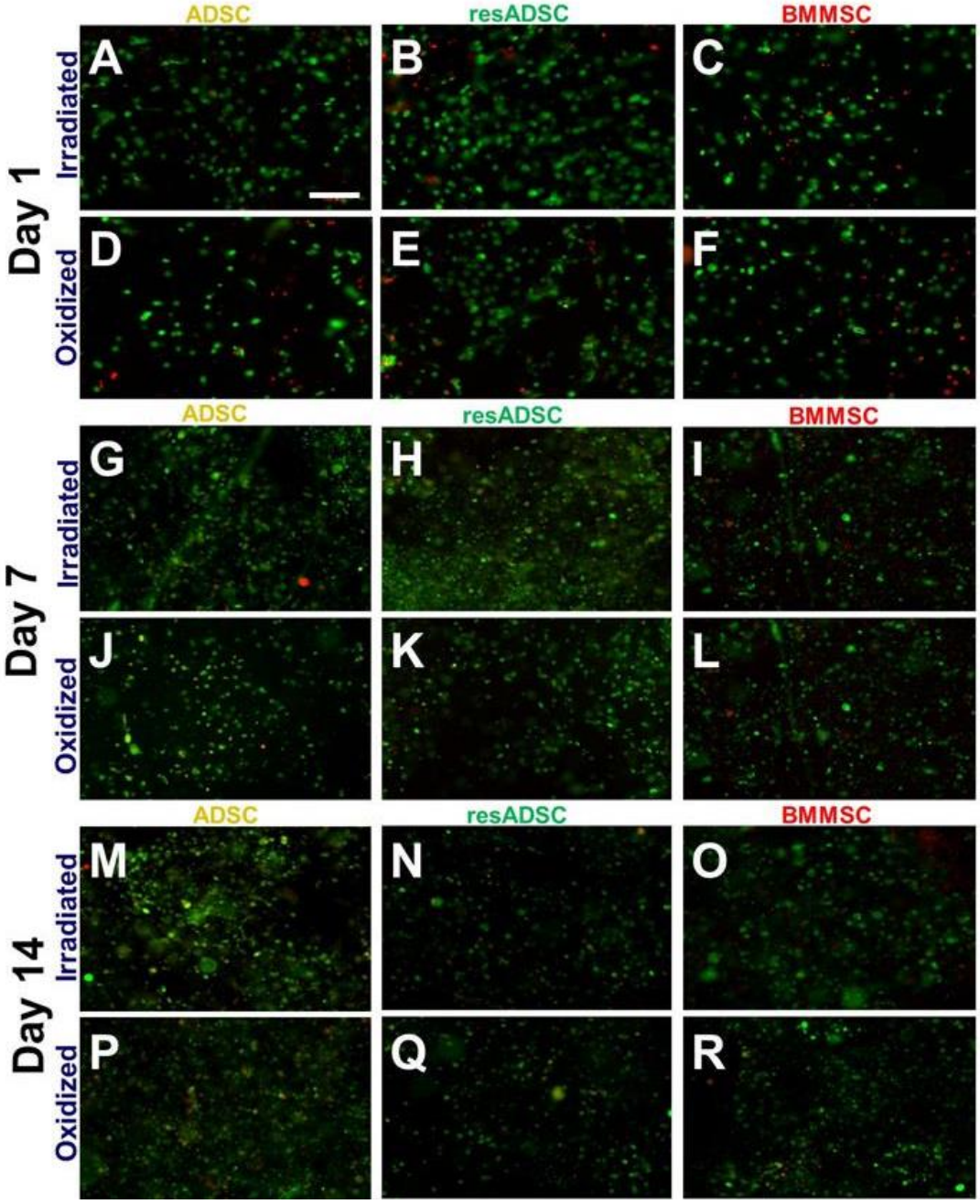

Figure 4.5 Representative images of ADSCs, resveratrol treated ADSCs, and BMMSCs over a 14 day time course. Scale bar = 100 µm.

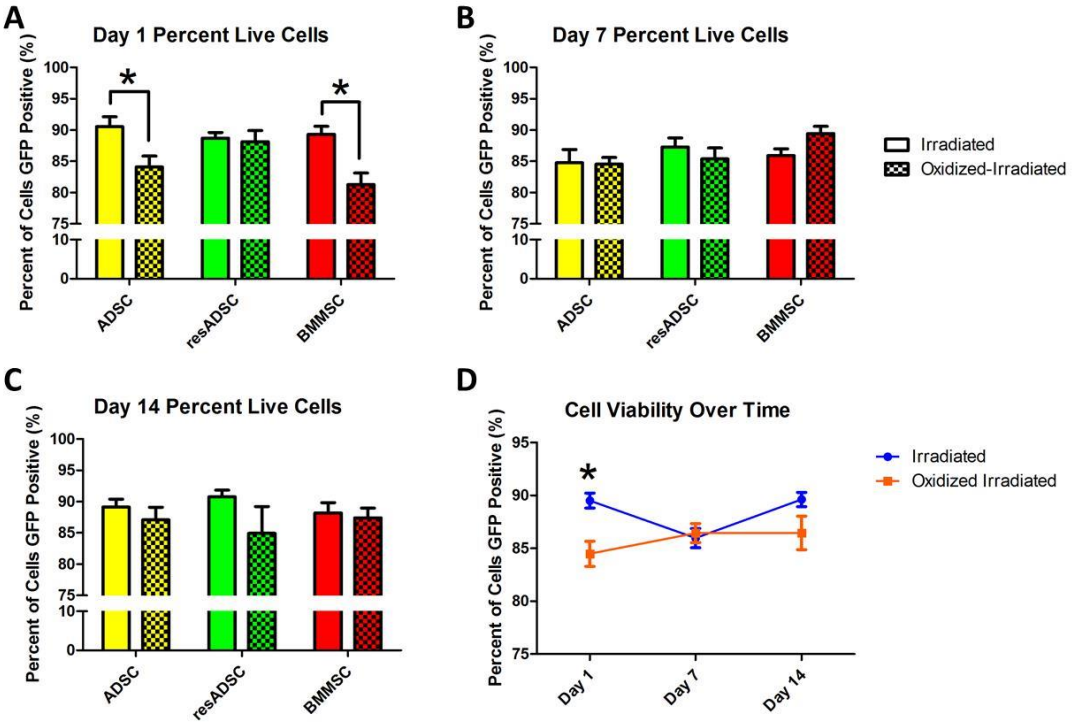

Figure 4.6 Quantification of live cells in alginate hydrogels at day 1 (A), day 7 (B), and day 14 (C). Analysis of the effect of alginate oxidation over time in terms of cell viability (D). * $p<0.05$ significantly higher than oxidized-irradiated for that cell group.

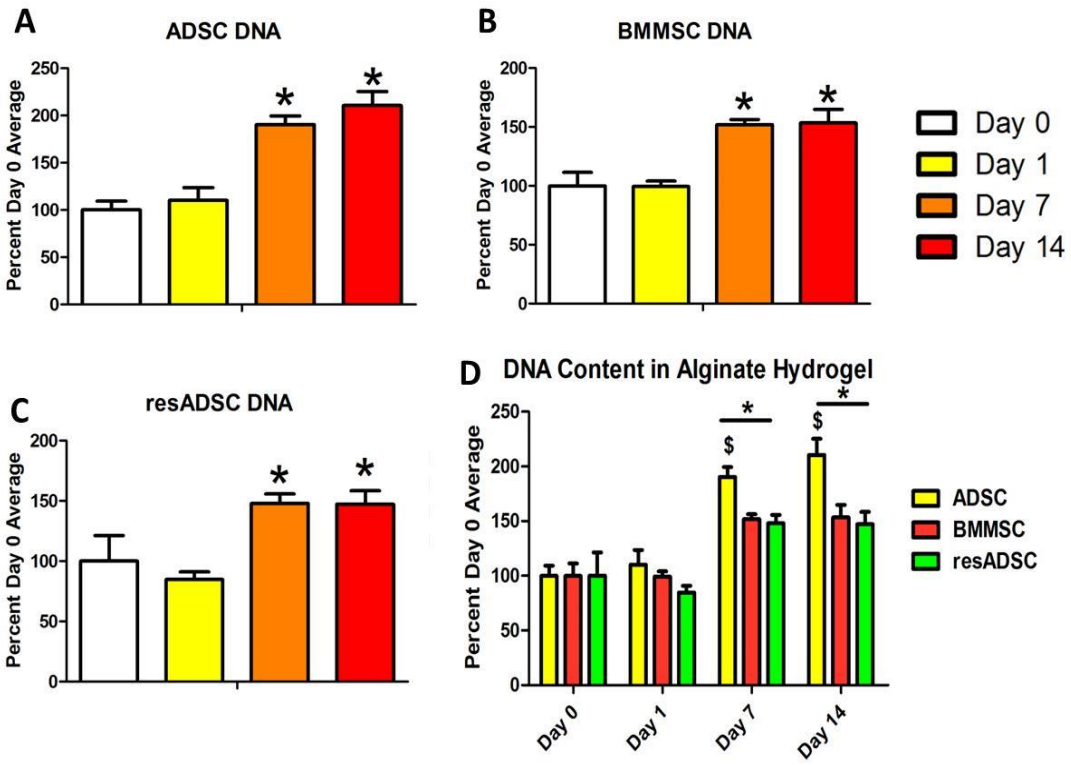

Figure 4.7 DNA levels in irradiated alginate hydrogels at day 1 (A), day 7 (B), and day 14 (C). Analysis of the effect of cell type in irradiated alginate over time in terms of cell viability (D). * $p<0.05$ significantly higher than day 1 and day 0 levels, $ $p<0.05$ significantly higher than other cell groups for that time point.

with the Picogreen DNA assay, as a significant increase in the DNA content of the hydrogel constructs between days 1 and 7 was observed for ADSC, resveratrol treated ADSC, and BMMSC cell types (Figure 4.7). When we pooled the cell groups to assess a difference in viability between the irradiated and oxidized-irradiated gel systems we observed a significant difference in cell viability with the irradiated hydrogel possessing greater viability than the oxidized hydrogel at an early time point. However at later time points there were no significant differences in the viability of the two hydrogel systems.

Degradation Kinetics of Irradiated and Oxidized-Irradiated Alginate Hydrogels *In vitro*

As the graphs above show, we observed an initial loss of approximately 20% in both the irradiated alginate gels and in the oxidized irradiated gels after only 24 hours in culture (Figure 4.8). This initial loss is most likely due to the loss of hydrogel that was not fully cross-linked. At day 7 we observed no significant differences in terms of mass loss between the two different hydrogel systems. After 14 days, the oxidized irradiated hydrogels demonstrated greater mass loss than the irradiated hydrogels. Further, we observed some differences in the cell groups between the irradiated and oxidized gels after 14 days in culture, suggesting the cells may be facilitating degradation via hydrolysis in the oxidized gels. However, these differences did not achieve significance.

Subcutaneous Ectopic Mineralization in Alginate Hydrogels

Micro-CT imaging and processing showed that the adipose derived stem cell loaded hydrogels lacked the presence of robust mineralization relative to acellular controls (Figure 4.9). Both resveratrol treated and untreated ADSCs produced less than 2

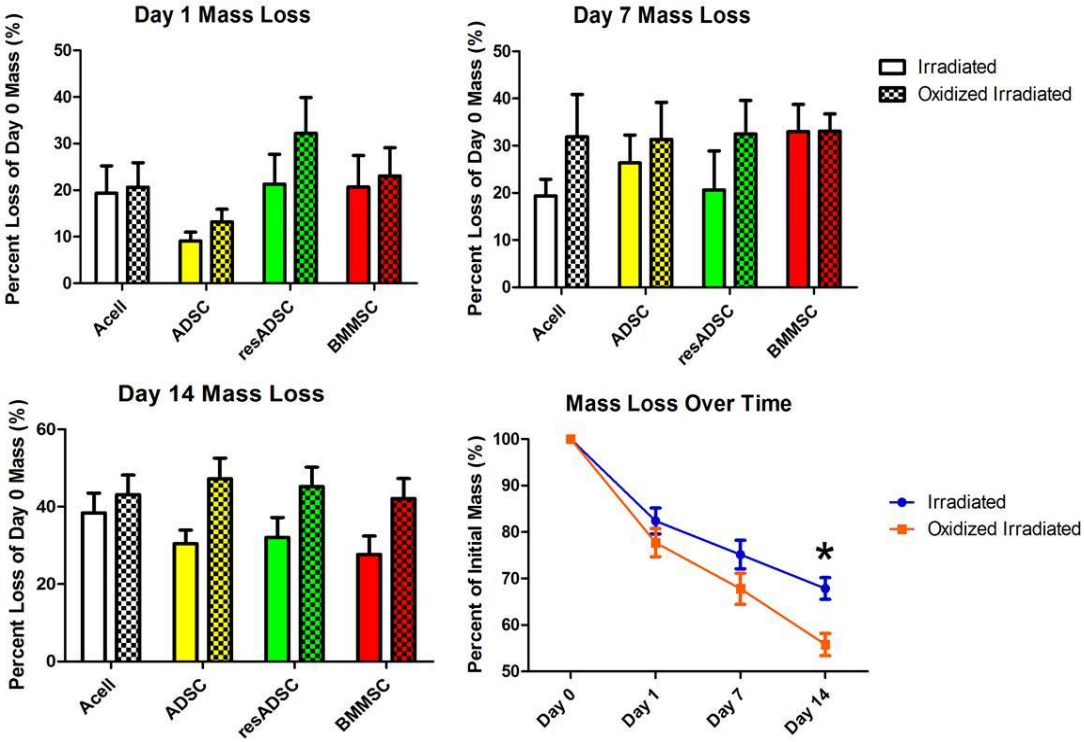

Figure 4.8 Mass loss of both irradiated and oxidized alginate hydrogels over the14 day time course. Grouping of the different cell types showed that at day 14 there was a significant increase in the total mass lost in oxidized-irradiated hydrogels. * $p<0.05$.

mm^3 of mineralized tissue and there was no effect of resveratrol treatment. The bone marrow and acellular groups produced the most ectopic mineralization *in vivo* as shown in the 3-D reconstructions (Figure 4.10). The acellular group had a mean of 13.7 mm^3 of mineralized tissue. Interestingly, 3 out of the 6 cellular samples produced robust bone formation, while the other 3 did not. The bone marrow derived stem cell group with BMP co-delivery had a mean of 31.8 mm^3 of mineralized matrix and all 6 samples produced robust bone formation. This group was significantly higher than all other groups. Removal of either the alginate hydrogel carrier or the BMP-2 resulted in a significant decrease in ectopic mineralization, demonstrating that the alginate hydrogel, BMP-2 and BMMSC cell source are all needed for consistent mineralization.

Histological Analysis of Harvested Alginate Hydrogels

Following micro-CT scanning, samples were decalcified and prepared for histology. Histological analysis was performed using H&E and Safranin-O stains, and further the presence of implanted cells was tested via immunohistochemistry for GFP positive cells. The presence of cells was observed in acellular constructs demonstrating host cell invasion into the hydrogel (Figure 4.11). ADSC loaded hydrogels had very little positive staining for mineralized tissue. In contrast, there were large areas of mineralization observed in BMMSC load hydrogels, consistent with the micro-CT data. For carrier free hydrogels, the majority of tissue present was granular and fibrous as there was no hydrogel in the construct to impede penetration of host tissue. GFP positive cells were found in cell-loaded constructs with hydrogels, but were not found in acellular constructs or constructs lacking hydrogels as expected. A majority of the cells present

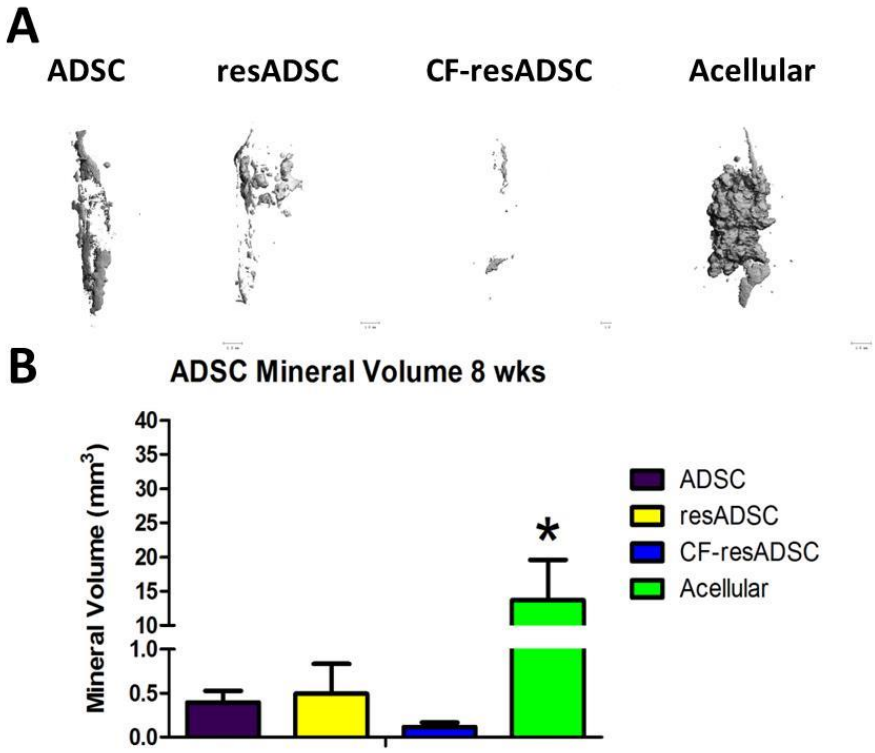

Figure 4.9. Representative micro-CT reconstructions of ADSC loaded alginate hydrogels and an acellular control (A). Quantification of mineralized tissue (B). * $p<0.05$ significantly greater than all other groups.

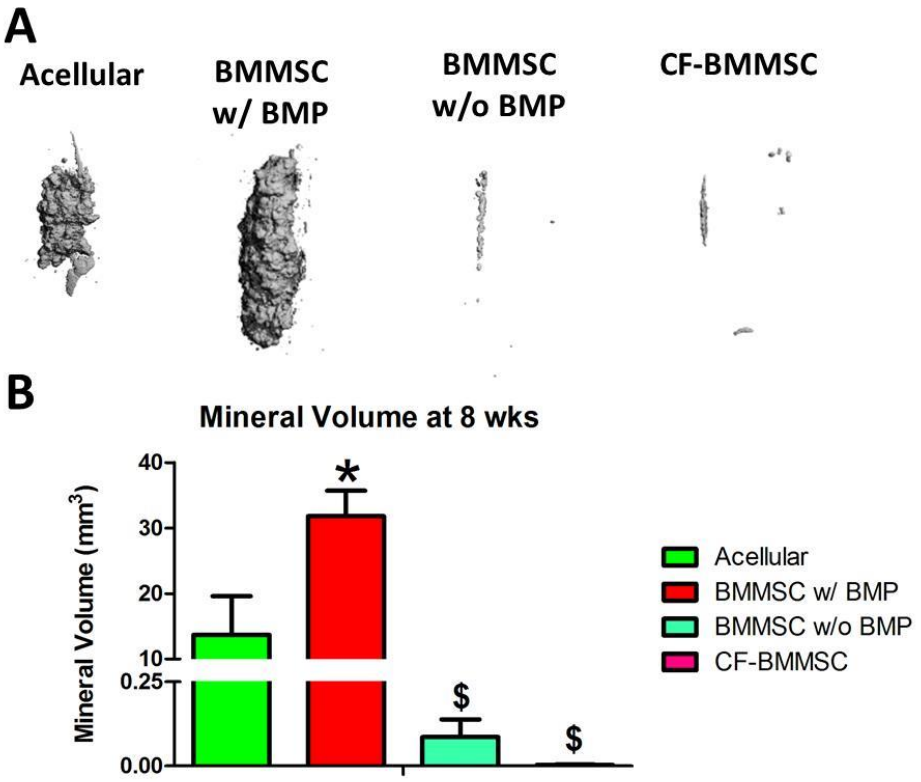

Figure 4.10. Representative micro-CT reconstructions of BMMSC loaded alginate hydrogels and an acellular control (A). Quantification of mineralized tissue (B). * $p<.05$ significantly greater than all other groups, $ $p<0.05$ significantly less than acellular constructs.

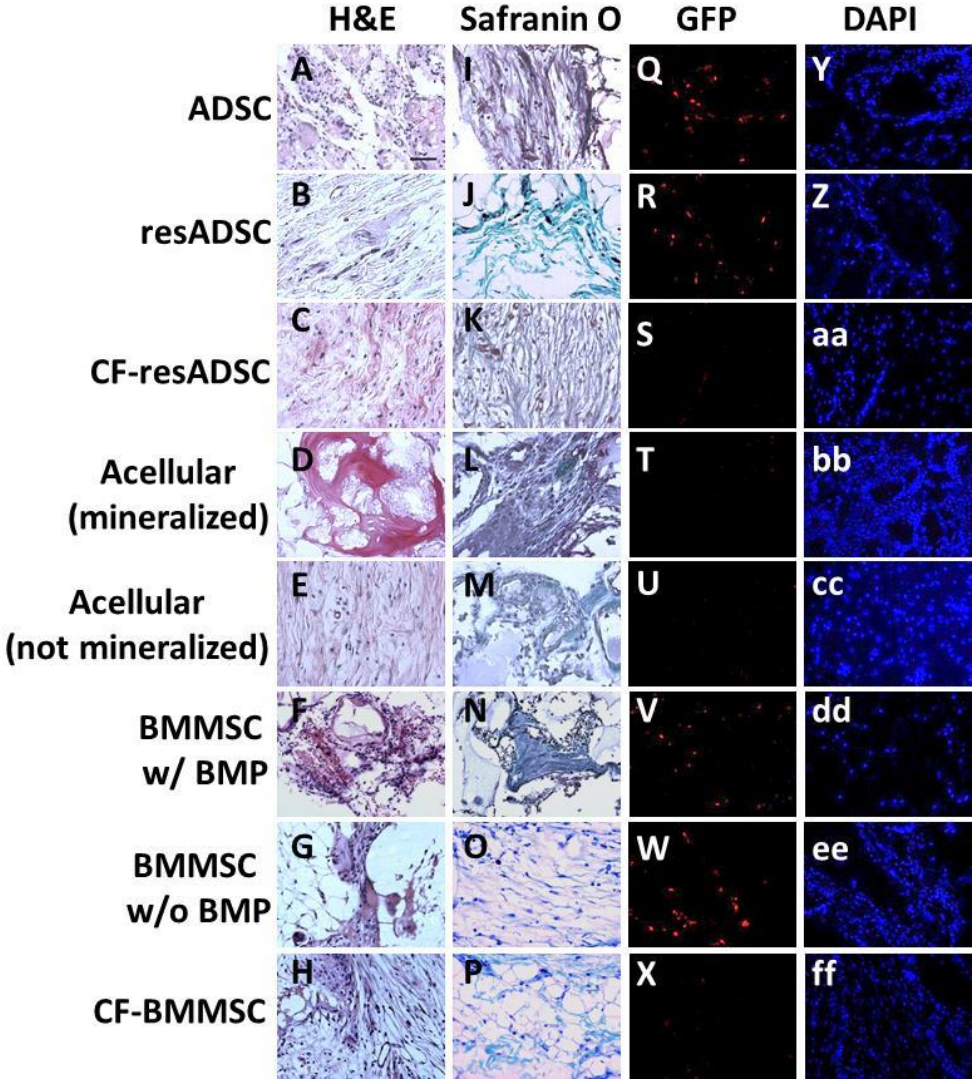

Figure 4.11. Representative histological section of alginate hydrogels H&E (A-H), Safranin-O (I-P), GFP (Q-X) and DAPI (Y-ff) were performed. Scale Bar = 100 µm.

were not positive for GFP demonstrating that the majority of the cells present in the construct after 8 weeks are invading host cells.

DISCUSSION

This set of experiments sought to investigate PEG and alginate based hydrogels as an injectable cell delivery vehicle for bone tissue engineering. Results demonstrated differences in the cell viability and bone formation potential of both materials. Alginate hydrogels had higher cell viability and facilitate greater ectopic mineral formation than PEG based hydrogels. We further demonstrated that implanted cells embedded into the hydrogels survive *in vivo*, and an effect of implanted cells was observed with bone marrow mesenchymal stem cells in alginate hydrogels. Finally, adipose derived stem cell loaded hydrogels had significantly less ectopic mineralization relative to acellular constructs in the alginate system.

The limited success of our PEG hydrogels is most likely due to the formulation of PEG chosen in this study. The PEGDA system lacked sites for enzymatic degradation, ultimately resulting in limited resorption of the hydrogel once implanted *in vivo*. Others have had greater success using PEG based materials for bone tissue engineering. Saito used a composite PLA and PEG based material for BMP-2 delivery and noted robust mineralization *in vivo* (Saito, Okada et al. 2001). However their system incorporated enzymatically degradable links that also allowed for controlled release of BMP-2. A study that had non-degrading PEG based hydrogel demonstrated that extremely large doses of BMP-2, up to 120 µg, are necessary to achieve bone formation *in vivo* (Murakami, Saito et al. 2002). Thus, the lack of resorption and low dose of BMP-2 in

our PEGDA system likely prevented host cells from reacting with the osteoinductive factor, thus limiting the amount of mineralized tissue production, as observed in the micro-CT reconstructions. In addition, the lower cell viability observed in PEG hydrogels compared to alginate is likely due to the TEMED and APS cross-linking system employed in these experiments. This system crosslinks the acrylate groups via generation of free radicals. Duan noted significant cell death in the incorporation of NIH/3T3 cells in APS and TEMED treated cultures (Duan, Zhu et al. 2005). Therefore, the generation of free radicals likely had a detrimental effect on the cells incorporated into the hydrogel thereby leading to lower viability at 14 days.

When applied to bone defect models, the presence of irradiated alginate is still detectable at 12 weeks (Boerckel, Kolambkar et al. 2011). The presence of alginate might have an inhibitory effect on the bone mechanics if it is unable to be remodeled by the host cells. We therefore examined partially oxidized irradiated alginate to determine differences in cell viability and degradation rates compared to irradiated alginate alone. Others have shown that oxidation of the alginate backbone increases its degradation *in vitro* (Bouhadir, Lee et al. 2008). In both the ADSCs and BMMSC groups, we observed a significant difference in cell viability 24 hours after encapsulation between the irradiated and oxidized-irradiated hydrogels. When forming the gels, the α-MEM that served as the dissolving agent of the oxidized alginate displayed a yellowish hue once the alginate was completely dissolved, indicative of a slightly acidic environment. This acidity may have had a detrimental effect on the cell viability at early time points, and attribute to why no differences were observed between irradiated and oxidized-irradiated hydrogels at later time points. The degradation kinetics of the irradiated and oxidized-

irradiated alginate hydrogels was relatively similar over the 14 day time course. The cells incorporated into the alginate hydrogels were in growth media and given no differentiation signals. As such, the cells had no incentive to remodel their environment which may account for the limited differences in the degradation of the hydrogels.

The difference between the results in the adipose and bone marrow mesenchymal stem cells for *in vivo* bone formation is most likely attributable to two factors: 1) cytokine signaling to host cells, and 2) time for host cell invasion. Histological analysis of our samples demonstrated a large host cell invasion into the hydrogels. In the case of adipose derived stem cells, we hypothesize that cellular waste products are likely degrading the BMP-2 present in the hydrogel preventing host cells from seeing the osteoinductive factor. Further, the BMP-2 dose chosen in this study may have been too low to induce robust cytokine activity from the ADSCs. Dudas was able to see an effect of adipose derived stem cells treated with BMP-2 at a higher dose on a gel foam scaffold in a calvarial defect (Dudas, Marra et al. 2006). Others have shown that additional factors besides BMP-2 are necessary to induce osteogenic differentiation of ADSCs (Knippenberg, Helder et al. 2006). As such, in our current system the ADSCs are likely having two detrimental effects on bone formation: too low of an osteoinductive factor signaling to stimulate endogenous host cells, and degradation of the delivered growth factor preventing endogenous cell mediated bone formation as seen in acellular hydrogels. We believe the reverse case is true for the bone marrow mesenchymal stem cells. For BMMSCs, we believe the BMP-2 is causing an up-regulation of osteoinductive factor signaling, which is why these constructs produce consistent robust mineralization compared to acellular constructs. Early time point studies examining the gene and

protein production of ADSCs and BMMSCs in these systems are needed to evaluate these hypotheses.

SUMMARY

In this study we examined the ability of both natural and synthetic hydrogels to support viability *in vitro* and ectopic mineralization *in vivo*. Results showed that extruding the hydrogel via injection in the PEG hydrogel system resulted in greater cell viability than molded hydrogels. In addition, there was an added benefit of incorporating the RGD cell attachment peptide sequence into the PEG hydrogel. However, when applied to an ectopic subcutaneous mineralization model, little mineralization was observed. There was a large amount of hydrogel still present within the nanofiber mesh tube, inhibiting tissue ingrowth. Conversely, alginate hydrogels demonstrated greater cell viability *in vitro* and supported ectopic mineralization in *vivo*. Few differences were found in cell viability in irradiated and oxidized-irradiated alginate hydrogels, and degradation kinetics were largely similar over a 14 day time course. Irradiated hydrogels were tested for as an injectable cell delivery vehicle for ectopic mineralization. Results showed that co-delivery of BMP-2 and BMMSCs generates robust deposits of mineralized tissue consistently. Adipose derived stem cell loaded hydrogels lacked robust mineralized tissue relative to acellular controls. Further, despite the effectiveness of resveratrol in increasing the osteogenic mineralization of ADSCs *in vitro*, pre-treatment resulted in no added benefit *in vivo*. Taken together, these results suggest that incorporation of BMMSCs and BMP-2 into an irradiated alginate based hydrogel will be an effective therapeutic intervention for a cell based tissue engineering approach in a non-healing bone defect model.

CHAPTER 5: EFFECT OF DELIVERY TIME ON THE REGENERATION OF BONE IN A NON-HEALING SEGMENTAL BONE DEFECT

ABSTRACT

The healing of critically sized diaphyseal defects remains a clinical problem. A stem cell based approach is an attractive option for current treatment techniques. In this set of studies, we sought to examine the ability of stem cells to heal a critically sized defect in the femur of the rat using an alginate based hydrogel as an injectable carrier for bone marrow mesenchymal stem cells (BMMSCs). We further investigated whether delaying the time of implantation altered the healing response. Potential delayed delivery time points were determined by examining tissue infiltration into empty defects over a 14 day time course. We next attempted to deliver our therapeutic using a blind percutaneous technique into the defect site at 14 days without reopening and reinjuring the tissue surrounding the defect site. Inaccurate delivery resulted in unhealed defects, with the hydrogel mineralizing in surrounding tissues. It was further observed that at 14 days there is too much infiltrated tissue to deliver the hydrogel. We therefore altered our technique with a second procedure at 7 days and injected the hydrogel with as little damage to surrounding tissues as possible. Quantification of mineralized tissue demonstrated that delaying the injection of the hydrogel for 7 days resulted in less bone formation than immediate delivery of the hydrogel, however BMMSC incorporation resulted in greater bone formation than acellular constructs for both the immediate and delayed treatment groups by 12 weeks. We therefore conclude that immediate delivery

of alginate hydrogels with BMMSCs is an effective strategy for the treatment of large bone defects.

INTRODUCTION

In the case of volumetric bone loss, such as traumatic injury or in tumor resection, loss of progenitor cells or damage to surrounding tissue can limit the endogenous healing capacity of the patient, resulting in nonunion of the defect (Bruder and Fox 1999). There is a large clinical need for effective treatment of such defects. According to the United States Bone and Joint Decade, musculoskeletal conditions are the most commonly reported health conditions in U.S. citizens, occurring in roughly 48% of the population. Beyond the associated physical afflictions is the enormous financial burden - $849 billion in 2004 alone (Decade 2009). Bone grafting procedures have an annual incident occurrence greater than 500,000, resulting in a cost greater than $2.5 billion in the United States alone (Laurencin, Khan et al. 2006).

Current clinical treatment modalities for management of large bone defects are limited and often ineffective. The clinical gold standard for treatment of large segmental bone defects is autologous bone grafting. This procedure, however, is severely constrained by a limited supply of available graft material, insufficient structural properties, and significant donor site morbidity. Another often-employed treatment is allograft tissue obtained from cadavers. Again, this treatment possesses significant limitations, including an unacceptably high rate of post-implantation failure. This is largely attributable to an inability of the graft tissue to fully revascularize and remodel leading to decreased integration of the graft to the host tissue. There are also additional

concerns with regard to disease transmission and immune rejection with allograft use (Nandi, Roy et al. 2010). The occurrence of refracture varies depending on the size of the graft, but has been reported to be as high as 25-35% (Sorger, Hornicek et al. 2001). As such, alternative treatment strategies are warranted to address the shortcomings of current treatment modalities.

A new grafting approach has emerged in the clinical treatment of large bone defects: the Masquelet technique. In this procedure, a multi-step operation is undertaken to heal a diaphyseal defect. The first procedure consists of debridement of the bone and surrounding soft tissue, and the placement of a large cement spacer in the area of a bone defect (Nauth, McKee et al. 2011). The spacer serves two functions: first, the spacer prevents fibrous tissue invasion into the defect site, and second, the foreign body response induced by the spacer will form a membrane surrounding the defect site (Giannoudis, Faour et al. 2011). The defect is fixed with an external stabilizer and the surrounding soft tissues are allowed to heal. In the second procedure, the spacer is removed with as little disruption of the newly formed membrane as possible, and trabecular bone chips are placed in the defect site to allow healing. This technique has been shown to be effective both in animal models and in clinical practice for tibia and femur defects (Klaue, Knothe et al. 2009, Stafford and Norris 2010). The membrane surrounding the spacer has been shown to be well vascularized and expresses angiogenic and osteogenic factors, including BMP-2, thereby inducing bone formation in the defect site (Pelissier, Masquelet et al. 2004).

While the Masquelet technique has been shown to be effective in the treatment of long bone defects, it is still dependent on the harvesting of autologous or allograft tissue.

Utilizing stem cells and osteoinductive growth factors in a tissue engineering approach for bone regeneration may alleviate the need for grafting substrates. Previous studies in our lab have demonstrated that injectable alginate based hydrogels are in effective strategy for growth factor delivery in the treatment of critically sized diaphyseal defects in a guided bone regeneration technique (Boerckel, Kolambkar et al. 2011, Kolambkar, Boerckel et al. 2011). However, we have not investigated incorporating stem cells into the alginate hydrogel delivery system, nor have we assessed timing of delivery of the alginate hydrogel to the defect site.

The purpose of this study was to investigate the use of an injectable alginate hydrogel system loaded with bone marrow mesenchymal stem cells to heal a critically sized diaphyseal defect in the femur of the rat. We hypothesized that delaying the delivery of stem cells to the defect site would lead to greater bone regeneration. Tissue infiltration between the creation of the defect and the delivery of the hydrogel would allow for greater nutrient exchange and a possible increase in the recruitment of endogenous osteoprogenitors to the defect site. Potential delayed delivery time points were determined by examining tissue infiltration into empty defects over a 14 day time course. We next attempted to deliver our therapeutic using a blind percutaneous technique into the defect site at 14 days without reopening and reinjuring the tissue surrounding the defect site. Inaccurate delivery resulted in unhealed defects, with the hydrogel mineralizing in surrounding tissues. We therefore employed a two-step surgery technique, similar to the Masquelet technique previously described albeit without a spacer in the defect site. The second procedure at 7 days involved injecting the hydrogel

with as little damage to surrounding tissues as possible. All studies used a non-healing dose of BMP-2 to assess the influence of cells in the repair process.

METHODS

GFP BMMSC Isolation

Genetically modified Sprague Dawley rats that express GFP ubiquitously (SD-Tg(GFP)2BalRrrc) were obtained from the Rat Resource and Research Center (RRRC, Columbia, MO). 3 males weighing 120-150 grams were euthanized and bone marrow harvested as described previously. Femurs and tibias were harvested aseptically. The epiphyseal ends were cut on both ends and the marrow flushed out in α-MEM into tissue culture plates. After 1 hour, the media was collected and then re-plated onto new tissue culture plates. 48 hours later the media was aspirated off and the adherent cells grown to 90% confluence, with media changes occurring every 48 hours. The cells were cryopreserved following expansion.

Alginate Hydrogel Formation

Alginate hydrogels were prepared as described previously (Boerckel, Kolambkar et al. 2011). Sterile irradiated RGD functionalized alginate was obtained from FMC Biopolymer (FMC Biopolymer, Philadelphia, PA). Alginate hydrogels were prepared by dissolving the lyophilized powder in α-MEM to a 3% w/v solution. The 3% w/v solution was then diluted to a 2% solution with either α-MEM or α-MEM containing 1 million cells. For BMP-2 containing gels, rat serum albumin (RSA, Sigma Aldrich, St. Louis, MO) was dissolved in 4 mM hydrochloric acid to obtain a .1% solution and mixed with the lyophilized BMP-2 protein. The BMP-2 solution was added to a syringe at a concentration of 1 μg/150 μL of hydrogel. Non-BMP-2 containing hydrogels just

received the RSA carrier solution. All solutions were sterilely mixed in 1 mL syringes with Luer-Lok connectors (Cole-Palmer, Vernon Hill, IL). Alginate hydrogels were prepared immediately prior to the surgical procedure.

PCL Nanofiber Mesh Tube Formation

PCL nanofiber mesh tubes were developed as described previously (Kolambkar, Boerckel et al. 2011). Poly (ε-caprolactone) (PCL) pellets (Sigma-Aldrich, St. Louis, MO) were dissolved in a 90:10 volume ratio of hexafluoro-2-propanol (HFP):dimethylformamide (DMF) (Sigma-Aldrich) to obtain a 12% (w/v) polymer solution. The solution was stirred overnight and until the solution was homogenous. The polymer solution was loaded in a 5 mL syringe (Becton-Dickinson, Franklin Lakes, NJ), and a 22 gauge blunt stainless steel needle (Jensen Global Inc., Santa Barbara, CA) was attached to the syringe end. The syringe was mounted on a syringe pump (Harvard Apparatus, Holliston, MA) set at a rate of 0.75 mL/hr. Electrospun fibers were collected on foil covering a copper plate (McMaster-Carr, Atlanta, GA) which was placed at a distance of 20-23 centimeters from the needle end. Fibers were electrospun for 5 hours at a voltage of 15-20 kV, supplied by a high voltage power supply (Gamma High Voltage Research, Ormond Beach, FL). The residual solvent from the meshes was allowed to evaporate by placing them in a dessicator until use. Sheets of electrospun nanofibers were cut via laser cutter (Universal Laser Systems, Scottsdale, AZ) into 12mm x 18 mm squares, with 1 mm holes perforating the middle of the mesh to allow nutrient transport. Meshes were removed from the foil by submerging them in 70% ethanol (VWR, West Chester, PA). The rectangular mesh samples were then wrapped around a stainless steel mandrel (McMaster-Carr, Atlanta, GA) to form a tube approximately 5 mm in diameter

and 12 mm length. The overlapping edges of the mesh were secured via UV glue (DYMAX Corporation, Torrington, CT), which was cured with a LED spot curing lamp (DYMAX Corporation). Tubes were then placed in ethanol for overnight evaporation. Prior to use, tubes were washed thrice with PBS (Mediatech Inc., Manassas, VA.)

Surgical Procedures

Female RNU Nude Rats (Harlan, Tampa, FL) aged 14 weeks underwent a bilateral segmental defect procedure as described previously (Oest, Dupont et al. 2007, Kolambkar, Boerckel et al. 2011). Briefly, diaphyseal defects were performed in the femur. Defects were stabilized with a polysulfone internal fixation plate modified with two holes in the center to allow for injection into the defect site (Appendix C). Following attachment of the fixation plate, an 8 mm segment of bone was removed from the diaphysis. A PCL nanofiber mesh tube was then placed in the defect site. For the empty defect and delayed defect groups, the defect site was left unfilled with the surrounding muscle sutured and the skin closed with wound clips. Groups receiving immediate treatment had a hydrogel implanted into the defect site, followed by closure.

For percutaneous delivery, following closure of the skin the internal fixation plate was palpated and the center holes of the plate were found by probing with a needle. The syringe containing the appropriate hydrogel was then guided through the hole and 150 µL of hydrogel was delivered to the defect site. The same procedure was followed for delayed implantation animals at 14 days prior to removal of the wound clips from the initial surgery.

For animals receiving two procedures, the animal was reopened 7 days post creation of the defect. Briefly, the wound clips from the initial surgery were removed.

Table 5.1. Groups for Percutaneous Delivery of Hydrogel

Group	Hydrogel	Cells	BMP-2	Implantation Day
BMP + Cells	RGD Alginate	1e6 GFP BMMSC	1.0 µg	0, 14 Days
BMP	RGD Alginate	None	1.0 µg	0, 14 Days
Carrier Free	None	1e6 GFP BMMSC	1.0 µg	0, 14 Days

Table 5.2. Groups for 2nd Procedure Delivery of Hydrogel

Group	Hydrogel	Cells	BMP-2	Implantation Day
No BMP	RGD Alginate	None	None	0, 7 Days
BMP	RGD Alginate	None	1.0 µg	0, 7 Days
BMP + Cells	RGD Alginate	1e6 GFP BMMSC	1.0 µg	0, 7 Days

Scabbed tissue was cut away from the initial incision using a scalpel, and the initial incision was reopened. The medial sutures in the surround muscle were cut, and the syringe containing the appropriate hydrogel was then guided through the center holes of the fixation plate and 150 μL of hydrogel was delivered inside the nanofiber mesh. The muscle was then re-sutured around the fixation plate, and the skin closed via wound clips.

Faxitron Radiograph Imaging

Digital radiographs (Faxitron MX-20 Digital; Faxitron X-ray Corp., Wheeling, IL) were performed at an exposure time of 11 s and a voltage of 25 kV with the animals under anesthesia. Animals were imaged at weeks 2, 4, and 8 and 12 post defect creation.

Micro-CT Imaging

Live animal *in vivo* micro-CT scans (VivaCT 40, Scanco Medical, Basserdorf, Switzerland) were performed with a 38.0 micron voxel size at a voltage of 55 kVp and a current of 109 μA. Analysis of newly formed bone was done with a lower threshold of 125, corresponding to approximately half the threshold of native cortical bone. The scans were segmented such that only bone inside the nanofiber mesh was included in the analysis. Scans were performed at 4, 8 and 12 weeks post defect creation.

Ex-vivo scans of harvested femurs were performed at a 21 micron resolution. To assess bone remodeling on the ends of the defect site in empty defects over a 14 day time course, samples were scanned and the first 25 slices adjacent to the defect site were segmented for trabecular bone in the medullary cavity.

Histological Analysis

Samples were decalcified in Immunocal (Decal Chemcial Corporation, Tallman, NY) and prepared for paraffin processing. Histological analysis was performed using H&E staining for general morphology, and Safranin-O for mineralized tissues.

Immunohistochemistry was performed for pan macrophage presence in decalcified empty defects via CD68 staining according to the manufacturer protocol (AbD Serotec, Bio-Rad, Raleigh, NC). Depariffinized sections were stained for the presence of GFP using a primary GFP antibody according to manufacturer instructions (Abcam, Cambridge MA). Briefly, our immunohistochemistry procedure was as follows: a 1:100 solution of primary antibody to PBS was placed on sectioned tissue and incubated overnight at 4 degrees Celsius. A secondary fluorescently tagged Texas-Red antibody was incubated for 1 hour. Samples were then cover slipped and imaged at 10X magnification using the Zeiss Axio Observer. Sections were also stained for nuclei using DAPI (Invitrogen) to discern antibody tagged cells from implanted cells.

Statistical Analysis

Data are presented as the mean and standard error. Data was analyzed via ANOVA with a Tukey's post hoc test for significance. Significance was determined with an alpha level of .05.

RESULTS

Empty Defect Characterization

An 8 millimeter segmental defect was created in the femur and a poly-caprolactone nanofiber mesh was implanted into the defect site. After the mesh was implanted, the muscle and skin were sutured and closed leaving the defect site empty. At days 3, 7 and 14 femurs were harvested and examined for tissue infiltration into the defect site. Micro-CT imaging showed that little bone formation occurred in the defect site over the 14 day time course (Figure 5.1A). Analysis of the cancellous bone in the medullary cavity demonstrated that on the proximal side of the defect there was bone

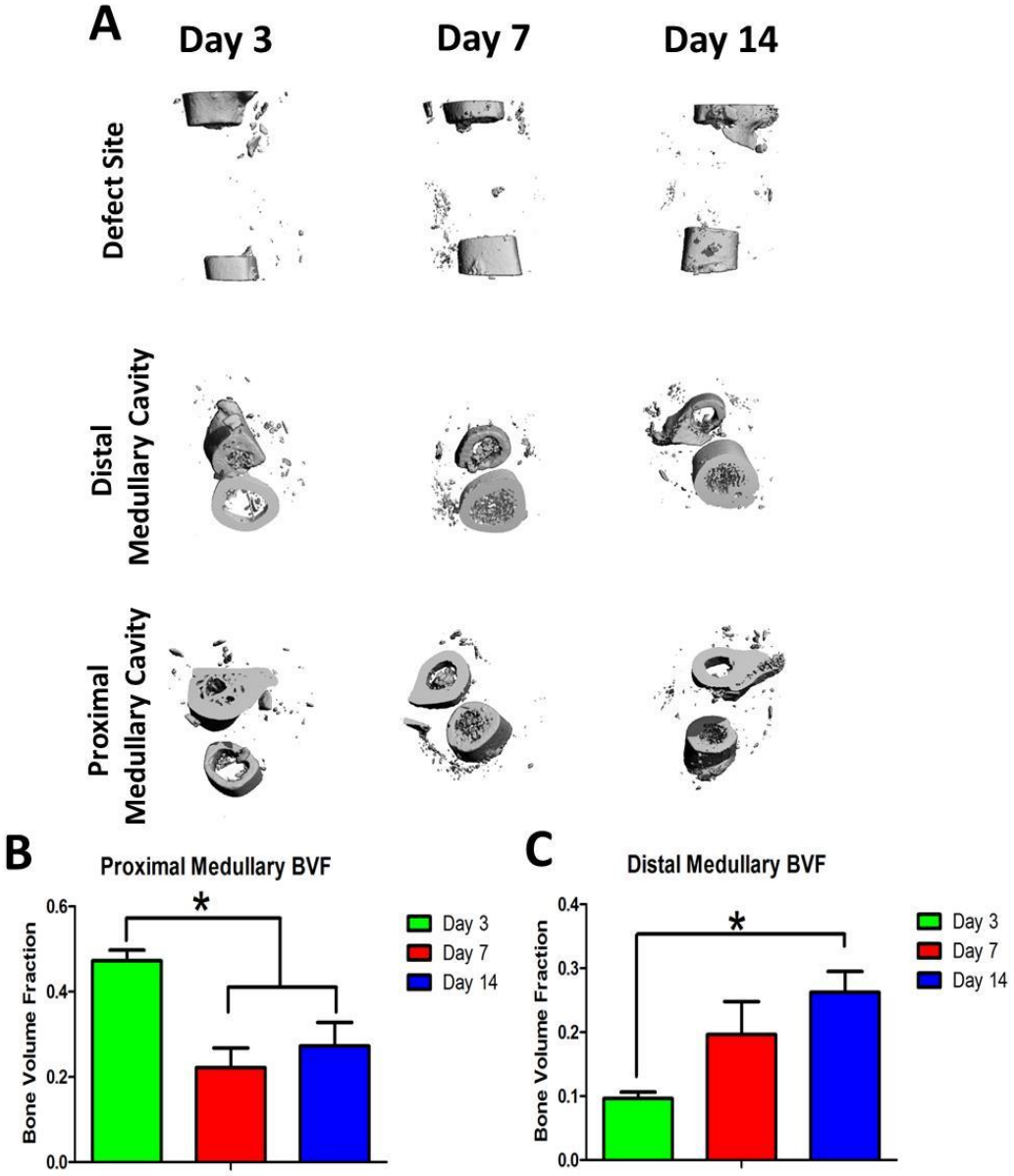

Figure 5.1 Micro-CT reconstructions of empty segmental defects over a 14 day time course (A). Quantification of cancellous bone volume fraction in the medullary cavity in the bone ends adjacent to the defect site (B). * $p<0.05$.

remodeling causing a significant decrease in the cancellous bone volume fraction over time (Figure 5.1B). Conversely, on the distal side there was a significant increase in the cancellous bone in the medullary cavity (Figure 5.1C). It should be noted that both sides approached similar bone volume fractions by day 14, and demonstrates bone remodeling occurs quickly after the creation of the defect.

Histological analysis showed that over the 14 day time course there is a gradual filling of the defect site with granular tissue. At day 3 the defect site is still largely empty and there are few macrophages present in the defect site (Figure 5.2). Polymorphonuclear cells, indicative of neutrophils, were observed in the defect site and at the bone ends. By day 7 there is more tissue present in the defect site. Immunohistochemistry for macrophages showed a large presence of CD68 positive cells in the defect site demonstrating macrophage infiltration (Figure 5.3). A large polymorphonuclear cell presence was also observed via H&E staining. By day 14, the defect site is nearly filled with host tissue (Figure 5.4). On the bone ends, the tissue had an organized structure which may be indicative of the beginning of 'end capping', where the periosteum bridges the cortices adjacent to the defect site in critically sized defects that do not achieve union. There was also a large presence of macrophages and polymorphonuclear cells present in the defect site at this time. The presence of host tissue suggested that the implanted cells would be able to achieve nutrient exchange facilitating their survival. Further, as one of the goals of this work is to determine if a carrier is needed for cell delivery at a delayed time point, the 14 day time point possibly allows for implanted cells to graft into the infiltrated host tissue. We therefore chose 14 days as our delayed implantation time point.

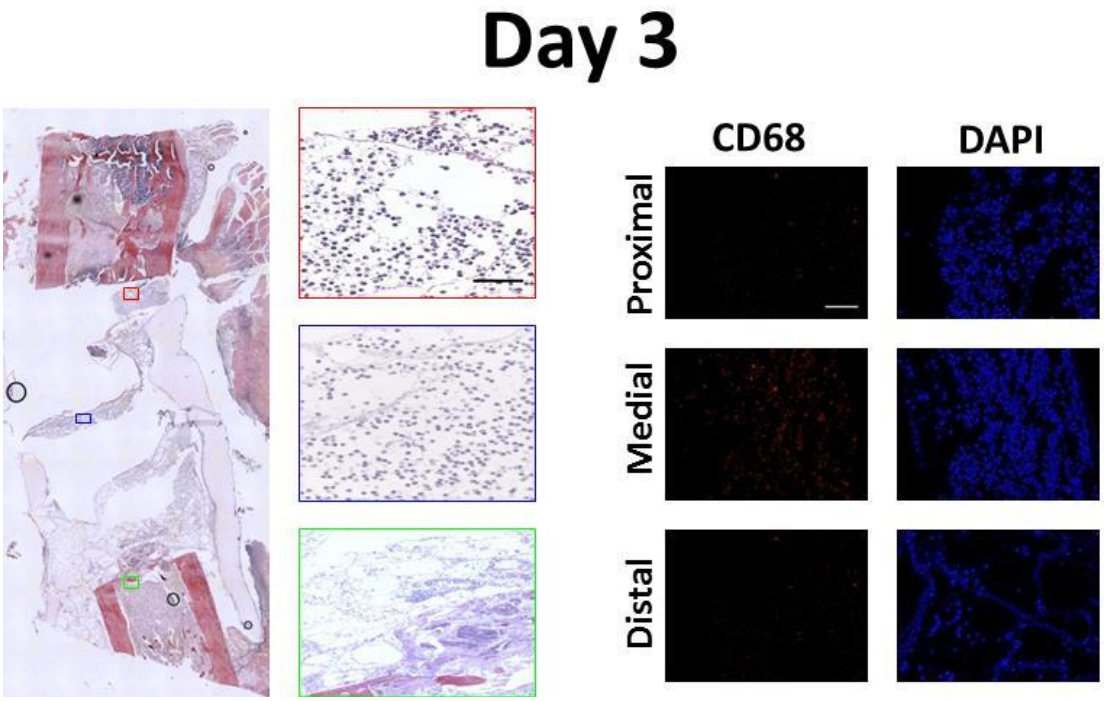

Figure 5.2 Histological analysis of 8 millimeter empty defects 3 days post defect creation. H&E Stain and immunohistochemistry for CD68. Scale Bar =100 µm.

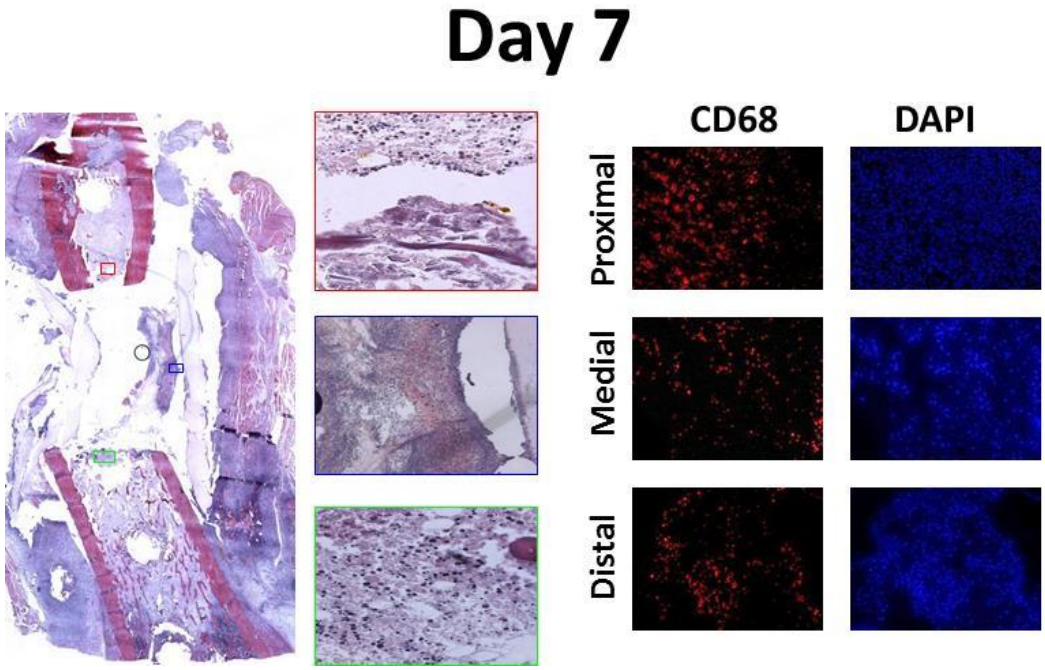

Figure 5.3 Histological analysis of 8 millimeter empty defects 7 days post defect creation. H&E Stain and immunohistochemistry for CD68.

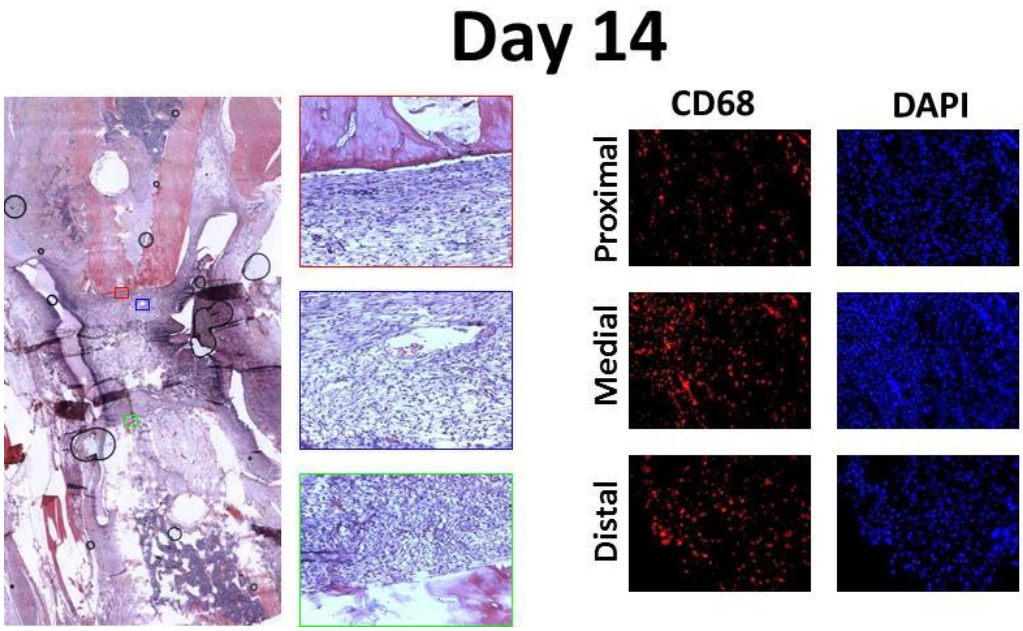

Figure 5.4 Histological analysis of 8 millimeter empty defects 14 days post defect creation. H&E Stain and immunohistochemistry for CD68.

Percutaneous Delivery of Hydrogels to Segmental Bone Defect

With the identification of a delayed time point of 14 days, we performed a study to investigate the difference between immediate delivery and delayed delivery of the therapeutics. Groups tested were: 1) Alginate hydrogels loaded with 1 million GFP BMMSCs and 1 μg of BMP-2, 2) cell free alginate hydrogels containing 1 μg of BMP-2, and 3) carrier free constructs consisting of cells in α-MEM and 1 μg of BMP-2. All constructs were delivered percutaneously with the immediate injection occurring after the animal had been sutured and stapled following the segmental defect surgery. The delayed time point injections occurred just prior to wound clip removal from the initial surgery.

The results show that the percutaneous delivery of the hydrogel through the skin is highly variable in terms of location of the hydrogel. Particularly for the immediate time point, many of the hydrogels were delivered past the defect site and into the surrounding tissue (Figures 5.5, 5.6, 5.7). Despite the inaccuracy of the delivery of therapeutics, some observations about the effectiveness of the therapeutics at the two different time points can be obtained. For the immediate injection, all 5 of the cell loaded alginate hydrogels mineralized with 4 mineralizing ectopically in the surrounding muscle and the 1 sample delivered accurately mineralizing in the defect site (Figure 5.5). For cell free hydrogels, 3 out of 5 produced mineral all of which were ectopically in the surrounding muscle (Figure 5.6). This rate of mineralization for these two groups agrees with what was observed in the subcutaneous model for the groups respectively as discussed in Chapter 4. For the carrier free, none of the samples mineralized ectopically or in the defect site. For one sample mineralization along the mesh was observed (Figure

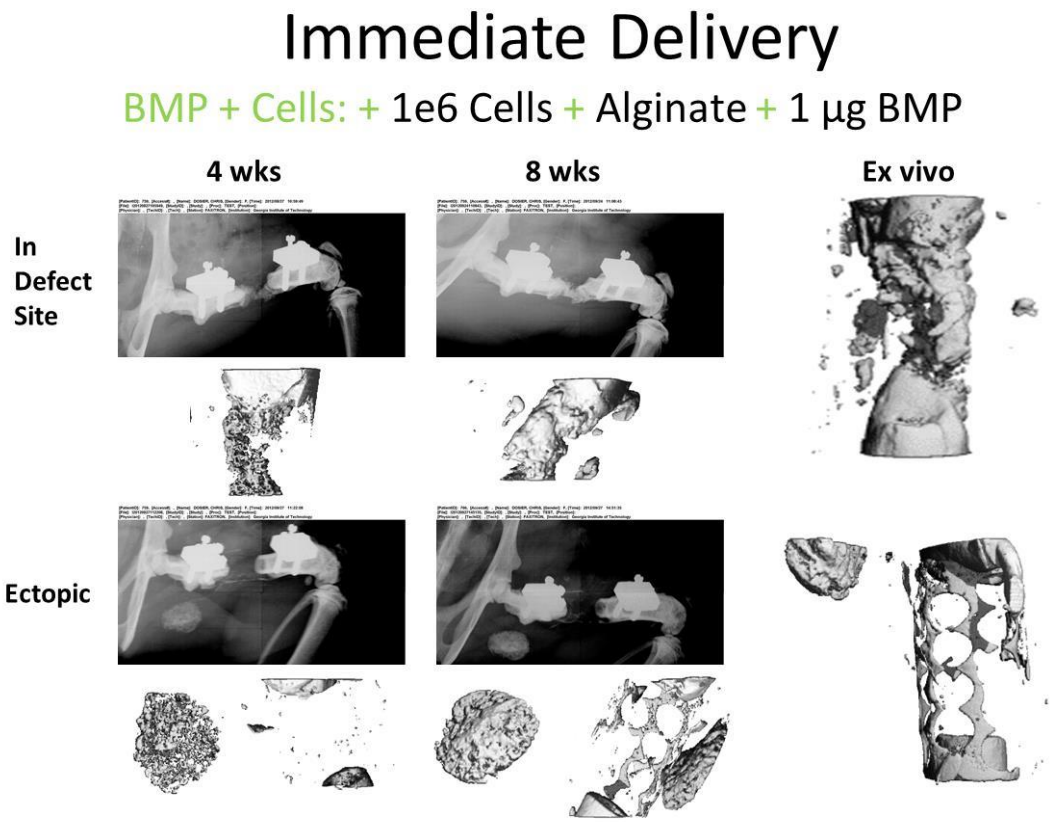

Figure 5.5 Radiograph and Micro-CT reconstruction of percutaneously delivered hydrogel containing BMP-2 and BMMSCs. Top row shows a hydrogel delivered to the defect site. Bottom row shows a representative ectopic mineralization sample due to inaccurate delivery.

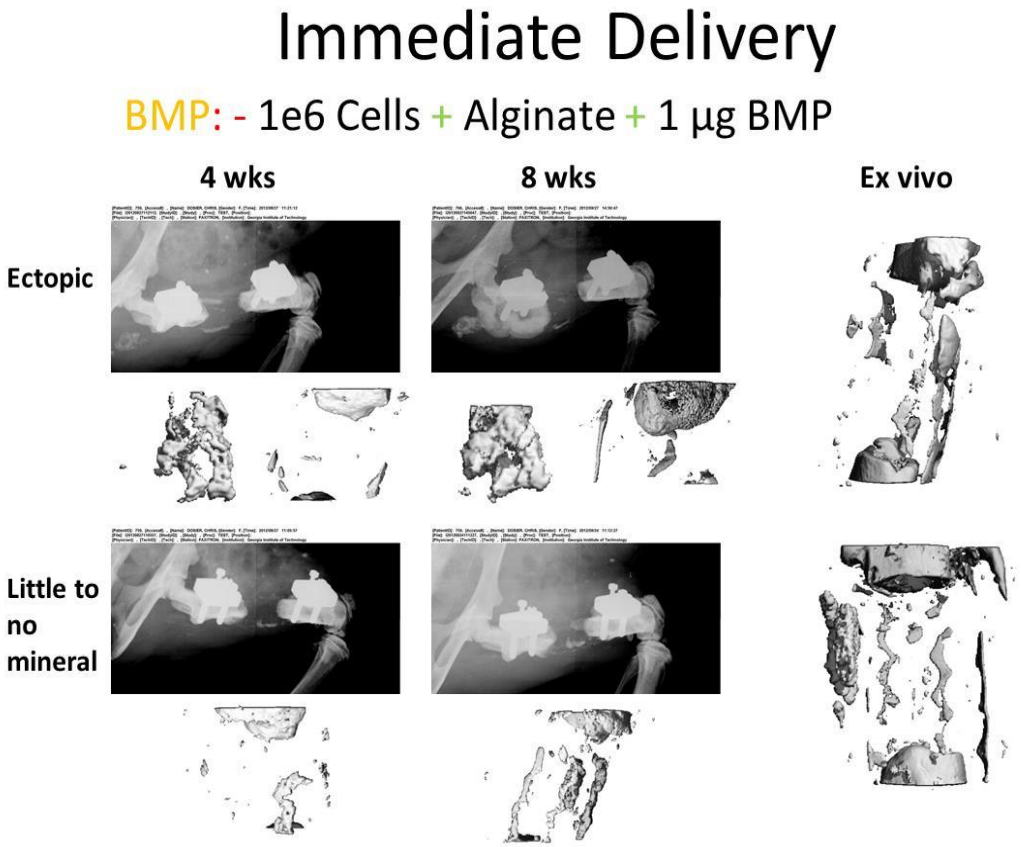

Figure 5.6 Radiograph and Micro-CT reconstruction of percutaneously delivered hydrogel containing BMP-2. A representative ectopic mineralization sample due to inaccurate delivery is shown in the top row. Bottom row is a representative of a sample with little bone formation observed anywhere in the limb.

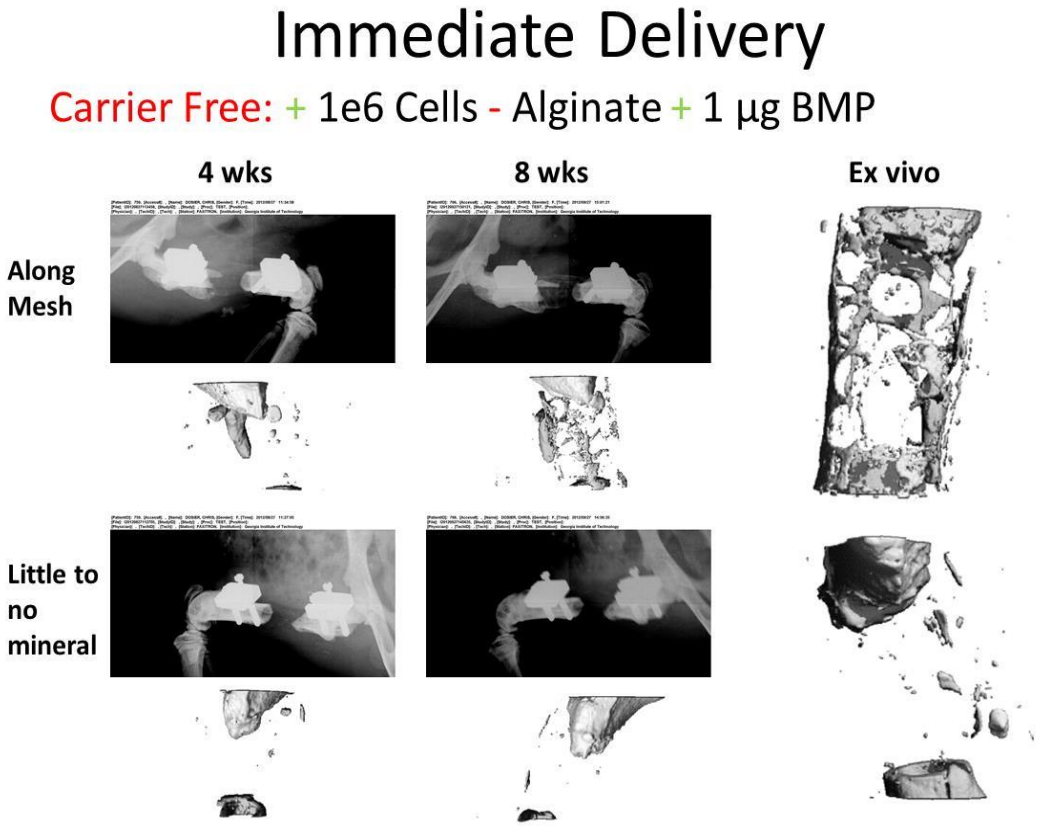

Figure 5.7 Radiograph and Micro-CT reconstruction of percutaneously delivered solution of cells and BMP-2. The top row shows a mesh with significant mineralization, possibly due to cell attachment to the mesh. Bottom row is a representative of a sample with little bone formation observed anywhere in the limb.

5.7). The lack of mineralization is most likely attributable to ambulation of the limb resulting in dispersion of the therapeutic since there is no hydrogel to retain the cells and BMP-2 at the injection site.

With more experience in delivering the hydrogels percutaneously, the delayed delivery hydrogels were delivered closer to the defect site. However in some samples part of the hydrogel ended up outside the nanofiber mesh. Results demonstrate that for the acellular constructs the mineralization response appears to be less than what was observed with 1 µg of BMP-2 in previous studies in our lab (Boerckel, Kolambkar et al. 2011). This is possibly due to failure of delivery of the entire 150 µL to the defect site and also the presence of host tissue retarding the ability of the hydrogel and BMP-2 to form a continuous volume of bone. For cell-loaded constructs, there appears to be a similar amount of bone formation compared to the acellular constructs, with the issues just described previously also possibly confounding the results (Figure 5.8). For the carrier free group, there appears to be little bone formation in any samples. Like the immediate injection results for this group, ambulation of the limb may be resulting in dispersion of the therapeutic following injection. Due to the variability of the hydrogel delivery location in these experiments, the mineral production was not quantified as it is impossible to ascertain whether any difference would be due to the therapeutic intervention or the volume actually delivered to the defect site.

Immediate versus Delayed Bone Formation with 2nd Procedure

Accuracy of delivery prevented quantification of differences in the groups tested, however we were able to discern that the group lacking hydrogel is ineffective for bone

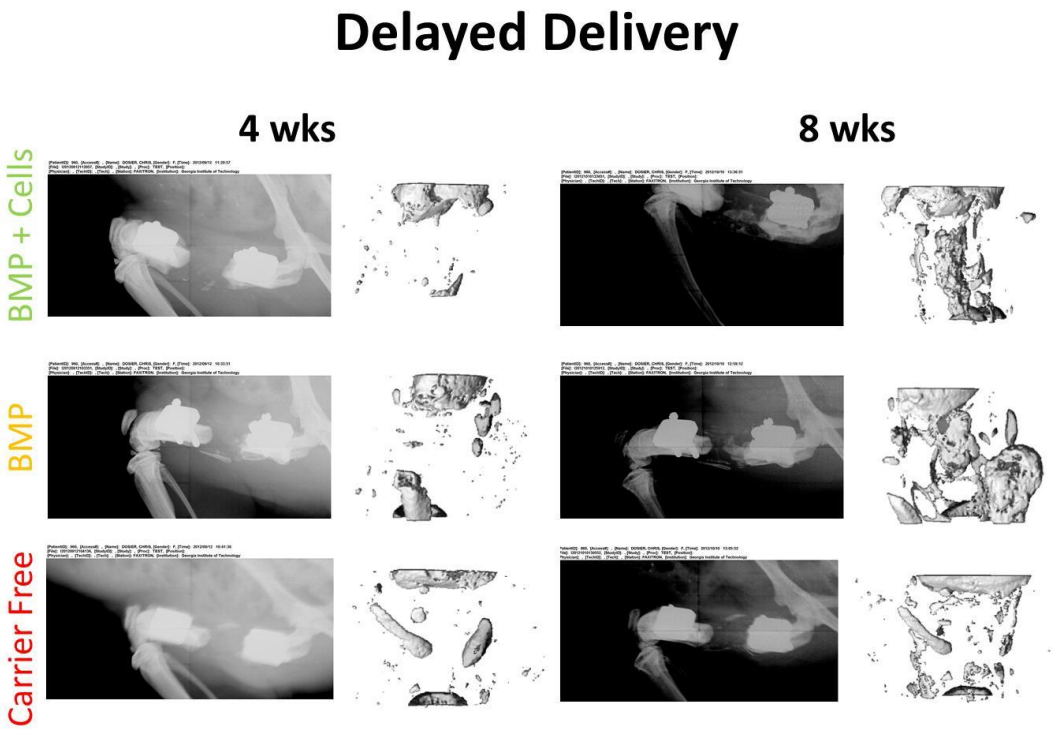

Figure 5.8 Radiograph and Micro-CT reconstruction of percutaneously delivered constructs 14 days after creation of the defect for the different constructs tested.

formation, as well as the 14 day time point being too late to deliver 150 µL of hydrogel into the defect site. Therefore, we altered the surgical procedure to allow for the defect site to be visible to ensure accurate delivery, and moved up our delayed time point further to 7 days. The groups tested in this new procedure were: an alginate hydrogel lacking BMP-2 or BMMSC incorporation (No BMP), an alginate hydrogel with BMP-2 (BMP), and an alginate hydrogel with BMP-2 and 1 million BMMSCs (BMP + Cells).

At 4 weeks, *in vivo* micro-CT showed that there was little mineral in the defect site. No differences were observed between any groups and no effect of timing of delivery was detected (Figure 5.9). *In vivo* micro-CT analysis at 8 weeks demonstrated that little to no bone formation occurs in the alginate hydrogels without BMP-2 (Figure 5.10). For immediate delivery samples, the addition of BMP-2 causes a significant increase in the bone volume over non-BMP-2 containing hydrogels. The group with the most mineral at the 8 week time point is the immediate delivery group containing 1 million cells. This group was significantly greater than the BMP-2 and non-BMP-2 containing hydrogels, as well as the delayed cell implantation group containing cells. In several samples mineral is present throughout the defect site and is approaching a bridged defect. Interestingly, delayed therapeutic implantation resulted in significantly less mineralization in the BMP-2 containing hydrogels and the BMP-2 with cells hydrogels. There were no significant differences observed between any of the groups for the delayed therapeutic delivery, and none of the defects were bridged by this time point.

Similar results were observed at 12 weeks, albeit with elevated levels of bone volume compared to 8 weeks (Figure 5.11). Again there was a significant increase in bone volume for hydrogels containing BMP-2 over non-BMP-2 containing hydrogels.

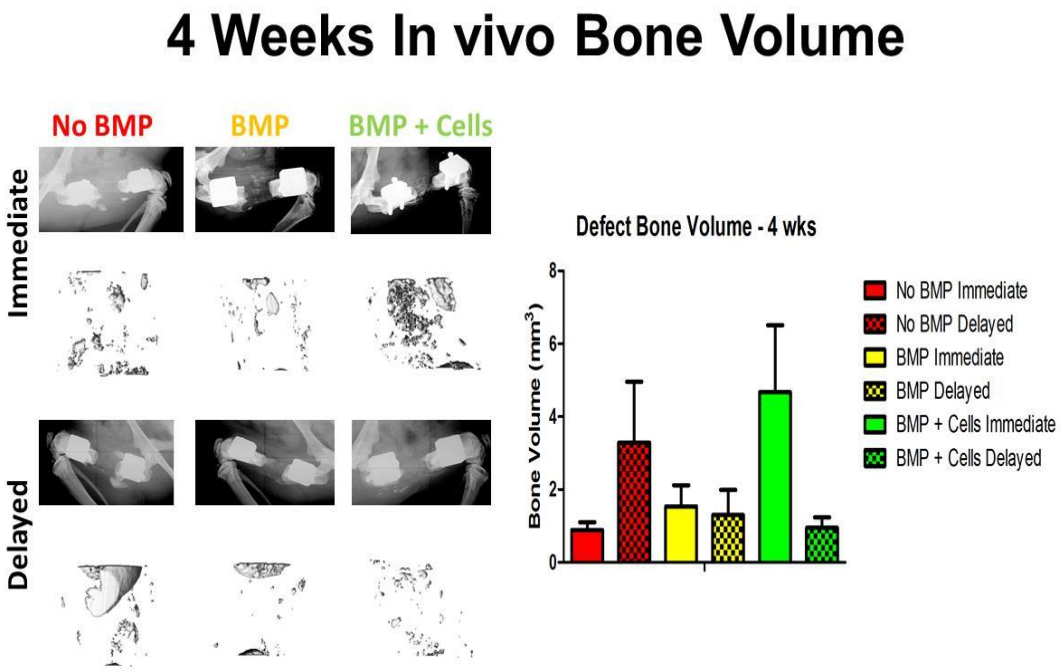

Figure 5.9 Radiographs and micro-CT reconstructions of immediate and delayed delivery hydrogels at 4 weeks post implantation.

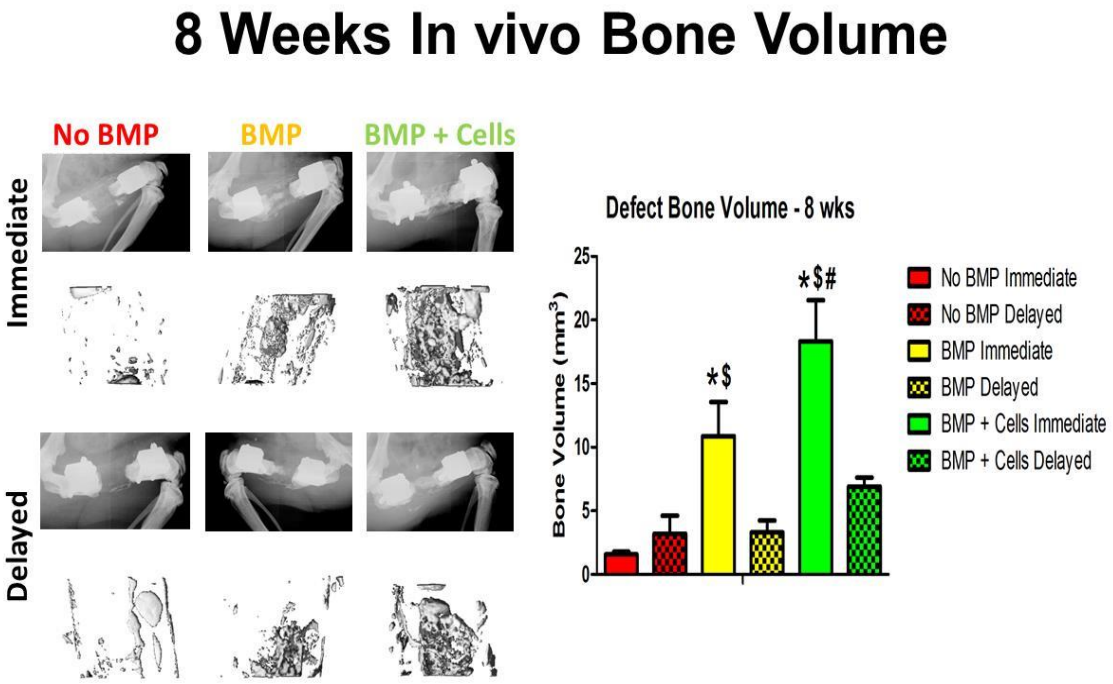

Figure 5.10 Radiographs and micro-CT reconstructions of immediate and delayed delivery hydrogels at 8 weeks post implantation. * $p<0.05$ significantly greater than No BMP, # $p<0.05$significantly greater than BMP, $$p<0.05$ significantly greater than delayed for that group.

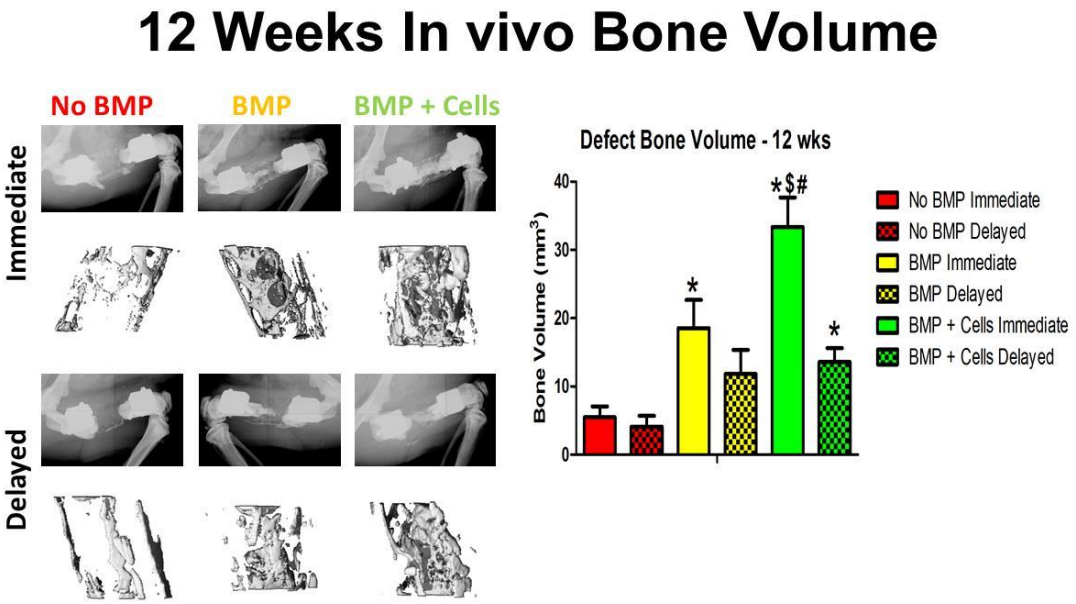

Figure 5.11 Radiographs and micro-CT reconstructions of immediate and delayed delivery hydrogels at 12 weeks post implantation. * $p<0.05$ significantly greater than No BMP, # $p<0.05$significantly greater than BMP, $$p<0.05$ significantly greater than delayed for that group.

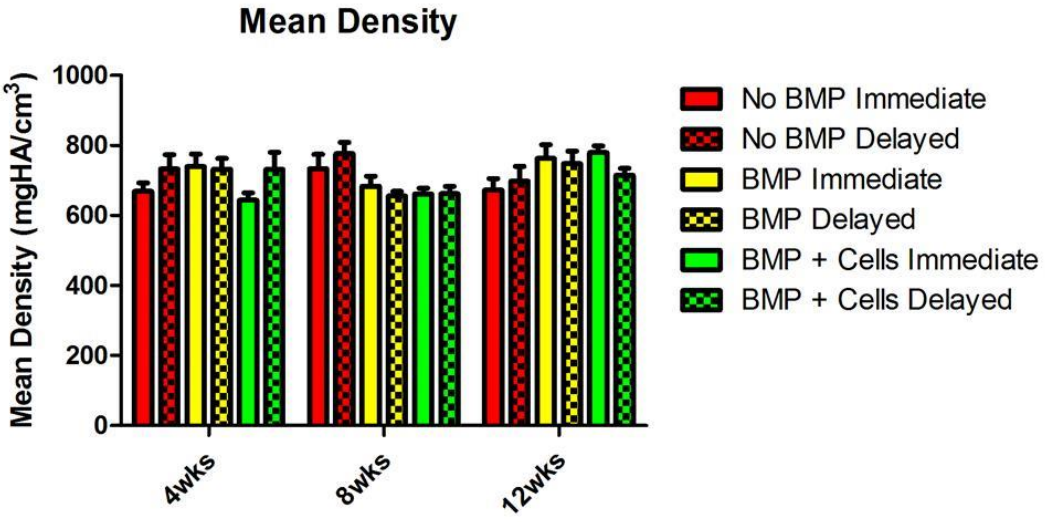

Figure 5.12 Mean mineral density of newly formed bone in tested hydrogels at 4, 8 and 12 weeks.

The immediately delivered hydrogel containing BMP-2 and cells had significantly greater bone volume than BMP-2 only and non-BMP-2 loaded hydrogels. For the delayed samples, a significant effect of including cells and BMP-2 was observed over non-BMP-2 loaded hydrogels. However, this group still had significantly less mineral than the immediately delivered counterpart. Analysis of the mean mineral density revealed no significant differences among any of the groups for any time point (Figure 5.12), indicating a similar level of bone maturity despite treatment or delivery time point.

Histological Analysis

H&E and Safranin-O staining of hydrogels lacking BMP-2 showed the presence of fibrous tissue along with remnants of alginate hydrogel. No areas of mineralization were observed in the defect site for both the immediate and delayed samples for this group (Figure 5.13 and Figure 5.14). For BMP-2 containing hydrogels, areas of mature bone were observed. For both immediate and delayed samples, areas of alginate hydrogel were still observable after 12 weeks. Interestingly, in cell loaded alginate hydrogels, the alginate has cells present in the hydrogel while acellular hydrogels lack cells (arrows in Figure 5.12 and Figure 5.13). Most of these cells however do not stain for nuclei on H&E, suggesting the cells are no longer functional after 12 weeks. Some cells are found along the surface of mineralized tissue, possibly indicating implanted cell bone formation.

Immunohistochemistry for GFP showed very little positive staining, suggesting that by 12 weeks most of the implanted cells are no longer alive (Figure 5.14). This confirms what is seen in the H&E and Safranin-O stains of cell loaded constructs, where

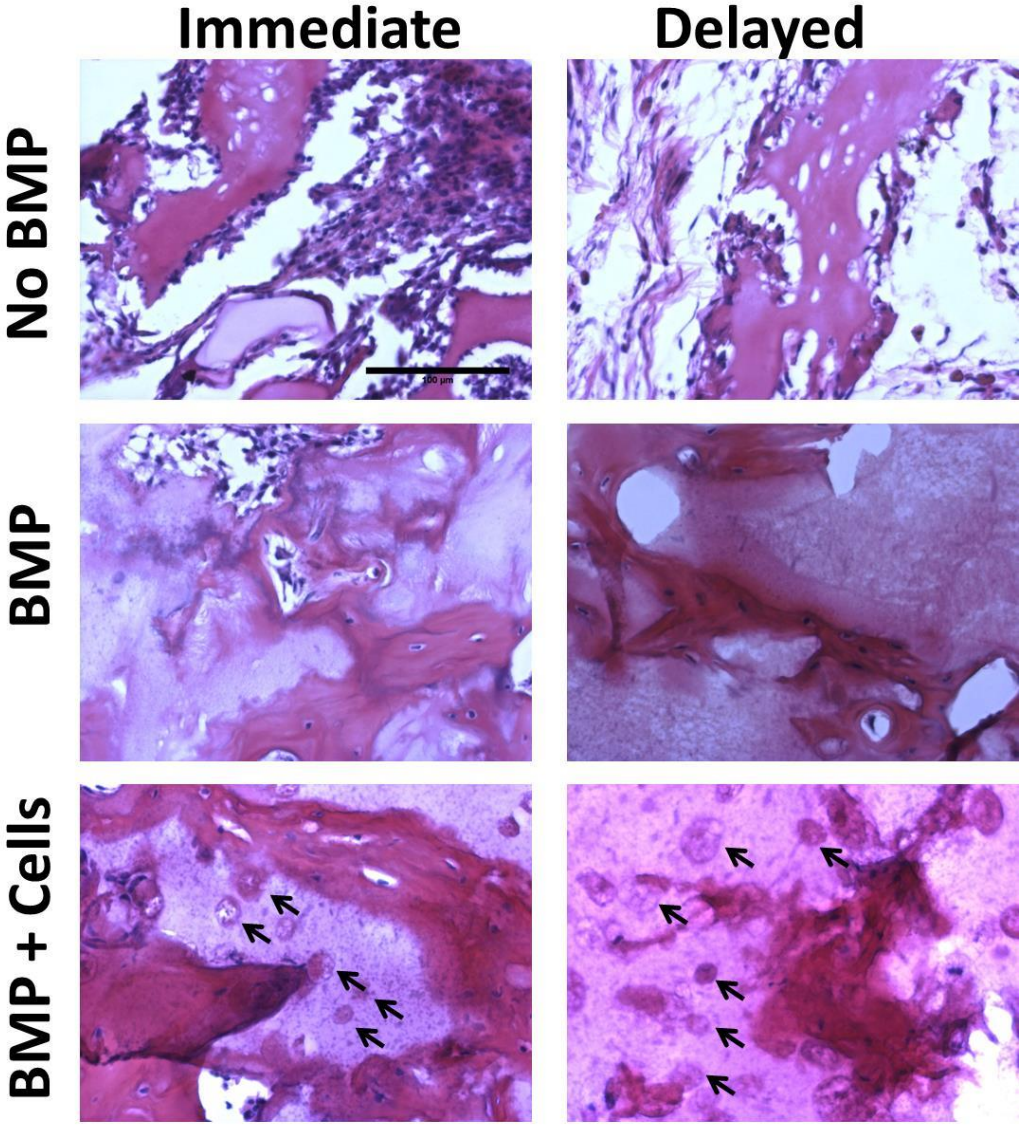

Figure 5.13 H&E staining of constructs after 12 weeks. Cell loaded alginate hydrogels still showed the presence of cells after 12 weeks (arrows). Scale bar = 100 µm.

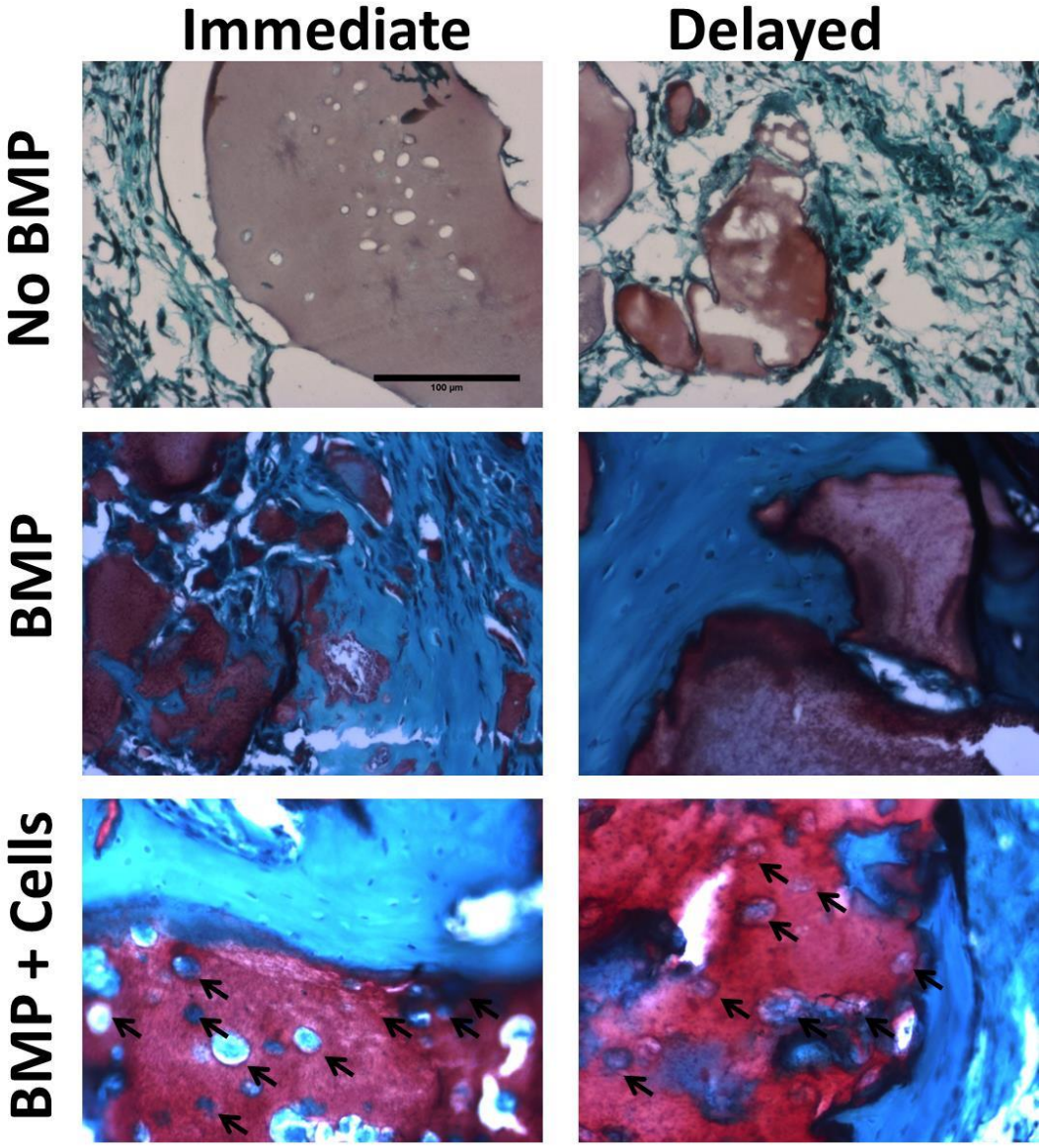

Figure 5.14 Safranin-O staining of constructs after 12 weeks. Cell loaded alginate hydrogels still showed the presence of cells after 12 weeks (arrows). Scale bar = 100 µm.

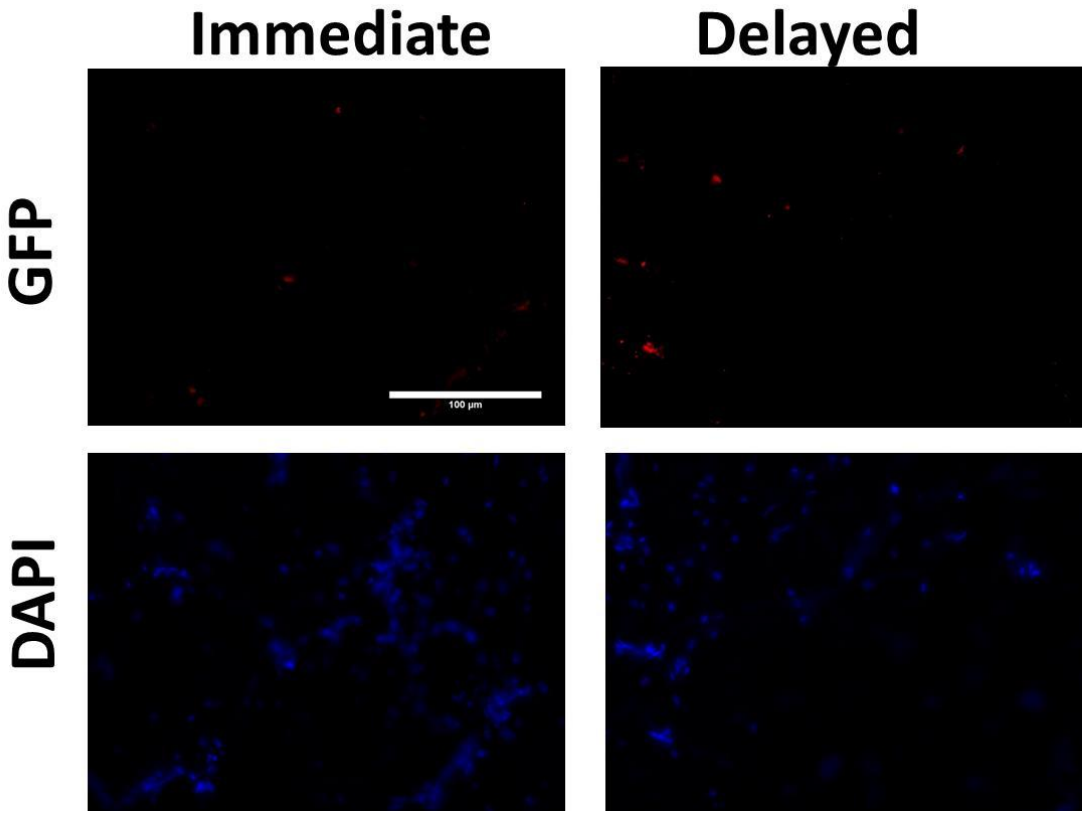

Figure 5.15 Immunohistochemistry for GFP positive cells after 12 weeks in cell loaded alginate hydrogels. Scale bar = 100 µm.

the lack of nuclei suggest that the cells are no longer metabolically active. Most of the cells visible in the H&E and Safranin-O stains did not stain positive for GFP.

DISCUSSION

The objective of this study was to examine the ability of stem cell loaded alginate hydrogels to regenerate bone tissue in a critically sized diaphyseal defect. We first characterized empty defects to identify possible delayed delivery time points of the hydrogel to the defect. We found that by 7 days there was tissue infiltration but not total filling of the defect. By day 14, the defect was nearly completely filled with host tissue. We next evaluated a percutaneous delivery approach to heal the defect. It was determined that the blind, percutaneous injections resulted in inaccurate volume delivery to the defect site, hampering comparison of hydrogel groups. The 14 day time point was initially chosen as one of the test groups lacked a hydrogel carrier, but this group failed to show robust bone formation in the defect site. In addition, little bone formation was observed most likely due to the large amount of host tissue impeding robust mineralization spanning the defect site. Finally, we adapted a delivery approach similar to the Masquelet technique where the defect site is reentered through the initial incision and the therapeutic delivered to the defect site. Despite accurate delivery of the hydrogels in this technique, we observed a detrimental effect of delayed implantation compared to immediate implantation. However, a beneficial effect of stem cell delivery was observed over acellular hydrogels at both time points. Acellular samples consistently did not achieve bridging of the defect, while cell loaded constructs did achieve bridging of the defect in a majority of samples.

The characterization of empty defects revealed some interesting results about the host response to the volumetric bone loss. As expected, there was a gradual increase in host tissue over time, with the defect being filled by 14 days. Interestingly, by day 7 there was a reduction in cancellous bone volume fraction in the proximal end of the defect site. Conversely, there was an increase in bone volume fraction on the distal end. The two bone volume fractions remodeled to relatively the same level. Histology further demonstrated that the tissue began to organize on the ends of the defect site. It is well known that non-healing defects will undergo 'end-capping' where the periosteum forms cortical bone over the bone end. Our data suggests that this process begins by 14 days with remodeling of the tissue adjacent to the defect site.

Attempts to deliver stem cells to regenerate a tissue post injury have not been performed for orthopedic applications. Limited studies have been performed for delayed progenitor cell delivery for neural tissue regeneration, restoring vascular supply in the brain (Kawabori, Kuroda et al. 2012, Kawabori, Kuroda et al. 2012). However, most investigation into timing of delivery of mesenchymal stem cells has involved regeneration of cardiac muscle tissue due to damage from myocardial infarction. Several clinical studies have investigated the use of mesenchymal stem cells to repair damaged muscle tissue due to myocardial infarct (Schachinger, Erbs et al. 2006, Schachinger, Erbs et al. 2006, Traverse, Henry et al. 2009, Traverse, Henry et al. 2010, Traverse, Henry et al. 2011). Given the delicate state of patients following a myocardial infarction, researchers sought to determine whether harvesting of autologous mesenchymal stem cells two to three weeks from the infarct and injecting them into the left ventricular wall would have a benefit on heart function (Traverse, Henry et al. 2010). It was reported that

delivery of 150 million autologous MSCs resulted in no added benefit in terms of ejection volumes from the left ventricular lobe (Traverse, Henry et al. 2010, Traverse, Henry et al. 2011). However, others have had success in giving stem cells to patients 5-7 days post infarct and seeing improvements in heart function (Schachinger, Erbs et al. 2006, Schachinger, Erbs et al. 2006). These studies show that timing of delivery is critical in order to achieve a therapeutic effect.

Our time points were chosen as we hypothesized the presence of endogenous tissue in the defect site may facilitate nutrient and waste exchange of the delivered stem cells, provide attachment sites for the cells as well as recruit more host progenitors before the BMP-2 could be degraded. However, given our results, our delivery time may have been too late. The amount of granular tissue in the defect site may have inhibited bone formation, and the BMP-2 may have been degraded by inflammatory cells at the defect site, limiting endogenous host cell recruitment. In addition, during the second surgical procedure we did not clear the defect site of infiltrated tissue. A possible consequence of this is limited space for the hydrogel at the 7 day time point, similar to what was observed in the 14 day delivery samples. An alternative hypothesis is that immediate delivery of osteoinductive factors significantly affects the endogenous cells recruited to the defect site. The mechanisms underlying our results need further study.

As stated previously, we adapted a form of the Masquelet technique in order to relieve the need for graft materials by delivering biologics. The Masquelet technique calls for a cement block in the defect site to prevent fibrous tissue invasion. Our membrane was perforate, allowing tissue invasion. We hypothesized that allowing some tissue infiltration into the defect would have a beneficial effect on our delivered biologics

thus leading to an increase in bone formation. A true test of the Masquelet technique with our alginate hydrogel system may elucidate some of the shortcomings of our current approach which uses a synthetic membrane and allows host tissue infiltration. For instance, comparison of the two techniques would allow for the effect of the granular tissue in the defect site on the delivered BMP-2 to be determined as well as any effect on delivered cell viability.

SUMMARY

In this study we demonstrated that inclusion of BMMSC into alginate hydrogels leads to greater bone formation in a non-healing diaphyseal defect compared to acellular hydrogels. Empty defect characterization identified two potential time points for delayed delivery of therapeutics. However, it was demonstrated that immediate delivery of the therapeutic results in more bone formation than a delayed time point of 7 days. It should be noted that acellular constructs consistently did not achieve bridging of the defect, while cell loaded constructs had a majority of the samples with bridged defects. These results may be attributable to a degradation of osteogenic factors by inflammatory cells present in the defect site at the delayed time point. Alternatively, immediate delivery of osteoinductive factors may significantly affect the endogenous cells recruited to the defect site, resulting in greater bone formation long term.

CHAPTER 6: SUMMARY AND IMPLICATIONS

SYNOPSIS

Tissue engineering offers an attractive alternative to current clinical treatment methods as stem cells, polymer scaffolds, and growth factors can be delivered to provide short term benefit and promote a long term host response to heal critically sized defects. In particular, cell based therapies have the potential to alleviate the use of grafts from host tissue and allogeneic tissue sources. In addition, co-delivery with growth factors could recruit host cells to a defect site as well as promote the differentiation of implanted cells. These tools allow for a large assortment of potential strategies to address many developmental diseases and traumatic injuries.

The goal of this thesis was to evaluate cell based tissue engineering strategies utilizing adult stem cells, growth factors, and hydrogels to regenerate bone tissue *in vivo*. We first evaluated adipose derived stem cells (ADSCs) as a potential cell source for bone tissue engineering (Chapter 3, Specific Aim I) by performing a rigorous examination of their osteogenic potential in 3-D. We next tested two hydrogel systems, poly-ethylene glycol hydrogels and alginate hydrogels, as cell carriers for *in vivo* bone tissue engineering (Chapter 4, Specific Aim II). We demonstrated that the alginate system supported robust *in vivo* bone formation when bone marrow mesenchymal stem cells (BMMSCs) were co-delivered with BMP-2. Finally, we took what we learned from Specific Aim II and applied them in a critically sized diaphyseal defect in the femur of the rat. We demonstrated that incorporation of bone marrow mesenchymal stem cells leads to greater *in vivo* bone formation than acellular hydrogels (Chapter 5, Specific Aim

III). It was further demonstrated that immediate delivery of the hydrogel leads to a greater amount of bone formation than delaying the delivery of the therapeutic. Taken together, we provide new insights into effective delivery strategies for cell based bone tissue engineering techniques.

SPECIFIC AIM I

The objective of this Specific Aim was to evaluate the osteogenic potential of ADSCs in order to utilize them in a bone defect model *in vivo*. Adipose derived stem cells have the advantage of being more abundant than other stem cell sources, making them an attractive cell source for bone tissue engineering. A summary of the results of tasks for this Specific Aim are provided below.

Resveratrol Treatment of Rat ADSCs

Resveratrol was identified as a potential pharmacological agent to increase the osteogenic potential of ADSCs. The simultaneous suppression of PPAR-γ and stimulation of Runx-2 made resveratrol an ideal candidate to promote osteogenic differentiation of ADSCs. 2-D analysis of cells for the dose of resveratrol initially identified 25μM as an effective dose. However, for tissue engineering the behavior of cells in a 3-D environment provides more insight into how they might perform *in vivo*. When we tested this with rat ADSCs in the 3-D PCL/collagen scaffold system, we observed an increase in mineralized matrix production at early time points. Further, a 7 day pre-treatment of the cells prior to seeding on the scaffold was shown to be sufficient to increase the mineralized matrix production compared to continuous treatment, which was not significantly higher than untreated cells. When we later performed a dose

dependency study in 3-D using the pre-treatment regimen, we noted that lower doses of resveratrol than 25 μM resulted in greater mineralized matrix, particularly at later time points. This is most likely due to increasing the early differentiation in higher doses, sacrificing proliferative capacity once seeded on the scaffolds. However, for *in vivo* bone applications, the effect of cell delivery can be presumed to be early as the cells will function primarily as paracrine signaling agents. We therefore chose to use the 12.5 μM dose for future *in vivo* studies.

Resveratrol Treatment of Human ADSCs

Of interest for clinical applications, human ADSC osteogenic potential was also investigated using the resveratrol treatment regimen. Dosage differences between hADSCs and rADSCs were observed. In particular, the high dose of 25 μM has a detrimental effect on mineralized matrix production in 3-D for hADSCs. When we performed a dose response, we observed similar results to rADSCs at lower doses, with a dose of 12.5 μM being the most effective at early time points, and 6.25 μM being the most effective at later time points.

Comparison of rADSC and hADSC Mineralized Matrix

Histological and surface analysis demonstrated differences in the mineralized matrix produced by rADSCs and hADSCs. rADSCs produced significantly more mineral than hADSCs in the 3-D culture environment. Further, the mineralized matrix is more mature as rADSC had a higher mean mineral density than hADSC constructs. Differences in the maturity of the mineralized matrix were also observed over time, with the mean density increasing between time points. Also observed was a difference in the

cellularity of the mineralized matrix. hADSCs had areas of high cellularity, while rADSCs had much larger nodules of mineral.

Concurrent Treatment of Resveratrol and BMP-2

As delivery of BMP-2 has been shown to be necessary to induce ADSC differentiation *in vivo*, the concurrent treatment of resveratrol and BMP-2 on rADSC mineralized matrix production was evaluated. We observed that the short 48 hour treatment of BMP-2 resulted in no added benefit in terms of mineralized matrix production. This is most likely attributable to the long culture time and 4 week span from the end of the BMP-2 treatment until the measurement of the mineralized matrix via micro-CT. By this time, the duration of culture in osteogenic media is most likely the dominant driver of mineralization. This assumption is supported by our 2-D alkaline phosphatase data, which showed BMP-2 treatment caused a significant increase in ALP activity at the shorter 14 day time point.

Implications

Taken together, these data imply that rADSCs are more osteogenic than hADSCs resulting in a greater amount of 3-D mineralized matrix production. These differences may be due to a higher metabolic activity than hADSCs. As such, rat derived stem cells were chosen as the cell source for future experiments. The short exposure time of BMP-2 may have been insufficient to detect an effect of BMP-2 treatment of ADSCs. A future study in which multiple short BMP-2 exposure times are used may lead to increased mineralized matrix, and may be a more accurate assessment of the effect of BMP-2 in long term cultures. Further, concurrent treatment of hADSCs with BMP-2 and resveratrol may increase their mineralized matrix production in the 3-D PCL/collagen

system. It would provide insight into the role of BMP-2 to test for the osteogenic gene expression of the cells in the 3-D culture system at early time points as well.

SPECIFIC AIM II

The objective of this Specific Aim was to evaluate hydrogels as an injectable cell delivery vehicle for bone tissue engineering. PEG and alginate based hydrogels were examined for their *in vitro* cell viability and *in vivo* bone formation in a subcutaneous ectopic mineralization model. A summary of the results of tasks for this Specific Aim are provided below.

In vitro Cell Viability in PEG Hydrogels

Using the PEG-DA hydrogel system, we observed that breaking up the hydrogel via injection resulted in greater cell viability than traditionally molded hydrogels. Further, incorporation of the cell attachment peptide RGD sustained greater cell viability at 14 days. Similar levels of cell viability were observed between ADSCs and BMMSCs. The APS/TEMED cross-linking system may have had a detrimental effect on the cell viability, as this system generates free radicals to cross-link the acrylate groups on the PEG backbone.

PEG Hydrogels as a Cell Delivery Vehicle for Bone Tissue Engineering

When implanted subcutaneously into RNU Nude rats, we observed very little ectopic mineralization in all of our groups. Incorporation of 2 µg of BMP-2 had no effect on the mineralized matrix production in the hydrogels. Micro-CT reconstructions showed that the ectopic mineralization that did occur was located primarily on the ends or the periphery of the implanted construct. Histological analysis showed the presence of

hydrogel still in the mesh tube, inhibiting new tissue formation. Few implanted cells were detected via immunohistochemistry, suggesting that any mineralization observed was endogenous cell driven.

In vitro Cell Viability in Alginate Hydrogels

Irradiated and oxidized irradiated alginate hydrogels were assessed for their *in vitro* cell viability. 24 hours after encapsulation, ADSC and BMMSC oxidized-irradiated hydrogels had lower cell viability than irradiated hydrogels. This is most likely due to the oxidized-irradiated hydrogels being more acidic, as noted by change in the phenol red indicator in α-MEM. By 7 days, all groups had similar cell viability. Analysis of the DNA content of the hydrogels showed that for all cell types there was an increase in cell number at 7 and 14 days. Compared to the PEG-DA hydrogel system, the alginate system had significantly greater cell viability at 14 days. These results suggest that alginate hydrogels are a viable cell delivery vehicle for an injectable bone tissue engineering system.

Degradation Kinetics of Irradiated and Oxidized Irradiated Alginate Hydrogels

The wet weight degradation of the two alginate based hydrogel systems was evaluated. Both hydrogels exhibited a similar degradation rate *in vitro*, and no significant differences in the amount of hydrogel left were detected until day 14. No differences were observed by incorporating cells into the hydrogel. At day 14, the oxidized-irradiated hydrogels had a significantly higher amount of mass loss compared to irradiated hydrogels. As the cells were cultured in standard growth media and remained undifferentiated, the cells were not induced to degrade the material. As such, the lack of major differences in the system are likely attributable to the culture conditions. Given the

similar degradation kinetics and cell viability, the irradiated alginate system was chosen as the hydrogel to test for *in vivo* bone formation.

Alginate Hydrogels as a Cell Delivery Vehicle for Bone Tissue Engineering

The irradiated alginate hydrogel system was investigated as an injectable cell delivery system for bone tissue engineering using a subcutaneous ectopic mineralization model. Micro-CT reconstructions and quantification demonstrated that ADSC loaded hydrogels had significantly less mineralized matrix relative to acellular hydrogels. This is most likely due to the ADSCs not secreting osteoinductive factors to promote bone formation from endogenous cells. Conversely, BMMSC inclusion resulted in a significant increase in bone formation compared to acellular hydrogels. This increase over acellular hydrogels suggests that the BMMSCs are producing osteoinductive factors that are promoting endogenous bone formation. This is further supported by only 50% of the acellular hydrogels producing robust mineralization, with the samples that did not mineralize likely not having enough BMP-2 still active in the hydrogel by the time host cells invaded the hydrogel. Histological analysis of explants showed that some implanted cells were still present in the constructs; however the majority of cells were host-derived cells.

Implications

The lack of mineralized tissue in the PEG system is most likely due to the non-resorption of the material. Future studies should incorporate enzymatically degradable cross-links, which will facilitate degradation of the material. This will result also in the presentation of more active growth factor, as the material will be broken down exposing

the BMP-2. As such, greater bone formation should be observed compared to the PEG-DA system.

The lack of mineralization in the ADSC groups in alginate hydrogels, and the robust mineralization of BMMSC loaded hydrogels, demonstrates that there is an effect of the type of cells on the bone formation response. We hypothesize that this is due to paracrine signaling and stimulation of endogenous progenitor cell differentiation. To evaluate this, it would be interesting to look at osteogenic protein expression of the implanted stem cells within the first 7 days of being implanted. Further, characterization of cells initially recruited to the hydrogel compared to non-BMP-2 containing gels might elucidate the dichotomy in the acellular hydrogel results.

SPECIFIC AIM III

The objective of this Specific Aim was twofold: 1) evaluate the ability of an injectable stem cell loaded alginate hydrogel to heal a critically sized femoral defect, and 2) assess the effect of timing of delivery of therapeutics for bone formation in the femoral defect. A summary of the results of tasks for this Specific Aim are provided below.

Characterization of Empty Defects

We first characterized empty segmental defects in terms of host tissue infiltration. As expected, we observed a gradual filling of the defect space when left empty over a 14 day time course. By day 14, the entire defect was filled with granular tissue. Macrophage presence was detected by day 3, however a larger presence was observed at days 7 and 14. The majority of the cells present in the defect site were polymorphonuclear cells (PNCs), indicative of neutrophils. These results suggest that the

inflammation response proceeds over the entire 14 day time course. Organization of the tissue adjacent to the bone ends was observable at day 14, indicative of the initiation of the bone 'end-capping' process in non-healing defects. Micro-CT analysis of the cancellous bone in the medullary cavity adjacent to the defect site suggested that the bone ends quickly remodel due to the creation of the defect. On the proximal end, there was a significant decrease in cancellous bone volume fraction. For the distal end, a significant increase in the cancellous bone volume fraction was observed, with both ends remodeling to a similar bone volume fraction.

Percutaneous Delivery of Injectable Alginate Hydrogels

Given our results with the empty defect characterization, we first attempted a percutaneous delivery approach with an immediate implantation of therapeutics and a delayed implantation at 14 days. The 14 day time point also allowed us to test delivery of cells and BMP-2 without a hydrogel carrier, as the host tissue would allow for engraftment of the cells. Unfortunately, blindly delivering the therapeutics to the defect site resulted in inaccurate delivery of the hydrogel, making quantitative comparisons unreasonable. However, with the micro-CT reconstructions some qualitative assessment of the bone formation in the limbs could be made.

For the immediate injection, all 5 of the cell loaded alginate hydrogels mineralized with 4 mineralizing ectopically in the surrounding muscle and the 1 sample delivered accurately mineralizing in the defect site. For cell free hydrogels, 3 out of 5 produced mineral all of which were ectopic in the surrounding muscle. This rate of mineralization for these two groups agrees with what was observed in the subcutaneous model for the groups respectively as discussed in Specific Aim II. For the carrier free

group, none of the samples mineralized ectopically or in the defect site. For one sample there was some mineralization along the mesh. The lack of mineralization is most likely due to ambulation of the limb resulting in dispersion of the therapeutic since there is no hydrogel to retain the cells and BMP-2 in the injection site.

With more experience in delivering the hydrogels blindly, the delayed delivery hydrogels were delivered closer to the defect site. However in some samples part of the hydrogel ended up outside the nanofiber mesh. Results demonstrate that for the acellular constructs the mineralization response appears to be less than what was observed with 1 µg of BMP-2 in previous studies in our lab (Boerckel, Kolambkar et al. 2011). This is possibly due to failure of delivery of the entire 150 µL to the defect site and also the presence of host tissue retarding the ability of the hydrogel and BMP-2 to form a continuous volume of bone. For cell loaded constructs, there appears to be a similar amount of bone formation compared to the acellular constructs. For the carrier free group, there appears to be little bone formation in any samples. Like the immediate injection results for this group, ambulation of the limb may be resulting in dispersion of the therapeutic following injection.

Immediate versus Delayed Bone Formation with 2nd Procedure

Accuracy of delivery prevented quantification of differences in the groups tested, however we were able to discern that the group lacking hydrogel is ineffective for bone formation, as well as the 14 day time point being too late to deliver 150 µL of hydrogel into the defect site. Future studies using a portable MRI system could improve the accuracy of delivery of the hydrogel percutaneously. However, due to resources we

altered the surgical procedure to allow for the defect site to be visible to ensure accurate delivery, and further moved up our delayed time point to 7 days.

At 4 weeks, *in vivo* micro-CT showed that there was little mineral in the defect site. No differences were observed between any groups and no effect of timing of delivery was detected. *In vivo* micro-CT analysis at 8 weeks demonstrated that little to no bone formation occurs in the alginate hydrogels without BMP-2 as expected. For immediate delivery samples, the addition of BMP-2 causes a significant increase in the bone volume over non-BMP-2 containing hydrogels. The group with the most mineral at the 8 week time point is the immediate delivery group containing 1 million BMMSCs. This group was significantly greater than the BMP-2 and non-BMP-2 containing hydrogels, as well as the delayed cell implantation group containing cells. Interestingly, delayed therapeutic implantation resulted in significantly less mineralization in the BMP-2 containing hydrogels and the BMP-2 with cells hydrogels. There were no significant differences observed between any of the groups for the delayed therapeutic delivery, and none of the defects were bridged by this time point. Similar results were observed at 12 weeks, albeit with elevated levels of bone volume compared to 8 weeks.

Histological Analysis of Bone Formation and Implanted Cell Presence

H&E and Safranin-O staining of hydrogels lacking BMP-2 showed the presence of fibrous tissue along with remnants of alginate hydrogel for both the immediate and delayed samples. No areas of mineralization were observed. BMP-2 containing hydrogels demonstrated areas of mature bone were observed. For both immediate and delayed samples, areas of alginate hydrogel were still observable after 12 weeks. Interestingly, in cell loaded alginate hydrogels, the alginate has cells present in the

hydrogel while acellular hydrogels lack cells. Most of these cells however do not appear to be functional after 12 weeks. Some cells are found along the surface of mineralized tissue, possibly indicating implanted cell bone formation. Immunohistochemistry for GFP showed very little positive staining, suggesting that by 12 weeks most of the implanted cells are no longer alive.

Implications

Our results, in terms of timing of delivery, suggest that the presence of BMP-2 early in the defect site may play a role in the types of cells initially recruited. It would be interesting to characterize the populations of cells recruited by placing a BMP-2 and non-BMP-2 loaded alginate hydrogel into the defect site. The presence of BMP-2 early may also have implications in terms of the vascular progenitor cells recruited as well, and this may ultimately impact bone formation.

As stated previously, we adapted a form of the Masquelet technique in order to relieve the need for graft materials by delivering biologics. The Masquelet technique calls for a cement block in the defect site to prevent fibrous tissue invasion. Our membrane was perforated, allowing tissue invasion as we hypothesized that allowing some tissue infiltration into the defect would have a beneficial effect on our delivered biologics thus leading to an increase in bone formation. A true test of the Masquelet technique with our alginate hydrogel system may elucidate some of the shortcomings of our current approach in using a synthetic membrane and allowing host tissue infiltration. For instance, comparison of the two techniques would allow us to determine the effect of the granular tissue in the defect site on the delivered BMP-2 as well as any effect on delivered cell viability.

CONCLUSIONS

A cell based tissue engineering approach for bone regeneration was developed in this thesis. We demonstrated that despite the increase in osteogenic potential of ADSC *in vitro* via resveratrol treatment, *in vivo* bone formation utilizing ADSCs is minimal. In contrast, the incorporation of BMMSCs results in robust bone formation *in vivo*. This was demonstrated in an injectable hydrogel system in an ectopic mineralization model. The creation of an injectable cell delivery system allowed us to evaluate temporal effects of therapeutic delivery. We demonstrated a temporal effect of delivery of the therapeutics into a segmental bone defect, in which delayed implantation results in less bone formation than immediate implantation. Taken together, we demonstrate that incorporation of adult stem cells into an injectable hydrogel is a viable system to promote repair of clinically challenging bone defects.

CHAPTER 7: FUTURE DIRECTIONS

The objective of this thesis was to evaluate the utility of adult stem cells for bone tissue engineering. Briefly, we first established an enrichment protocol for adipose derived stem cells that increases their mineralized matrix production *in vitro*. We next evaluated the potential of adipose derived stem cells and bone marrow mesenchymal stem cells to produce mineralized tissue in both ectopic and orthotopic sites via a biologically functionalized hydrogel. Our results demonstrate that adipose derived stem cells are inferior to bone marrow mesenchymal stem cells for *in vivo* bone tissue engineering. We further investigated the effect of delivery time on the amount of bone regeneration in a non-healing bone defect model. It was demonstrated that delayed delivery results in reduced bone formation compared to immediate delivery of the therapeutic. Taken together, this raises several questions about effective cell based tissue engineering strategies for bone regeneration.

Role of Cells

Our results show that adipose derived stem cells are able to form mineralized matrix *in vitro* when cultured in osteogenic media. Further, pre-treatment with resveratrol increases the mineralized matrix production in a 3-D culture environment. However, pre-treatment with resveratrol is insufficient to promote robust mineralization *in vivo*, even with the co-delivery of the potent osteoinductive factor BMP-2. This suggests that ADSCs require a large osteogenic stimulus to produce mineralized tissue. One way to possibly increase the *in vivo* mineralization potential of ADSCs in our hydrogel system would be to incorporate both undifferentiated ADSCs and osteogenic differentiated ADSCs into the same construct. Park demonstrated that ADSCs cultured

in osteogenic media on PLGA scaffolds for 4 weeks are able to regenerate a tibial defect (Park, Zhou et al. 2012). Just as important as mineralized matrix production is the ability to revascularize a defect site. Undifferentiated ADSCs have been shown to have positive effects on angiogenesis *in vivo* (Mazo, Hernández et al. 2012). As such, incorporation of both osteogenic differentiated and undifferentiated ADSCs may improve bone formation in the hydrogel system. This could first be studied in the ectopic mineralization model to analyze dosages of differentiated and undifferentiated cells in order to identify optimal concentrations for mineralized tissue production.

As stated previously, the dichotomy of results between ADSC groups in alginate hydrogels and BMMSC loaded hydrogels demonstrates that there is an effect of the type of cells implanted on the bone formation response *in vivo*. We hypothesize that this is due to paracrine signaling and stimulation of endogenous progenitor cell differentiation. To evaluate this, the osteogenic protein expression of the implanted stem cells within the first 7 days of implantation could be evaluated. Our results further demonstrate that endogenous cell recruitment is vital to robust bone formation. Characterization of cells initially recruited to hydrogels containing BMP-2 compared to non-BMP-2 containing gels would provide insight into early cytokine signaling and host cell recruitment to the hydrogel. Identification of differences in cell recruitment could potentially provide therapeutic targets to increase the retention of circulating osteoprogenitors to the mineralization site.

Role of the Cell Carrier

In Specific Aim I, we used a PCL/collagen system to evaluate the osteogenic potential of ADSCs. It was later shown that while this system has utility *in vitro*, its

application for in vivo applications is limited (Appendix A). It was further shown that cells seeded onto PCL nanofiber meshes and implanted into the segmental defect results in cell death within the first 72 hours. These results demonstrated the need for a cell carrier that would facilitate cell viability *in vivo*.

In Specific Aim II, we investigated PEG and alginate based hydrogels for *in vitro* cell viability and *in vivo* bone formation. Both systems showed they sustained cell viability *in vitro* over a 14 day time course, with alginate having a higher degree of viability compared to PEG based systems. The lack of mineralized tissue in the PEG system is most likely due to the non-resorption of the material. Incorporation of enzymatically degradable cross-links will facilitate greater degradation of the material. As such, the presentation of more active growth factor would occur as the material will be broken down exposing the BMP-2. Thus greater bone formation should be observed compared to the PEG-DA system. In Specific Aim II and Specific Aim III, alginate hydrogels supported robust bone formation *in vivo* when coupled with BMP-2 and BMMSCs. In the segmental defect, histological analysis demonstrated that large pockets of hydrogel are still present in the defect site at 12 weeks.

Taken together, these results show that the method of delivery of cells is an important criterion for successful bone tissue engineering strategies. Further, degradation of the hydrogel is necessary for new tissue formation. Oxidation of the alginate back bone has been shown to increase the degradation rate of the hydrogel (Bouhadir, Lee et al. 2008). Oxidizing the back bone may result in greater degradation of the hydrogel, allowing for greater new bone formation in the defect site. A second strategy may be to lower the weight percentage of the alginate hydrogel. However, the retention of the cells

and BMP-2 are necessary for robust bone formation, as constructs lacking hydrogel did not mineralize *in vivo*. As such, a study looking at different weight percentages of alginate hydrogels is likely to show a positive effect of the reduction in alginate weight percentage until the hydrogel is unable to retain shape and leaks out of the defect space. Finally, another strategy of further irradiating the alginate backbone to reduce the molecular weight of the alginate hydrogel chains may also facilitate greater degradation. The average molecular weight of our alginate was 50 kDa. Lowering the weight percentage should provide greater degradation kinetics ultimately leading to greater bone formation *in vivo*.

Role of Timing of Delivery

We demonstrated in Specific Aim III that delayed implantation of therapeutics results in reduced bone formation in a non-healing bone defect. This suggests that the presence of BMP-2 early in the defect site may play a role in the types of cells initially recruited. As stated previously, it would be interesting to characterize the populations of cells recruited by placing a BMP-2 and non-BMP-2 loaded alginate hydrogel into the defect site. The presence of BMP-2 early may also have implications in terms of the vascular progenitor cells recruited to the defect site as well, and this may ultimately impact the regenerative capacity of the defect.

In order to accurately deliver the hydrogel, we had to implement a two-step surgical procedure that allowed the defect site to be visible to the surgeon. It is possible that the second surgery is having a detrimental effect on the healing response. Adopting a purely percutaneous approach by using a portable MRI machine to ensure accurate delivery of the therapeutic to the defect site would bypass the need for the second

procedure. This may produce a better result than our two-step surgical procedure and warrants further study.

Mimicking a Clinical Situation

An experiment that may mimic clinical procedures would be to use the Masquelet technique discussed previously to place a spacer into a bone defect site. At the same time, autologous stem cells from the bone marrow can be harvested in the contralateral femur. After expansion of the cells *in vitro*, simultaneously allowing growth of the membrane surrounding the spacer *in vivo*, the autologous cells could then be delivered in a hydrogel and bone formation could be assessed. A large animal model, such as in sheep or goats, would also provide insight into the scale-up ability of the hydrogel system and the amount of cells needed for a clinical application. These would be powerful experiments to test the use of autologous cells for large diaphyseal bone defect regeneration.

APPENDIX A: MOTIVATION FOR ADOPTING HYDROGELS AS A CELL DELIVERY VEHICLE

Prior to adopting the hydrogel approach to deliver stem cells, we first evaluated the PCL/Collagen system as a delivery vehicle for stem cells *in vivo*. 3 million untreated and resveratrol pre-treated rat ADSCs were seeded onto the PCL/Collagen scaffold as described in Chapter 3. The constructs were cultured overnight in growth media, and then implanted into a segmental bone defect as described in Chapter 5.

Micro-CT quantification of mineralized matrix showed virtually no bone formation within the scaffold. Nearly all bone formation that was in the defect site was

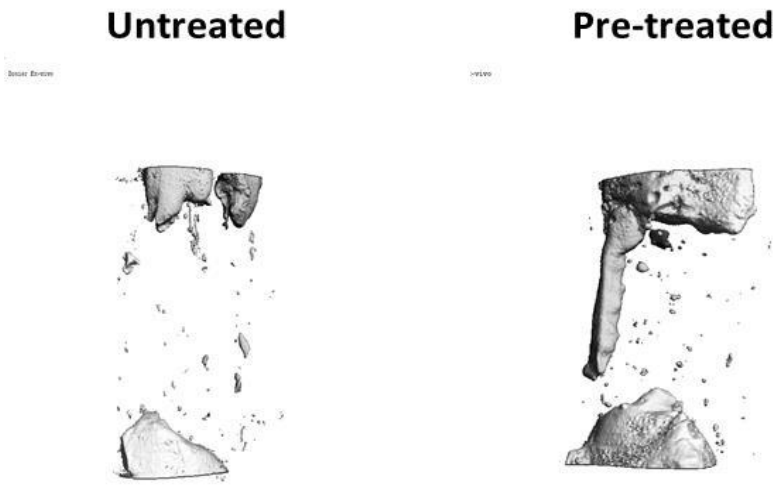

Figure A.1. Ex vivo Micro-CT reconstruction of ADSCs seeded on PCL/Collagen scaffolds and implanted into the segmental defect after 12 weeks.

due to the periosteal response. End-capping of the bone was observed indicating that the physiologic response of our implants was similar to a non-union.

This study was followed up by seeding 1 million GFP ADSCs onto a PCL nanofiber mesh tube and implanting them into the defect site. The meshes were then explanted and imaged for GFP cells after 3 days. Our results showed that we had high

cell viability on the mesh tubes prior to implantation. When explanted and examined after 3 days, almost all of the cells were no longer visible on the mesh (Figure A.2).

This indicated that having the cells readily exposed to the implant environment such as in the case of the PCL/Collagen scaffold may have a detrimental effect on the bone regeneration potential of implanted cells. We therefore chose to investigate hydrogels, as the hydrogel would offer some protection of the implanted cells from the initial host response, as well as facilitate diffusion of nutrients and waste products due to their high water content.

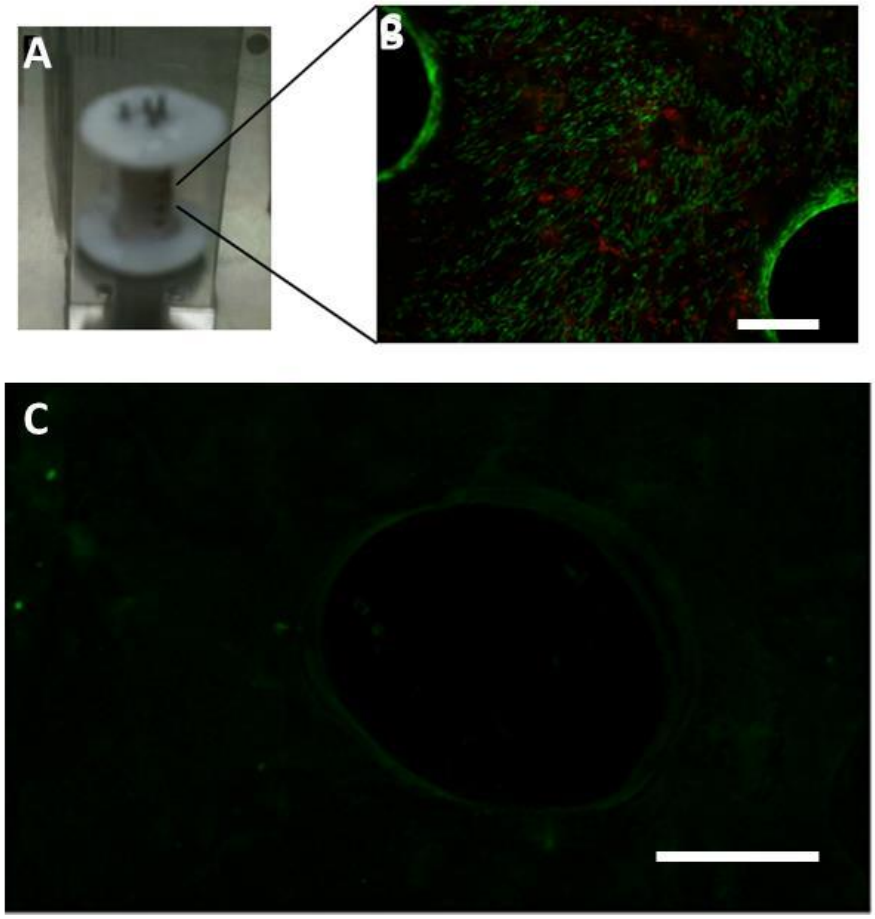

Figure A.2. GFP ADSC presence prior (B) and after (C) implantation into a segmental defect for 3 days. Scale Bar = 500 µm.

APPENDIX B: STABILITY OF GFP SIGNAL IN ADSCs and BMMSCs

Given the need to be able to track cell survival *in vivo*, we isolated adipose derived stem cells and bone mesenchymal stem cells from genetically modified rats that ubiquitously express green fluorescent protein (GFP). Characterization of GFP ADSCs showed that the cells were highly proliferative, with as many as 18 doublings through 8 passages (data not shown). We further characterized the cell source in terms of the amount of green fluorescent protein expressed through multiple passages. Qualitative analysis showed that the GFP signal was easily detectable, and further that the GFP signal was stable over multiple passages and cell doublings (Fig. B.1). This is an important criterion as it ensures that we will be able to track the cells ex vivo via fluorescent microscopy allowing us to detect cell survival after implantation. Bone marrow mesenchymal stem cells demonstrated similar results in terms of proliferation as well as stable GFP expression over multiple passages.

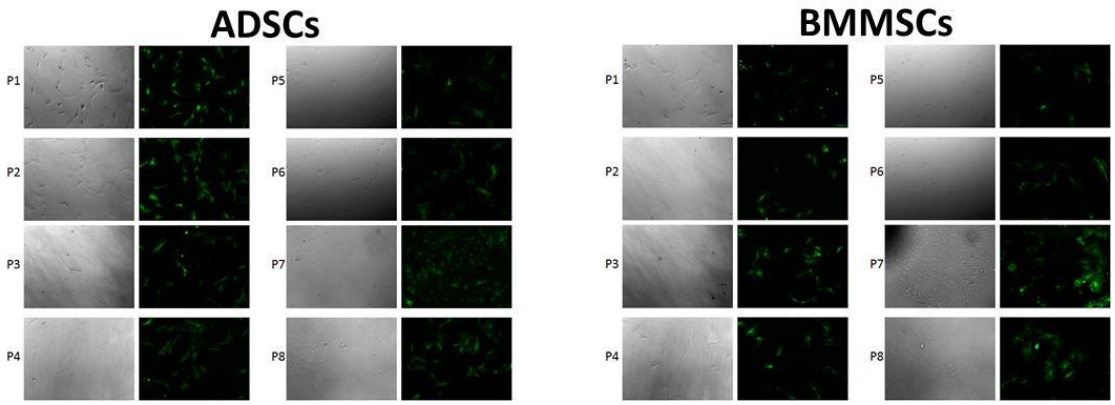

Figure B.1. Fluorescence of GFP ADSCs and BMMSCs through 8 passages and 18 doublings.

APPENDIX C: MODIFIED FIXATION PLATE DRAWINGS TO ALLOW PERCUTANEOUS DELIVERY OF HYDROGELS

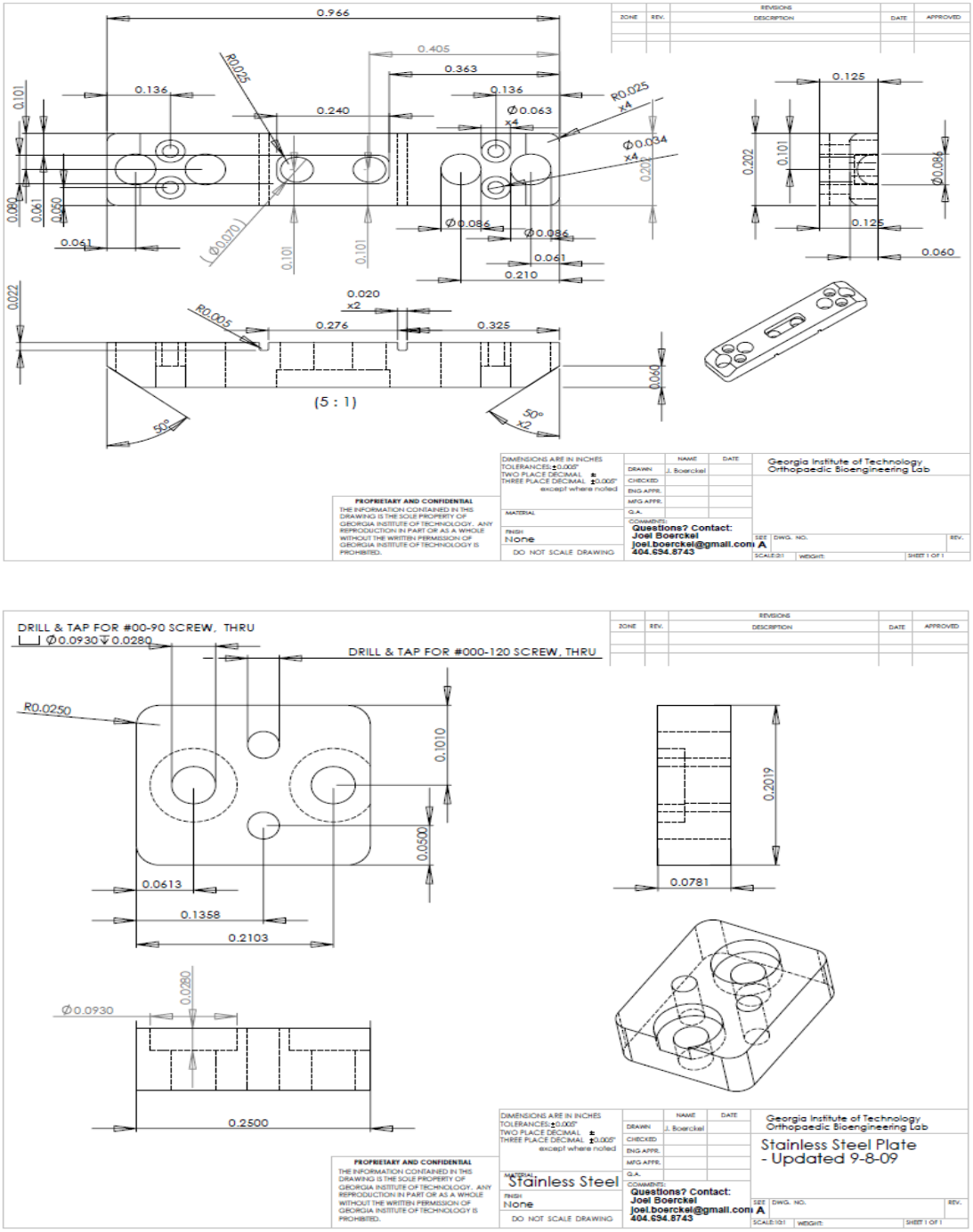

Figure C.1. Solid Works drawings of modified internal fixation plate to allow percutaneous delivery of hydrogels.

REFERENCES

Alberts, B. (2002). Molecular Biology of the Cell, Garland Science.

Alsberg, E., K. Anderson, A. Albeiruti, R. Franceschi and D. Mooney (2001). "Cell-interactive alginate hydrogels for bone tissue engineering." Journal of dental research **80**(11): 2025-2029.

Amini, A. R., C. T. Laurencin and S. P. Nukavarapu (2012). "Bone tissue engineering: recent advances and challenges." Crit Rev Biomed Eng **40**(5): 363-408.

Antonucci, I., L. Stuppia, Y. Kaneko, S. Yu, N. Tajiri, E. C. Bae, S. H. Chheda, N. L. Weinbren and C. V. Borlongan (2011). "Amniotic fluid as a rich source of mesenchymal stromal cells for transplantation therapy." Cell Transplant **20**(6): 789-795.

Arnhold, S., H. Klein, I. Semkova, K. Addicks and U. Schraermeyer (2004). "Neurally selected embryonic stem cells induce tumor formation after long-term survival following engraftment into the subretinal space." Investigative ophthalmology & visual science **45**(12): 4251-4255.

Awad, H. A., M. Quinn Wickham, H. A. Leddy, J. M. Gimble and F. Guilak (2004). "Chondrogenic differentiation of adipose-derived adult stem cells in agarose, alginate, and gelatin scaffolds." Biomaterials **25**(16): 3211-3222.

Backesjo, C. M., Y. Li, U. Lindgren and L. A. Haldosen (2006). "Activation of Sirt1 decreases adipocyte formation during osteoblast differentiation of mesenchymal stem cells." J Bone Miner Res **21**(7): 993-1002.

Baer, D. G., et al. (2004). "Bone and Soft Tissue Trauma Research at the USAISR, in RTO HFM Symposium on "Combat Casualty Care in Ground Based Tactical Situations: Trauma Technology and Emergency Medical Procedures"." St Pete Beach, USA.

Baron, R. (1993). Primer on the metabolic bone diseaseas and disorders of mineral metaboism. New York, Raven Press.

Bauer, T. W. and G. F. Muschler (2000). "Bone Graft Materials: An Overview of the Basic Science." Clinical Orthopaedics and Related Research **371**: 10-27.

Betz, M. W., A. B. Yeatts, W. J. Richbourg, J. F. Caccamese, D. P. Coletti, E. E. Falco and J. P. Fisher (2010). "Macroporous hydrogels upregulate osteogenic signal expression and promote bone regeneration." Biomacromolecules **11**(5): 1160-1168.

Blum, J. S., M. A. Barry, A. G. Mikos and J. A. Jansen (2003). "In vivo evaluation of gene therapy vectors in ex vivo-derived marrow stromal cells for bone regeneration in a rat critical-size calvarial defect model." Human gene therapy **14**(18): 1689-1701.

Boerckel, J. D., Y. M. Kolambkar, K. M. Dupont, B. A. Uhrig, E. A. Phelps, H. Y. Stevens, A. J. Garcia and R. E. Guldberg (2011). "Effects of protein dose and delivery system on BMP-mediated bone regeneration." Biomaterials **32**(22): 5241-5251.

Boissy, P., T. L. Andersen, B. M. Abdallah, M. Kassem, T. Plesner and J. M. Delaisse (2005). "Resveratrol inhibits myeloma cell growth, prevents osteoclast formation, and promotes osteoblast differentiation." Cancer Res **65**(21): 9943-9952.

Bono, C. and T. Einhorn (2005). "Overview of osteoporosis: pathophysiology and determinants of bone strength." The Aging Spine: 8-14.

Bouhadir, K. H., K. Y. Lee, E. Alsberg, K. L. Damm, K. W. Anderson and D. J. Mooney (2008). "Degradation of partially oxidized alginate and its potential application for tissue engineering." Biotechnology progress **17**(5): 945-950.

Breitbart, A. S., D. A. Grande, R. Kessler, J. T. Ryaby, R. J. Fitzsimmons and R. T. Grant (1998). "Tissue engineered bone repair of calvarial defects using cultured periosteal cells." Plastic and reconstructive surgery **101**(3): 567.

Breitbart, A. S., D. A. Grande, J. M. Mason, M. Barcia, T. James and R. T. Grant (1999). "Gene-enhanced tissue engineering: applications for bone healing using cultured periosteal cells transduced retrovirally with the BMP-7 gene." Annals of plastic surgery **42**(5): 488.

Bruder, S. P. and B. S. Fox (1999). "Tissue engineering of bone. Cell based strategies." Clin Orthop Relat Res(367 Suppl): S68-83.

Buckwalter, J. A., et al. (1996). "Bone biology. I: Structure, blood supply, cells, matrix, and mineralization. ." Instr Course Lect **45**: 371-386.

Buckwalter, J. A., et al. (1996). "Bone biology. II: Formation, form, modeling, remodeling, and regulation of cell function." Instr Course Lect **45**: 387-399.

Burdick, J. K. S. A. (2002). "Photoencapsulation of osteoblasts in injectable RGD-modified PEG hydrogels for bone tissue engineering." Biomaterials **23**: 4315-4323.

Byrne, D. P., D. Lacroix, J. A. Planell, D. J. Kelly and P. J. Prendergast (2007). "Simulation of tissue differentiation in a scaffold as a function of porosity, Young's modulus and dissolution rate: application of mechanobiological models in tissue engineering." Biomaterials **28**(36): 5544-5554.

Cahill, K. S., J. H. Chi, A. Day and E. B. Claus (2009). "Prevalence, complications, and hospital charges associated with use of bone-morphogenetic proteins in spinal fusion procedures." JAMA **302**(1): 58-66.

Cao, H. and N. Kuboyama (2010). "A biodegradable porous composite scaffold of PGA/beta-TCP for bone tissue engineering." Bone **46**(2): 386-395.

Caplan, A. I. (1991). "Mesenchymal stem cells." Journal of Orthopaedic Research **9**(5): 641-650.

Cohen, M. (2006). "The new bone biology: Pathologic, molecular, and clinical correlates." Am J Med Genet Part A **140A**: 2646–2706.

Comisar, W. A., N. H. Kazmers, D. J. Mooney and J. J. Linderman (2007). "Engineering RGD nanopatterned hydrogels to control preosteoblast behavior: a combined computational and experimental approach." Biomaterials **28**(30): 4409-4417.

Costa, C. D., F. Rohden, T. O. Hammes, R. Margis, J. W. Bortolotto, A. V. Padoin, C. C. Mottin and R. M. Guaragna (2011). "Resveratrol Upregulated SIRT1, FOXO1, and Adiponectin and Downregulated PPARgamma1-3 mRNA Expression in Human Visceral Adipocytes." Obes Surg.

Cowan, C. M., Y. Y. Shi, O. O. Aalami, Y. F. Chou, C. Mari, R. Thomas, N. Quarto, C. H. Contag, B. Wu and M. T. Longaker (2004). "Adipose-derived adult stromal cells heal critical-size mouse calvarial defects." Nat Biotechnol **22**(5): 560-567.

Dahlin, C., A. Johansson, M. Hoffman and A. Molenberg (2012). "Early biocompatibility of poly (ethylene glycol) hydrogel barrier materials for guided bone regeneration. An in vitro study using human gingival fibroblasts (HGF-1)." Clin Oral Implants Res.

De Coppi, P., A. Callegari, A. Chiavegato, L. Gasparotto, M. Piccoli, J. Taiani, M. Pozzobon, L. Boldrin, M. Okabe, E. Cozzi, A. Atala, P. Gamba and S. Sartore (2007). "Amniotic fluid and bone marrow derived mesenchymal stem cells can be converted to smooth muscle cells in the cryo-injured rat bladder and prevent compensatory hypertrophy of surviving smooth muscle cells." J Urol **177**(1): 369-376.

de Wert, G. and C. Mummery (2003). "Human embryonic stem cells: research, ethics and policy." Human reproduction **18**(4): 672-682.

Deasy, B. M., R. J. Jankowski and J. Huard (2001). "Muscle-derived stem cells: characterization and potential for cell-mediated therapy." Blood Cells, Molecules, and Diseases **27**(5): 924-933.

Decade, U. S. B. a. J. (2009). "Why is the Bone and Joint Decade Important?" http://www.usbjd.org/about/index.cfm?pg=important.cfm.

Dominici, M., K. Le Blanc, I. Mueller, I. Slaper-Cortenbach, F. Marini, D. Krause, R. Deans, A. Keating, D. Prockop and E. Horwitz (2006). "Minimal criteria for defining multipotent mesenchymal stromal cells. The International Society for Cellular Therapy position statement." Cytotherapy **8**(4): 315-317.

Duan, S., W. Zhu, L. Yu and J. Ding (2005). "Negative cooperative effect of cytotoxicity of a di-component initiating system for a novel injectable tissue engineering hydrogel." Chinese Science Bulletin **50**(11): 1093-1096.

Dudas, J. R., K. G. Marra, G. M. Cooper, V. M. Penascino, M. P. Mooney, S. Jiang, J. P. Rubin and J. E. Losee (2006). "The osteogenic potential of adipose-derived stem cells for the repair of rabbit calvarial defects." Annals of plastic surgery **56**(5): 543-548.

Dupont, K. M., K. Sharma, H. Y. Stevens, J. D. Boerckel, A. J. García and R. E. Guldberg (2010). "Human stem cell delivery for treatment of large segmental bone defects." Proceedings of the National Academy of Sciences **107**(8): 3305-3310.

Einhorn, T. A. (1998). "The cell and molecular biology of fracture healing." Clinical orthopaedics and related research **355**: S7-S21.

Erdman, C. P., C. R. Dosier, R. Olivares-Navarrete, C. Baile, R. E. Guldberg, Z. Schwartz and B. D. Boyan (2011). "Effects of Resveratrol on Enrichment of Adipose-derived Stem Cells and their Differentiation to Osteoblasts in Two and Three Dimensional Cultures." Journal of Tissue Engineering and Regnerative Medicine **Submitted, In Press**.

Erices, A., P. Conget and J. J. Minguell (2000). "Mesenchymal progenitor cells in human umbilical cord blood." Br J Haematol **109**(1): 235-242.

Feng, X. and J. M. McDonald (2011). "Disorders of bone remodeling." Annual Review of Pathology: Mechanisms of Disease **6**: 121-145.

Fernández-Tresguerres Hernández-Gil, I., et.al. (2006). "Physiological bases of bone regeneration II. The remodeling process." Med Oral Patol Oral Cir Bucal **11**: E151-157.

Fini, M., A. Motta, P. Torricelli, G. Giavaresi, A. N. Nicoli, M. Tschon, R. Giardino and C. Migliaresi (2005). "The healing of confined critical size cancellous defects in the presence of silk fibroin hydrogel." Biomaterials **26**(17): 3527.

Firth, A. L. and J. X. Yuan (2012). "Identification of functional progenitor cells in the pulmonary vasculature." Pulm Circ **2**(1): 84-100.

Fraser, J. K., I. Wulur, Z. Alfonso and M. H. Hedrick (2006). "Fat tissue: an underappreciated source of stem cells for biotechnology." Trends Biotechnol **24**(4): 150-154.

Friedenstein, A. J., S. Piatetzky, II and K. V. Petrakova (1966). "Osteogenesis in transplants of bone marrow cells." J Embryol Exp Morphol **16**(3): 381-390.

Gan, Y., K. Dai, P. Zhang, T. Tang, Z. Zhu and J. Lu (2008). "The clinical use of enriched bone marrow stem cells combined with porous beta-tricalcium phosphate in posterior spinal fusion." Biomaterials **29**(29): 3973-3982.

Giannoudis, P. V., O. Faour, T. Goff, N. Kanakaris and R. Dimitriou (2011). "Masquelet technique for the treatment of bone defects: tips-tricks and future directions." Injury **42**(6): 591-598.

Gimble, J. and F. Guilak (2003). "Adipose-derived adult stem cells: isolation, characterization, and differentiation potential." Cytotherapy **5**(5): 362-369.

González, Y., M. Cerrolaza and C. González (2009). "Poroelastic analysis of bone tissue differentiation by using the boundary element method." Engineering Analysis with Boundary Elements **33**(5): 731-740.

Guldberg, R. E., M. E. Oest, K. Dupont, A. Peister, E. Deutsch, Y. Kolambkar and D. Mooney (2007). "Biologic augmentation of polymer scaffolds for bone repair." J Musculoskelet Neuronal Interact **7**(4): 333-334.

Hale, B. W., L. R. Goodrich, D. D. Frisbie, C. W. McIlwraith and J. D. Kisiday (2012). "Effect of scaffold dilution on migration of mesenchymal stem cells from fibrin hydrogels." Am J Vet Res **73**(2): 313-318.

Hasharoni, A., Y. Zilberman, G. Turgeman, G. A. Helm, M. Liebergall and D. Gazit (2005). "Murine spinal fusion induced by engineered mesenchymal stem cells that conditionally express bone morphogenetic protein-2." Journal of Neurosurgery: Spine **3**(1): 47-52.

Hattori, H., M. Sato, K. Masuoka, M. Ishihara, T. Kikuchi, T. Matsui, B. Takase, T. Ishizuka, M. Kikuchi and K. Fujikawa (2004). "Osteogenic potential of human adipose tissue-derived stromal cells as an alternative stem cell source." Cells Tissues Organs **178**(1): 2-12.

Hauser, P. V., R. De Fazio, S. Bruno, S. Sdei, C. Grange, B. Bussolati, C. Benedetto and G. Camussi (2010). "Stem cells derived from human amniotic fluid contribute to acute kidney injury recovery." Am J Pathol **177**(4): 2011-2021.

Hicok, K. C., T. V. Du Laney, Y. S. Zhou, Y.-D. C. Halvorsen, D. C. Hitt, L. F. Cooper and J. M. Gimble (2004). "Human adipose-derived adult stem cells produce osteoid in vivo." Tissue engineering **10**(3-4): 371-380.

Hu, Y., C. Zhang, S. Zhang, Z. Xiong and J. Xu (2003). "Development of a porous poly (L-lactic acid)/hydroxyapatite/collagen scaffold as a BMP delivery system and its use in healing canine segmental bone defect." Journal of Biomedical Materials Research Part A **67**(2): 591-598.

Huang, Y. C., D. Kaigler, K. G. Rice, P. H. Krebsbach and D. J. Mooney (2004). "Combined Angiogenic and Osteogenic Factor Delivery Enhances Bone Marrow Stromal Cell-Driven Bone Regeneration." Journal of Bone and Mineral Research **20**(5): 848-857.

Ikeuchi, M., A. Ito, Y. Dohi, H. Ohgushi, H. Shimaoka, K. Yonemasu and T. Tateishi (2003). "Osteogenic differentiation of cultured rat and human bone marrow cells on the surface of zinc-releasing calcium phosphate ceramics." J Biomed Mater Res A **67**(4): 1115-1122.

Iwasaki, M., H. Nakahara, K. Nakata, T. Nakase, T. Kimura and K. Ono (1995). "Regulation of proliferation and osteochondrogenic differentiation of periosteum-derived cells by transforming growth factor-beta and basic fibroblast growth factor." The Journal of bone and joint surgery. American volume **77**(4): 543.

Javazon, E. H., D. C. Colter, E. J. Schwarz and D. J. Prockop (2001). "Rat marrow stromal cells are more sensitive to plating density and expand more rapidly from single-cell-derived colonies than human marrow stromal cells." Stem Cells **19**(3): 219-225.

Kadiyala, S., N. Jaiswal and S. P. Bruder (1997). "Culture-expanded, bone marrow-derived mesenchymal stem cells can regenerate a critical-sized segmental bone defect." Tissue engineering **3**(2): 173-185.

Karageorgiou, V., L. Meinel, S. Hofmann, A. Malhotra, V. Volloch and D. Kaplan (2004). "Bone morphogenetic protein-2 decorated silk fibroin films induce osteogenic differentiation of human bone marrow stromal cells." Journal of Biomedical Materials Research Part A **71**(3): 528-537.

Kawabori, M., S. Kuroda, M. Ito, H. Shichinohe, K. Houkin, Y. Kuge and N. Tamaki (2012). "Timing and cell dose determine therapeutic effects of bone marrow stromal cell transplantation in rat model of cerebral infarct." Neuropathology.

Kawabori, M., S. Kuroda, T. Sugiyama, M. Ito, H. Shichinohe, K. Houkin, Y. Kuge and N. Tamaki (2012). "Intracerebral, but not intravenous, transplantation of bone marrow stromal cells enhances functional recovery in rat cerebral infarct: an optical imaging study." Neuropathology **32**(3): 217-226.

Kern, S., H. Eichler, J. Stoeve, H. Klüter and K. Bieback (2006). "Comparative analysis of mesenchymal stem cells from bone marrow, umbilical cord blood, or adipose tissue." Stem cells **24**(5): 1294-1301.

Kim, K. H., L. Jeong, H. N. Park, S. Y. Shin, W. H. Park, S. C. Lee, T. I. Kim, Y. J. Park, Y. J. Seol, Y. M. Lee, Y. Ku, I. C. Rhyu, S. B. Han and C. P. Chung (2005). "Biological efficacy of silk fibroin nanofiber membranes for guided bone regeneration." J Biotechnol **120**(3): 327-339.

Kimelman, N., G. Pelled, G. A. Helm, J. Huard, E. M. Schwarz and D. Gazit (2007). "Review: gene-and stem cell-based therapeutics for bone regeneration and repair." Tissue engineering **13**(6): 1135-1150.

Klaue, K., U. Knothe, C. Anton, D. H. Pfluger, M. Stoddart, A. C. Masquelet and S. M. Perren (2009). "Bone regeneration in long-bone defects: tissue compartmentalisation? In vivo study on bone defects in sheep." Injury **40**: S95-S102.

Knippenberg, M., M. Helder, B. Zandieh Doulabi, P. Wuisman and J. Klein-Nulend (2006). "Osteogenesis versus chondrogenesis by BMP-2 and BMP-7 in adipose stem cells." Biochemical and biophysical research communications **342**(3): 902-908.

Knippenberg, M., M. N. Helder, B. Zandieh Doulabi, P. I. Wuisman and J. Klein-Nulend (2006). "Osteogenesis versus chondrogenesis by BMP-2 and BMP-7 in adipose stem cells." Biochem Biophys Res Commun **342**(3): 902-908.

Kojimoto, H., N. Yasui, T. Goto, S. Matsuda and Y. Shimomura (1988). "Bone lengthening in rabbits by callus distraction. The role of periosteum and endosteum." Journal of Bone & Joint Surgery, British Volume **70**(4): 543-549.

Kolambkar, Y. M., J. D. Boerckel, K. M. Dupont, M. Bajin, N. Huebsch, D. J. Mooney, D. W. Hutmacher and R. E. Guldberg (2011). "Spatiotemporal delivery of bone morphogenetic protein enhances functional repair of segmental bone defects." Bone **49**(3): 485-492.

Kolambkar, Y. M., K. M. Dupont, J. D. Boerckel, N. Huebsch, D. J. Mooney, D. W. Hutmacher and R. E. Guldberg (2011). "An alginate-based hybrid system for growth factor delivery in the functional repair of large bone defects." Biomaterials **32**(1): 65-74.

Kurata, K., T. J. Heino, H. Higaki and H. K. Väänänen (2006). "Bone Marrow Cell Differentiation Induced by Mechanically Damaged Osteocytes in 3D Gel-Embedded Culture." Journal of Bone and Mineral Research **21**(4): 616-625.

Laurencin, C., Y. Khan and S. F. El-Amin (2006). "Bone graft substitutes." Expert review of medical devices **3**(1): 49-57.

Levi, B., J. S. Hyun, D. T. Montoro, D. D. Lo, C. K. Chan, S. Hu, N. Sun, M. Lee, M. Grova, A. J. Connolly, J. C. Wu, G. C. Gurtner, I. L. Weissman, D. C. Wan and M. T. Longaker (2012). "In vivo directed differentiation of pluripotent stem cells for skeletal regeneration." Proc Natl Acad Sci U S A **109**(50): 20379-20384.

Li, S. and L. Huang (2000). "Nonviral gene therapy: promises and challenges." Gene therapy **7**(1): 31-34.

Luca, L., A. L. Rougemont, B. H. Walpoth, L. Boure, A. Tami, J. M. Anderson, O. Jordan and R. Gurny "Injectable rhBMP-2-loaded chitosan hydrogel composite: Osteoinduction at ectopic site and in segmental long bone defect." J Biomed Mater Res A.

Mackie, E., Y. Ahmed, L. Tatarczuch, K.-S. Chen and M. Mirams (2008). "Endochondral ossification: how cartilage is converted into bone in the developing skeleton." The international journal of biochemistry & cell biology **40**(1): 46-62.

Majola, A., S. Vainionpää, K. Vihtonen, M. Mero, J. Vasenius, P. Törmälä and P. Rokkanen (1991). "Absorption, biocompatibility, and fixation properties of polylactic acid in bone tissue: an experimental study in rats." Clin Orthop **268**(7): 260-269.

Marks, S. C., Jr. and S. N. Popoff (1988). "Bone cell biology: the regulation of development, structure, and function in the skeleton." Am J Anat **183**(1): 1-44.

Maroni, P., A. T. Brini, E. Arrigoni, L. de Girolamo, S. Niada, E. Matteucci, P. Bendinelli and M. A. Desiderio (2012). "Chemical and genetic blockade of HDACs enhances osteogenic differentiation of human adipose tissue-derived stem cells by oppositely affecting osteogenic and adipogenic transcription factors." Biochem Biophys Res Commun **428**(2): 271-277.

Maximow, A. A. (1924). "Relation of blood cells to connective tissues and endothelium." Physiological Reviews **4**(4): 533-563.

Mazo, M., S. Hernández, J. Gavira, G. Abizanda, M. Araña, T. López-Martínez, C. Moreno, J. Merino, A. Martino-Rodríguez and A. Uixeira (2012). "Treatment of reperfused ischemia with adipose-derived stem cells in a preclinical swine model of myocardial infarction." Cell transplantation.

Mekala, N., R. Baadhe and S. Parcha (2013). "Study on Osteoblast like Behavior of Umbilical Cord Blood Cells on Various Combinations of PLGA Scaffolds Prepared by Salt Fusion." Current stem cell research & therapy.

Murakami, N., N. Saito, H. Horiuchi, T. Okada, K. Nozaki and K. Takaoka (2002). "Repair of segmental defects in rabbit humeri with titanium fiber mesh cylinders

containing recombinant human bone morphogenetic protein-2 (rhBMP-2) and a synthetic polymer." Journal of biomedical materials research **62**(2): 169-174.

Murphy, C. M., M. G. Haugh and F. J. O'Brien (2010). "The effect of mean pore size on cell attachment, proliferation and migration in collagen–glycosaminoglycan scaffolds for bone tissue engineering." Biomaterials **31**(3): 461-466.

Nakagami, H., R. Morishita, K. Maeda, Y. Kikuchi, T. Ogihara and Y. Kaneda (2006). "Adipose tissue-derived stromal cells as a novel option for regenerative cell therapy." J Atheroscler Thromb **13**(2): 77-81.

Nandi, S. K., S. Roy, P. Mukherjee, B. Kundu, D. K. De and D. Basu (2010). "Orthopaedic applications of bone graft & graft substitutes: a review." Indian J Med Res **132**: 15-30.

Nauth, A., M. D. McKee, T. A. Einhorn, J. T. Watson, R. Li and E. H. Schemitsch (2011). "Managing bone defects." J Orthop Trauma **25**(8): 462-466.

Ni, Y. W., Y. S. Zhou, Y. S. Liu, B. J. Zeng and Y. W. Xu (2009). "[Comparison of biological characteristics of human, rabbit and rat adipose tissue-derived stromal cells in vitro]." Beijing Da Xue Xue Bao **41**(1): 95-99.

Niemeyer, P., K. Fechner, S. Milz, W. Richter, N. P. Suedkamp, A. T. Mehlhorn, S. Pearce and P. Kasten (2010). "Comparison of mesenchymal stem cells from bone marrow and adipose tissue for bone regeneration in a critical size defect of the sheep tibia and the influence of platelet-rich plasma." Biomaterials **31**(13): 3572-3579.

Niemeyer, P., M. Kornacker, A. Mehlhorn, A. Seckinger, J. Vohrer, H. Schmal, P. Kasten, V. Eckstein, N. P. Sudkamp and U. Krause (2007). "Comparison of immunological properties of bone marrow stromal cells and adipose tissue-derived stem cells before and after osteogenic differentiation in vitro." Tissue Eng **13**(1): 111-121.

Oest, M. E., K. M. Dupont, H. J. Kong, D. J. Mooney and R. E. Guldberg (2007). "Quantitative assessment of scaffold and growth factor-mediated repair of critically sized bone defects." Journal of orthopaedic research **25**(7): 941-950.

Ornitz, D. M. and P. J. Marie (2002). "FGF signaling pathways in endochondral and intramembranous bone development and human genetic disease." Genes & development **16**(12): 1446-1465.

Osyczka, A. M., D. L. Diefenderfer, G. Bhargave and P. S. Leboy (2004). "Different effects of BMP-2 on marrow stromal cells from human and rat bone." Cells Tissues Organs **176**(1-3): 109-119.

Overman, J. R., E. Farre-Guasch, M. N. Helder, C. M. ten Bruggenkate, E. A. Schulten and J. Klein-Nulend (2013). "Short (15 minutes) bone morphogenetic protein-2 treatment stimulates osteogenic differentiation of human adipose stem cells seeded on calcium phosphate scaffolds in vitro." Tissue Eng Part A **19**(3-4): 571-581.

Owen, M. (1988). "Marrow stromal stem cells." J Cell Sci Suppl **10**: 63-76.

Park, B. H., L. Zhou, K. Y. Jang, H. S. Park, J. M. Lim, S. J. Yoon, S. Y. Lee and J. R. Kim (2012). "Enhancement of tibial regeneration in a rat model by adipose-derived stromal cells in a PLGA scaffold." Bone **51**(3): 313-323.

Park, J. B. (2011). "The use of hydrogels in bone-tissue engineering." Med Oral Patol Oral Cir Bucal **16**(1): e115-118.

Park, J. S., M. S. Shim, S. H. Shim, H. N. Yang, S. Y. Jeon, D. G. Woo, D. R. Lee, T. K. Yoon and K. H. Park (2011). "Chondrogenic potential of stem cells derived from amniotic fluid, adipose tissue, or bone marrow encapsulated in fibrin gels containing TGF-beta3." Biomaterials **32**(32): 8139-8149.

Patino, M. G., M. E. Neiders, S. Andreana, B. Noble and R. E. Cohen (2002). "Collagen: an overview." Implant dentistry **11**(3): 280-285.

Peister, A., E. R. Deutsch, Y. Kolambkar, D. W. Hutmacher and R. E. Guldberg (2009). "Amniotic fluid stem cells produce robust mineral deposits on biodegradable scaffolds." Tissue Eng Part A **15**(10): 3129-3138.

Peister, A., J. A. Mellad, B. L. Larson, B. M. Hall, L. F. Gibson and D. J. Prockop (2004). "Adult stem cells from bone marrow (MSCs) isolated from different strains of inbred mice vary in surface epitopes, rates of proliferation, and differentiation potential." Blood **103**(5): 1662-1668.

Peister, A., B. D. Porter, Y. M. Kolambkar, D. W. Hutmacher and R. E. Guldberg (2008). "Osteogenic differentiation of amniotic fluid stem cells." Biomed Mater Eng **18**(4-5): 241-246.

Peister, A., M. A. Woodruff, J. J. Prince, D. P. Gray, D. W. Hutmacher and R. E. Guldberg (2011). "Cell sourcing for bone tissue engineering: amniotic fluid stem cells have a delayed, robust differentiation compared to mesenchymal stem cells." Stem Cell Res **7**(1): 17-27.

Pek, Y. S., A. C. Wan and J. Y. Ying (2010). "The effect of matrix stiffness on mesenchymal stem cell differentiation in a 3D thixotropic gel." Biomaterials **31**(3): 385-391.

Pelissier, P., A. C. Masquelet, R. Bareille, S. M. Pelissier and J. Amedee (2004). "Induced membranes secrete growth factors including vascular and osteoinductive factors and could stimulate bone regeneration." J Orthop Res **22**(1): 73-79.

Perka, C., O. Schultz, R.-S. Spitzer, K. Lindenhayn, G.-R. Burmester and M. Sittinger (2000). "Segmental bone repair by tissue-engineered periosteal cell transplants with bioresorbable fleece and fibrin scaffolds in rabbits." Biomaterials **21**(11): 1145-1153.

Phelps, E. A., N. Landazuri, P. M. Thule, W. R. Taylor and A. J. Garcia "Bioartificial matrices for therapeutic vascularization." Proc Natl Acad Sci U S A **107**(8): 3323-3328.

Pittenger, M. F., A. M. Mackay, S. C. Beck, R. K. Jaiswal, R. Douglas, J. D. Mosca, M. A. Moorman, D. W. Simonetti, S. Craig and D. R. Marshak (1999). "Multilineage potential of adult human mesenchymal stem cells." science **284**(5411): 143-147.

Rai, B., J. L. Lin, Z. X. Lim, R. E. Guldberg, D. W. Hutmacher and S. M. Cool (2010). "Differences between in vitro viability and differentiation and in vivo bone-forming efficacy of human mesenchymal stem cells cultured on PCL-TCP scaffolds." Biomaterials **31**(31): 7960-7970.

Rayalam, S., M. A. Della-Fera and C. A. Baile (2011). "Synergism between resveratrol and other phytochemicals: Implications for obesity and osteoporosis." Mol Nutr Food Res.

Razzouk, S. and R. Sarkis (2011). "BMP-2: biological challenges to its clinical use." The New York state dental journal **78**(5): 37-39.

Rhee, S. C., Y. H. Ji, N. A. Gharibjanian, E. S. Dhong, S. H. Park and E. S. Yoon "In Vivo Evaluation of Mixtures of Uncultured Freshly Isolated Adipose-Derived Stem Cells and Demineralized Bone Matrix for Bone Regeneration in a Rat Critically Sized Calvarial Defect Model." Stem Cells Dev.

Rhee, S. C., Y. H. Ji, N. A. Gharibjanian, E. S. Dhong, S. H. Park and E. S. Yoon (2010). "In Vivo Evaluation of Mixtures of Uncultured Freshly Isolated Adipose-Derived Stem Cells and Demineralized Bone Matrix for Bone Regeneration in a Rat Critically Sized Calvarial Defect Model." Stem Cells Dev.

Richardson, S. M., J. M. Curran, R. Chen, A. Vaughan-Thomas, J. A. Hunt, A. J. Freemont and J. A. Hoyland (2006). "The differentiation of bone marrow mesenchymal stem cells into chondrocyte-like cells on poly-L-lactic acid (PLLA) scaffolds." Biomaterials **27**(22): 4069-4078.

Rowley, J. A. and D. J. Mooney (2002). "Alginate type and RGD density control myoblast phenotype." J Biomed Mater Res **60**(2): 217-223.

Saito, N., T. Okada, H. Horiuchi, N. Murakami, J. Takahashi, M. Nawata, H. Ota, K. Nozaki and K. Takaoka (2001). "A biodegradable polymer as a cytokine delivery system for inducing bone formation." Nature biotechnology **19**(4): 332-335.

Salinas, C. N. and K. S. Anseth (2008). "The influence of the RGD peptide motif and its contextual presentation in PEG gels on human mesenchymal stem cell viability." J Tissue Eng Regen Med **2**(5): 296-304.

Schachinger, V., S. Erbs, A. Elsasser, W. Haberbosch, R. Hambrecht, H. Holschermann, J. Yu, R. Corti, D. G. Mathey, C. W. Hamm, T. Suselbeck, B. Assmus, T. Tonn, S. Dimmeler, A. M. Zeiher and R.-A. Investigators (2006). "Intracoronary bone marrow-derived progenitor cells in acute myocardial infarction." N Engl J Med **355**(12): 1210-1221.

Schachinger, V., S. Erbs, A. Elsasser, W. Haberbosch, R. Hambrecht, H. Holschermann, J. Yu, R. Corti, D. G. Mathey, C. W. Hamm, T. Suselbeck, N. Werner, J. Haase, J. Neuzner, A. Germing, B. Mark, B. Assmus, T. Tonn, S. Dimmeler, A. M. Zeiher and R.-A. Investigators (2006). "Improved clinical outcome after intracoronary administration of bone-marrow-derived progenitor cells in acute myocardial infarction: final 1-year results of the REPAIR-AMI trial." Eur Heart J **27**(23): 2775-2783.

Schaffler, A. and C. Buchler (2007). "Concise review: adipose tissue-derived stromal cells--basic and clinical implications for novel cell-based therapies." Stem Cells **25**(4): 818-827.

Shang, Q., Z. Wang, W. Liu, Y. Shi, L. Cui and Y. Cao (2001). "Tissue-engineered bone repair of sheep cranial defects with autologous bone marrow stromal cells." Journal of Craniofacial Surgery **12**(6): 586-593.

Sheyn, D., I. Kallai, W. Tawackoli, D. Cohn Yakubovich, A. Oh, S. Su, X. Da, A. Lavi, N. Kimelman-Bleich, Y. Zilberman, N. Li, H. Bae, Z. Gazit, G. Pelled and D. Gazit (2011). "Gene-modified adult stem cells regenerate vertebral bone defect in a rat model." Mol Pharm **8**(5): 1592-1601.

Shockley, K. R., O. P. Lazarenko, P. J. Czernik, C. J. Rosen, G. A. Churchill and B. Lecka-Czernik (2009). "PPARgamma2 nuclear receptor controls multiple regulatory pathways of osteoblast differentiation from marrow mesenchymal stem cells." J Cell Biochem **106**(2): 232-246.

Simmons, C. A., E. Alsberg, S. Hsiong, W. J. Kim and D. J. Mooney (2004). "Dual growth factor delivery and controlled scaffold degradation enhance in vivo bone formation by transplanted bone marrow stromal cells." Bone **35**(2): 562-569.

Sorger, J. I., F. J. Hornicek, M. Zavatta, J. P. Menzner, M. C. Gebhardt, W. W. Tomford and H. J. Mankin (2001). "Allograft fractures revisited." Clinical orthopaedics and related research **382**: 66-74.

Stafford, P. R. and B. L. Norris (2010). "Reamer-irrigator-aspirator bone graft and bi Masquelet technique for segmental bone defect nonunions: a review of 25 cases." Injury **41 Suppl 2**: S72-77.

Suda, T., K. Kobayashi, E. Jimi, N. Udagawa and N. Takahashi (2001). "The molecular basis of osteoclast differentiation and activation." Novartis Found Symp **232**: 235-247; discussion 247-250.

Teixeira, S., H. Fernandes, A. Leusink, C. van Blitterswijk, M. P. Ferraz, F. J. Monteiro and J. de Boer (2010). "In vivo evaluation of highly macroporous ceramic scaffolds for bone tissue engineering." J Biomed Mater Res A **93**(2): 567-575.

Traverse, J. H., T. D. Henry, S. G. Ellis, C. J. Pepine, J. T. Willerson, D. X. Zhao, J. R. Forder, B. J. Byrne, A. K. Hatzopoulos and M. S. Penn (2011). "Effect of intracoronary delivery of autologous bone marrow mononuclear cells 2 to 3 weeks following acute myocardial infarction on left ventricular function." JAMA: The Journal of the American Medical Association **306**(19): 2110-2119.

Traverse, J. H., T. D. Henry, D. E. Vaughan, S. G. Ellis, C. J. Pepine, J. T. Willerson, D. X. Zhao, L. M. Simpson, M. S. Penn, B. J. Byrne, E. C. Perin, A. P. Gee, A. K. Hatzopoulos, D. H. McKenna, J. R. Forder, D. A. Taylor, C. R. Cogle, S. Baraniuk, R. E. Olson, B. C. Jorgenson, S. L. Sayre, R. W. Vojvodic, D. J. Gordon, S. I. Skarlatos, L. A. Moye, R. D. Simari and N. Cardiovascular Cell Therapy Research (2010). "LateTIME: a

phase-II, randomized, double-blinded, placebo-controlled, pilot trial evaluating the safety and effect of administration of bone marrow mononuclear cells 2 to 3 weeks after acute myocardial infarction." Tex Heart Inst J **37**(4): 412-420.

Traverse, J. H., T. D. Henry, D. E. Vaughn, S. G. Ellis, C. J. Pepine, J. T. Willerson, D. X. Zhao, L. B. Piller, M. S. Penn and B. J. Byrne (2009). "Rationale and design for TIME: A phase II, randomized, double-blind, placebo-controlled pilot trial evaluating the safety and effect of timing of administration of bone marrow mononuclear cells after acute myocardial infarction." American heart journal **158**(3): 356-363.

Tsai, M. S., S. M. Hwang, K. D. Chen, Y. S. Lee, L. W. Hsu, Y. J. Chang, C. N. Wang, H. H. Peng, Y. L. Chang, A. S. Chao, S. D. Chang, K. D. Lee, T. H. Wang, H. S. Wang and Y. K. Soong (2007). "Functional network analysis of the transcriptomes of mesenchymal stem cells derived from amniotic fluid, amniotic membrane, cord blood, and bone marrow." Stem Cells **25**(10): 2511-2523.

Tseng, P. C., S. M. Hou, R. J. Chen, H. W. Peng, C. F. Hsieh, M. L. Kuo and M. L. Yen (2011). "Resveratrol promotes osteogenesis of human mesenchymal stem cells by upregulating RUNX2 gene expression via the SIRT1/FOXO3A axis." Journal of Bone and Mineral Research **26**(10): 2552-2563.

Urist, M. R. (1965). "Bone: formation by autoinduction." Science **150**(3698): 893-899.

Usas, A., A. M. Ho, G. M. Cooper, A. Olshanski, H. Peng and J. Huard (2009). "Bone regeneration mediated by BMP4-expressing muscle-derived stem cells is affected by delivery system." Tissue Eng Part A **15**(2): 285-293.

Wei Hao, e. a. (2009). "Enhanced bone formation in large segmental radial defects by combining adipose-derived stem cells expressing bone morphogenetic protein 2 with nHA/RHLC/PLA scaffold." International Orthopaedics.

Weiner, S., Wagenr, H.D. (1998). "The Material Bone: Structure-Mechanical Function Relations." Annual Review of Materials Science **28**: 271-298.

Wheeler, D. L. and W. F. Enneking (2005). "Allograft bone decreases in strength in vivo over time." Clin Orthop Relat Res(435): 36-42.

Woodbury, D., E. J. Schwarz, D. J. Prockop and I. B. Black (2000). "Adult rat and human bone marrow stromal cells differentiate into neurons." J Neurosci Res **61**(4): 364-370.

Wozney, J. M. (2002). "Overview of Bone Morphogenetic Proteins." Spine **27**(16S): S2-S8.

Xu, Y., H. Meng, C. Li, M. Hao, Y. Wang, Z. Yu, Q. Li, J. Han, Q. Zhai and L. Qiu (2010). "Umbilical cord-derived mesenchymal stem cells isolated by a novel explantation technique can differentiate into functional endothelial cells and promote revascularization." Stem Cells Dev **19**(10): 1511-1522.

Yang, X. B., R. S. Bhatnagar, S. Li and R. O. Oreffo (2004). "Biomimetic collagen scaffolds for human bone cell growth and differentiation." Tissue engineering **10**(7-8): 1148-1159.

Yu, C., Y. G. Shin, A. Chow, Y. Li, J. W. Kosmeder, Y. S. Lee, W. H. Hirschelman, J. M. Pezzuto, R. G. Mehta and R. B. van Breemen (2002). "Human, rat, and mouse metabolism of resveratrol." Pharm Res **19**(12): 1907-1914.

Yu, N., A. Schindeler, M. Tagil, A. Ruys and D. Little (2012). "Application of BMPs and bisphosphonates in improving bone fracture healing." Frontiers in bioscience (Elite edition) **4**: 2647.

Zavan, B., C. Giorgi, G. P. Bagnara, V. Vindigni, G. Abatangelo and R. Cortivo (2007). "Osteogenic and chondrogenic differentiation: comparison of human and rat bone marrow mesenchymal stem cells cultured into polymeric scaffolds." Eur J Histochem **51 Suppl 1**: 1-8.

Zhang, Y., W. Li, T. Laurent and S. Ding (2012). "Small molecules, big roles - the chemical manipulation of stem cell fate and somatic cell reprogramming." J Cell Sci **125**(Pt 23): 5609-5620.

Zuk, P. A., M. Zhu, P. Ashjian, D. A. De Ugarte, J. I. Huang, H. Mizuno, Z. C. Alfonso, J. K. Fraser, P. Benhaim and M. H. Hedrick (2002). "Human adipose tissue is a source of multipotent stem cells." Mol Biol Cell **13**(12): 4279-4295.

Zuk, P. A., M. Zhu, H. Mizuno, J. Huang, J. W. Futrell, A. J. Katz, P. Benhaim, H. P. Lorenz and M. H. Hedrick (2001). "Multilineage cells from human adipose tissue: implications for cell-based therapies." Tissue Eng **7**(2): 211-228.